

Nano-scaled carbon fillers and their functional polymer composites

Citation for published version (APA):

Gomes Ghislandi, M. (2012). *Nano-scaled carbon fillers and their functional polymer composites*. [Phd Thesis 1 (Research TU/e / Graduation TU/e), Chemical Engineering and Chemistry]. Technische Universiteit Eindhoven. <https://doi.org/10.6100/IR733425>

DOI:

[10.6100/IR733425](https://doi.org/10.6100/IR733425)

Document status and date:

Published: 01/01/2012

Document Version:

Publisher's PDF, also known as Version of Record (includes final page, issue and volume numbers)

Please check the document version of this publication:

- A submitted manuscript is the version of the article upon submission and before peer-review. There can be important differences between the submitted version and the official published version of record. People interested in the research are advised to contact the author for the final version of the publication, or visit the DOI to the publisher's website.
- The final author version and the galley proof are versions of the publication after peer review.
- The final published version features the final layout of the paper including the volume, issue and page numbers.

[Link to publication](#)

General rights

Copyright and moral rights for the publications made accessible in the public portal are retained by the authors and/or other copyright owners and it is a condition of accessing publications that users recognise and abide by the legal requirements associated with these rights.

- Users may download and print one copy of any publication from the public portal for the purpose of private study or research.
- You may not further distribute the material or use it for any profit-making activity or commercial gain
- You may freely distribute the URL identifying the publication in the public portal.

If the publication is distributed under the terms of Article 25fa of the Dutch Copyright Act, indicated by the "Taverne" license above, please follow below link for the End User Agreement:

www.tue.nl/taverne

Take down policy

If you believe that this document breaches copyright please contact us at:

openaccess@tue.nl

providing details and we will investigate your claim.

Nano-scaled Carbon Fillers and their Functional Polymer Composites

PROEFSCHRIFT

ter verkrijging van de graad van doctor aan de
Technische Universiteit Eindhoven, op gezag van de
rector magnificus, prof. dr. ir. C.J. van Duijn, voor een
commissie aangewezen door het College voor
Promoties in het openbaar te verdedigen
op donderdag 14 juni 2012 om 16.00 uur

door

Marcos Gomes Ghislandi

geboren te Goiânia, Brazilië

Dit proefschrift is goedgekeurd door de promotor:
prof. dr. G. de With

Ghislandi, Marcos G.
Nano-scaled Carbon Fillers and their Functional Polymer Composites

Eindhoven University of Technology, 2012

A catalogue record is available from the Eindhoven University of Technology Library.
ISBN: 978-90-386-3169-1

Copyright 2012, Marcos Ghislandi

The research results described in this thesis form part of the research program of the Dutch Polymer Institute (DPI, PO Box 902, 5600 AX Eindhoven), project # 648.

Cover design: Marcos Ghislandi

Printed at the PrintService, Eindhoven University of Technology

"There are no facts, only interpretations."

F. Nietzsche

Table of Contents

1. Introduction	1
1.1 Conductive polymer nanocomposites	2
1.2 Nano-scaled carbon fillers	3
1.3 Processing of carbon-based polymer nanocomposites.....	5
1.3.1 Latex technology concept	6
1.4 Outline of the thesis	9
2. Graphene: Preparation and properties	13
2.1 Mechanical exfoliation of graphite	14
2.1.1 Micro-mechanical cleavage or scotch tape method	14
2.1.2 Liquid-phase sonication	16
2.2 Oxidation and reduction	16
2.2.1 Chemical reduction of graphene oxide	17
2.2.2 Thermal reduction of graphene oxide (GO).....	18
2.3 Chemical vapor deposition (CVD) and epitaxial grow.....	19
2.4 Techniques for evaluation of graphene and nanocomposites properties.....	20
3. Electrical conductivity of compacts of graphene, multi-wall carbon nanotubes, carbon black, and graphite powder	29
3.1 Introduction	30
3.2 Experimental.....	32
3.2.1 Materials	32
3.2.2 Paper preparation	33
3.2.3 Powder pressing	34
3.3 Results and discussion	35
3.3.1 Amount of powder for pressing	35
3.3.2 Density versus pressure.....	36
3.3.3 Conductivity versus pressure	39

3.3.4	Conductivity versus density	42
3.3.5	Orientation dependence.....	45
3.4	Conclusions	48
4.	Electrical conductivities of carbon powder nanofillers and their latex-based polymer composites	51
4.1	Introduction	52
4.2	Experimental.....	53
4.2.1	Materials	53
4.2.2	Characterization	53
4.2.3	Powder pressing	54
4.2.4	Paper film and composite processing.....	54
4.3	Results and Discussion	55
4.3.1	Powder and paper conductivities	56
4.3.2	Polymer composite processing, conductivity and percolation threshold	57
4.4	Conclusions	63
5.	Tip-enhanced Raman spectroscopy and mapping of graphene sheets.....	65
5.1	Introduction	66
5.2	Experimental.....	67
5.3	Results and Discussion	69
5.4	Conclusions	78
6.	Investigating the preparation routes to aqueous graphene dispersions and their influence on electrical conductivity of polymer composites.....	81
6.1	Introduction	82
6.2	Experimental.....	83
6.2.1	Chemicals and polymer latex	83
6.2.2	Preparation of graphene via chemical oxidation/reduction treatment.....	83
6.2.3	Preparation of graphene via chemical oxidation and thermal reduction treatment	84

6.2.4	Preparation of graphene sonicated in solution	84
6.2.5	Composites processing.....	84
6.2.6	Characterization	84
6.3	Results and Discussion	85
6.3.1	Graphene powder and dispersion analyses.....	85
6.3.2	PS/graphene composite analysis	89
6.4	Conclusions	93
 7. High performance graphene and MWCNTs-based PS/PPO composites via organic solvent dispersion.....		97
7.1	Introduction	98
7.2	Experimental.....	100
7.2.1	Materials and Characterization	100
7.2.2	Preparation of dispersions and composite processing.....	101
7.3	Results and discussion	102
7.3.1	Conductive Percolation Threshold.....	104
7.3.2	Thermo-Mechanical Properties.....	106
7.4	Conclusions	113
 Technology Assessment.....		117
 Summary.....		121
 Acknowledgements.....		125
 Curriculum Vitae.....		127
 List of Publications		128

Introduction

The chapter gives a general overview on carbon nanofillers and their respective conductive polymer composites. Nanocomposites processing methods are introduced with special focus on the latex technology concept. Finally, the scope of the project and outline of thesis are presented.

1.1 Conductive polymer nanocomposites

Composites are materials made by combination of two or more components with significantly different physical or chemical properties on a micro- or macro-scale. The constituents retain their identities, that is, they do not dissolve or merge completely into one another although they act in concert for a more desirable combination of properties.^[1] Moving to the nano-scale, nanocomposites can be defined as composites where at least one of the dimensions of its components is in the nanometer size range. In many applications, they surpass normal composites due to the exceptionally high surface area and/or aspect ratio of the reinforcing phase. Polymer nanocomposites can exhibit substantial property enhancements at extremely low filler content, reducing costs and weight of the final products.

Polymers are generally insulating materials from an electrical point of view. One way of improving their conductivity is the addition of conductive fillers. The conduction in filled polymers may result from the strong electric field effect between the conductive particles or just their direct physical contact. In the first case, processes such as tunneling, field emission and space charge-limited transport should be considered, resulting in a non-linear current-voltage response. In the second case, when conductive carbon particles are in direct contact, a continuous conducting network forms and the dependence between the current and voltage is more likely to be of the Ohmic type.^[2]

In composites of a polymer matrix with a conducting filler material, the conductivity often increases many orders of magnitude when the filler concentration becomes higher than a critical value. This critical content of conductive filler required to form continuous conducting paths allowing electrical conductivity through the polymer matrix is the so-called percolation threshold. According to theory, this threshold for random percolation is usually of the order of 10-20% in volume fraction for non-nanofillers.^[3-5]

In the field of conductive polymer nanocomposites researchers are usually aiming at a controlled and low percolation threshold and a satisfactory overall conductivity combined with enhanced mechanical properties. Tuning these properties is always a challenge, as many parameters are involved and play a role in the system, starting from the selection of the components (filler, polymer matrix plus, optional, surfactant), passing through the optimum ratio filler/matrix or filler/surfactant/matrix and finishing with one of the known

methods used for obtaining a homogeneous nanofiller dispersion and optimum processing of the composite.

1.2 Nano-scaled carbon fillers

Recent discoveries in the field of nanostructured carbon materials have broadened the horizon for exploiting their hidden outstanding properties, bringing their applications onto a new level. These carbon fillers are largely utilized for the fabrication of polymer composites, where they, dispersed in an insulating matrix, can provide thermo-mechanical reinforcement and/or a conductive path. Applications ranging from electronics (electrostatic dissipations, printed circuits, transparent conductive coatings) to automotive and aerospace sectors have been largely explored.^[6-9]

Graphite is the most stable form of carbon under standard conditions and has a layered, planar structure. In each layer, the carbon atoms are arranged in a hexagonal lattice with a bond length of 0.142 nm, while the distance between the layers is 0.335 nm.^[10] Natural graphite is largely consumed for refractories, steelmaking, brake linings, foundry facings and lubricants. To be used as a filler in polymer composites, commonly graphite intercalation compounds, which are compounds of graphite with atoms or molecules of alkali metals or mineral acids intercalated between the carbon layers,^[11,12] are used. The intercalation increases the interlayer spacing of graphite, weakening the interlayer interactions and facilitating exfoliation.^[13]

Carbon black (CB) is considered an amorphous form of carbon. It is a finely divided solid composed of primary particles of roughly spherical shape, with diameters between a few tens and a few hundreds of nanometers, that are fused together into aggregates.^[14] Because of its variable but low aspect ratio, we like to regard low-structured CB as a 'zero' dimensional carbon nanofiller (0D). CB is one of the most used conductive fillers because of its abundant availability, low density, good electrical conductivity, and low cost. The CB content at percolation threshold of many nanocomposites is usually high, ranging from 10 to 20 vol.%.^[15,16] However, there are also very spectacular cases where favorable inhomogeneity or fractal carbon black distributions lead to electrical conduction at a CB content as low as 0.03 wt.%.^[17]

The discovery of fullerene in 1985,^[18] another carbon allotrope in addition to graphite, diamond and amorphous carbon, revolutionized the field of carbon materials. Another breakthrough came a few years later, in 1991, when Iijima produced carbon nanotubes (CNTs) for the first time.^[19] Since then, a great deal of attention has been given to nanotubes, dispersed in composite materials, to exploit their exceptional mechanical and electrical properties.^[20,21] They are cylindrical nanostructures that can reach a gigantic length-to-diameter ratio. The high aspect ratios of the CNTs make these nanofillers virtually one-dimensional (1D). Nanotubes are normally named according to the number of shells or walls. Most single-walled nanotubes (SWCNTs) have a diameter close to 1 nanometer with a tube length that can be many millions of times longer. The structure of a SWCNT can be conceptualized by wrapping a one-atom-thick layer of graphite, called graphene, into a seamless cylinder.^[22] Multi-walled nanotubes (MWCNTs) consist of multiple rolled layers (concentric tubes) of graphite. Its individual shells can be described as SWCNTs, which can be metallic or semiconducting. Individual nanotubes naturally align themselves into "ropes" held together by van der Waals forces, more specifically, π -stacking.^[23, 24]

Although graphene has recently been discovered, it has already being used as a new nanofiller material for polymers. *"Graphene is a rapid rising star on the horizon of materials science and condensed-matter physics. This strictly two-dimensional material exhibits exceptionally high crystal and electronic quality, and despite its short history, has already revealed a cornucopia of new physics and potential applications. The most immediate application for graphene is in composite materials...."*^[25]

Graphene can be obtained from cheap graphite by the use of chemical or physical treatments, and its cost is expected be lower than that of MWCNTs, and much lower than that of SWCNTs. In fact, whereas carbon nanotubes can be regarded as rolled-up graphene sheets, the corresponding graphene sheets are two-dimensional (2D), but have aspect ratios similar to those of the corresponding nanotubes. In the case of graphene sheets, charge carriers can more easily bypass point defects in the sheet structure, which makes its charge transport behaviour less sensitive to chemical treatments.^[26,27] When incorporated as a nanofiller in a matrix, isolated graphene sheets are expected to impart exceptional mechanical (strength and stiffness), electrical (conductivity and dielectric), thermal (conductivity and flame retardancy), and gas barrier properties to the matrix polymer,

which will exceed those of nanocomposites based on other fillers such as layered silicates or CNTs.

Figure 1.1 shows the different carbon allotropes. In this work, graphite (3D), graphene (2D), MWCNTs (1D), and carbon black (0D) fillers are studied with focus on bulk conductivity behavior. Special attention is given to graphene, with a more detailed investigation of its properties depending on the manufacturing method. All the different fillers are used for the production of conductive polymer composites.

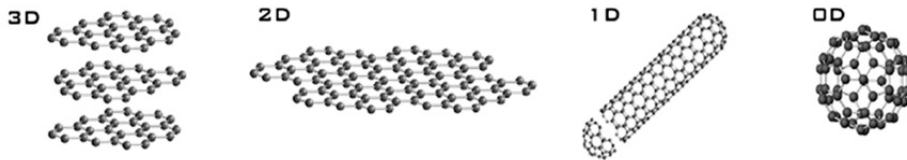


Figure 1.1 Graphene is a 2D building material for carbon materials of all other dimensionalities. It can be wrapped up into 0D buckyballs, rolled into 1D nanotubes or stacked into 3D graphite.

1.3 Processing of carbon-based polymer nanocomposites

Important points when using carbon nanofillers in nanocomposites are the dispersion of the filler in a polymer matrix as well as the quality of the filler–matrix interface; the bottleneck is that the as-produced fillers tend to be held together in bundles/agglomerates by very strong van der Waals interactions.

Various methods have been developed in recent years to efficiently disperse individual CNTs in a polymer matrix. Direct mixing of the CNTs and the polymer, with or without the help of a solvent, has proven to be efficient and appears to be the easiest and least laborious way to achieve this goal.^[28,29]

Solvent processing basically consists of three steps: dispersion of the filler in a suitable solvent (usually adding external energy, e.g. by ultra-sonication), addition of the polymer (which should also be soluble in the solvent), and removal of the solvent by evaporation or distillation. Due to the simplicity for preparation of polymer nanocomposites, it is expected that this methodology will continue to be developed.^[30-32]

Direct melt processing is commercially much more attractive than a solvent method, as it is more versatile and environmentally friendly. This strategy involves the direct inclusion of the carbon fillers into the molten polymer using generally an extruder.^[33] The drawbacks of this procedure are the lower degree of dispersion, even sometimes with the formation of millimeter-scale inhomogeneities, as compared to solvent blending, and manipulation difficulties during processing due to the low bulk density of the nanofillers.^[34] This lower degree of dispersion can then have a detrimental influence on the percolation threshold, conductivity values and mechanical properties. However, some studies report that the existence of a certain amount of agglomerates can be a key factor in lowering the value of the percolation threshold and in increasing the conductivity.^[35-38] In general, melt processing allows manufacturers many degrees of freedom with regard to the selection of polymer and choice of the filler content.^[39]

Modifying either the nanofiller surface itself or the polymer matrix by functionalization improves the quality of the interface between two components of the nanocomposite by enhancing the interfacial interactions, but this approach has some drawbacks. In one possible case, the interaction of the filler with the polymer is realized by covalent bonding, and in another case, by means of $\pi - \pi$ stacking. Both approaches lead to disturbances of the π -electron delocalization on the e.g. graphene/CNTs surfaces, which results in a significant deterioration of its electrical properties.

In-situ polymerization is another, less frequently used processing method. In this strategy the fillers are usually mixed with monomers or pre-polymers, with or without the presence of a solvent, and then the polymerization reaction proceeds by adjusting parameters such as temperature and time.^[33,34,40]

1.3.1 Latex technology concept

A frequently applied approach to incorporate nanofillers into a polymer matrix is based on the use of a third component, i.e. a surfactant. The methods for nanocomposite production inspired by the strategy utilizing surfactants are mainly based on the so-called latex-technology, although in-situ emulsion polymerization and spraying of surfactant-aided exfoliated nanofiller on polymer powder followed by dispersion in xylene and solution-casting have also been utilized.^[41-43] The basic concept consists of the generation

of a stable, mixed colloidal system in water containing both a suspension of individual nanofillers, stabilized by surfactant molecules, and polymer latex particles, also stabilized by surfactants. After the removal of water, usually done via freeze drying, the resulting powder can be processed by e.g. compression molding into the desired shape, preserving in most cases the dispersion and exfoliation of the filler inside the polymer matrix. Figure 1.2 illustrates the route used for the preparation of nanotubes-based polymer composites via latex technology.

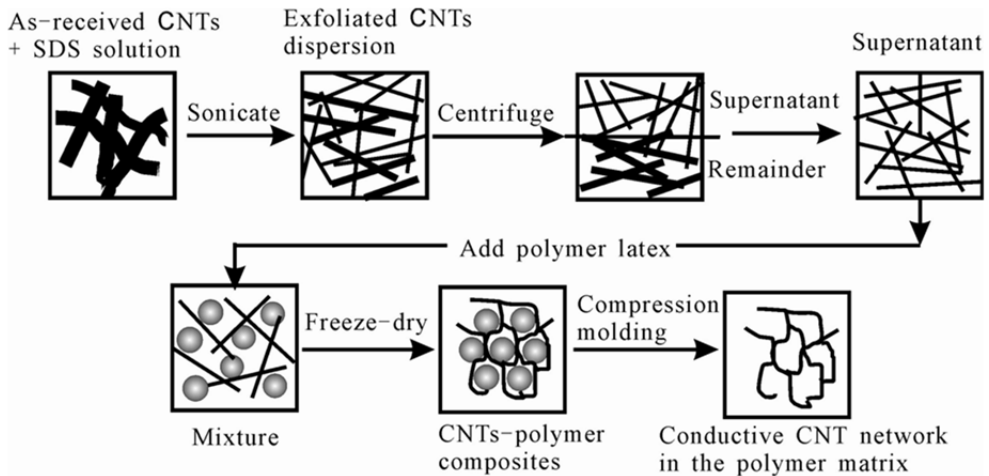


Figure 1.2 Schematic description of the multi-step process for preparation of CNT/polymer composites via latex technology.^[44] “Reprinted from ref. 44, with permission from Elsevier”.

The latex technology was initially successfully applied to prepare SWCNT/polymer composites. A very low percolation threshold of 0.3 wt.% SWCNTs in a polystyrene (PS) matrix^[45] and even lower percolation threshold of about 0.04 wt.% SWCNTs in poly(vinyl acetate) (PVAc)^[46] were reported. For MWCNTs in a PS matrix, the percolation was verified to be ~1.8 wt.%.^[44] A very similar latex-based process to disperse MWCNTs into a polymer matrix has been described earlier by Dufresne et al. and a percolation threshold of about 3 wt.% was reported.^[47]

As an initial stage of this PhD work, we used for the first time the same latex concept for the preparation of graphene/polystyrene nanocomposites.^[48] The study demonstrates that it is possible to apply the latex technology for the preparation of graphene-based

nanocomposites. Poly(sodium 4-styrene sulfonate) (PSS)-covered graphene platelets were firstly successfully prepared via a known oxidation/reduction method and dispersed in water by means of sonication. PSS stabilizes the platelets and prevents their aggregation, but at the same time, because of its bulkiness and non-conductive character, probably limits the electron transport at the graphene junctions in the final nanocomposites. Atomic force microscopy (AFM) showed that the thickness of the oxidized graphite platelets is about 1 nanometer, pointing to approximately 2-3 graphene layers. Relatively well-dispersed graphene sheets in the PS matrix could be visualized using a high charge contrast scanning electron microscopy (SEM) imaging technique. The final conductivities of the graphene/PS nanocomposites, obtained by both four point and local current measurement techniques, revealed interestingly high values up to 15 S/m, which can be achieved for low nanofiller loadings (1.6-2 wt.%). A pronounced percolation threshold exhibiting a quite low value around 0.8-0.9 wt.% was observed for the produced PS/graphene nanocomposites (see Figure 1.3).

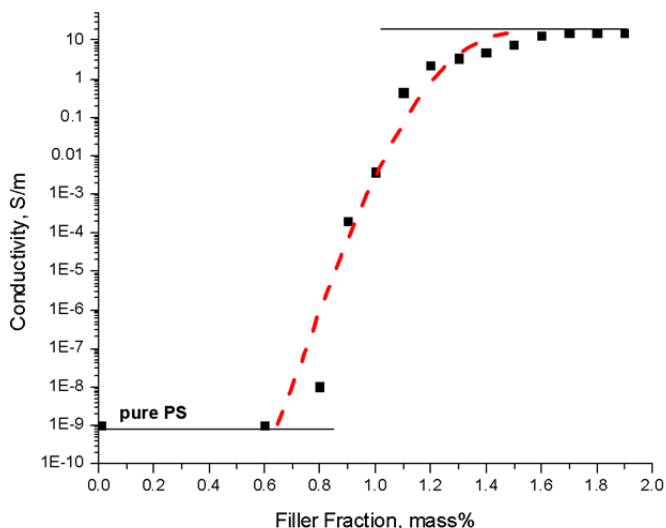


Figure 1.3 Electrical conductivity of graphene/PS composites as a function of graphene weight fraction.^[48]

The advantages of the latex technique are obvious: it is easy, versatile, reproducible, and reliable. This approach allows composite production with a relatively homogeneous dispersion of the nanofiller into the polymer matrix, low percolation thresholds and good

conductivity levels. It is very flexible with respect to the choice of the polymer matrix: it can be applied to any polymer that can either be synthesized by emulsion polymerization, or brought into a polymer latex form in another way. It does not require the use of toxic and inflammable solvents and is safe and environmentally friendly. Furthermore, since the nanofillers are not chemically modified, their properties are preserved. A drawback is that the mechanical properties of the nanocomposite can deteriorate because of the high amount of surfactant, necessary for the particles stabilization, but remaining present in the final polymer nanocomposite.

1.4 Outline of the thesis

The goal is to develop nano-scaled carbon-based polymer nanocomposites with different levels of nanofiller loading, using primarily the latex technology, and to optimize and compare their electrical properties. Special attention is given to graphene nanoparticles characterization and their respective polymer composites. To achieve this goal, a thorough study with respect to the conductivity and morphology of the as-received filler powders was firstly conducted.

Chapter 2 introduces the main methods utilized in this thesis work for the preparation of graphene. Microscopic and spectroscopic techniques used for characterization of graphene sheets and their respective polymer composites are briefly explained.

Chapter 3 presents a detailed electrical conductivity study of graphite, graphene, MWCNTs, and carbon black bulk powders. The goal is to obtain an understanding of the mechanical and electrical behavior of these powders during compaction or paper preparation process.

Chapter 4 extends the study to the conductivity and percolation threshold of Polypropylene (PP) nanocomposites produced via latex technology process, using the different carbon nanopowders studied in Chapter 3 as filler.

Chapter 5 focuses on the spectroscopic characterization of graphene platelets utilizing Raman and tip-enhanced Raman (TERS) spectroscopy. Enhancements of the intensity modes are for the first time reported and an investigation of graphene edge defects, with resolution within the nanometer range, is presented.

Chapter 6 compares the structural properties and dimensions of graphene sheets produced via different liquid-based preparation methods introduced in Chapter 2. Polystyrene (PS)/graphene composites are prepared via the latex concept using the different graphene platelets, and their respective final electrical conductivities and percolation thresholds are compared.

Chapter 7 proposes and tests a new method for the preparation of well-dispersed graphene/PS-Poly(p-phenylene oxide) composites, based on long-term ultra-sonication of the filler in an organic solvent, without the use of surfactants. The goal is to obtain a highly conductive composite at low filler contents and with reasonably high mechanical (stiffness/strength) properties.

References

- [1] W. D. Callister, *Material Science and Engineering: An Introduction*, 5th ed., John Wiley & Sons Inc, **1999**.
- [2] J. M. Margolis, *Conductive polymers and plastics*, Chapman and Hall, **1989**.
- [3] S. Dietrich, A. Amnon, *Introduction to percolation theory*, Taylor & Francis, **1994**.
- [4] A. Bunde, S. Havlin, *Fractals and disordered systems*, Springer, **1996**.
- [5] R. Viswanathan, M. B. Heaney, *Phys. Rev. Lett.* **1995**, 75, 4433.
- [6] J. G. Smith, D. M. Delozier, J. W. Connell, K. A. Watson, *Polymer* **2004**, 45, 6133.
- [7] J. H. Chen, M. Ishigami, C. Jang, D. R. Hines, M. S. Fuhrer, E. D. Williams, *Adv. Mater.* **2007**, 19, 3623.
- [8] H. X. Chang, G. F. Wang, A. Yang, X. M. Tao, X. Q. Liu, Y. D. Shen, Z. J. Zheng, *Adv. Funct. Mater.* **2011**, 20, 2893.
- [9] M. Lotya, Y. Hernandez, P. J. King, R. J. Smith, V. Nicolosi, L. S. Karlsson, F. M. Blighe, S. De, Z. M. Wang, I. T. McGovern, G. S. Duesberg, J. N. Coleman, *J. Amer. Chem. Soc.* **2009**, 131, 3611.
- [10] P. Delhaès, *Graphite and precursors*, Gordon & Breach, **2001**.
- [11] M. S. Dresselhaus, G. Dresselhaus, *Advances in Physics* **1981**, 30, 139.
- [12] G. H. Chen, D. J. Wu, W. U. Weng, C. L. Wu, *Carbon* **2003**, 41, 619.

-
- [13] B. Z. Jang, A. Zhamu, *J. Mater. Sci.* **2008**, *43*, 5092.
- [14] J. I. Paredes, M. Gracia, A. Martínez-Alonso, J. M. D. Tascón, *J. Colloid Interface Sci.* **2005**, *288*, 190.
- [15] H. G. Yoon, K. W. Kwon, K. Nagata, K. Takahashi, *Carbon* **2004**, *42*, 1877.
- [16] A. L. G. Saad, H. A. Aziz, O. I. H. Dimitry, *J. Appl. Polym. Sci.* **2004**, *91*, 1590.
- [17] D. van der Putten, J. T. Moonen, H. B. Brom, J. C. M. Brokken-Zijp, M. A. J. Michels, *Phys. Rev. Lett.* **1992**, *69*, 494.
- [18] H. W. Kroto, J. R. Heath, S. C. O'Brien, R. F. Curl, R. E. Smalley, *Nature* **1985**, *318*, 162.
- [19] S. Iijima, *Nature* **1991**, *354*, 56.
- [20] M. M. J. Treacy, T. W. Ebbesen, J. M. Gibson, *Nature* **1996**, *381*, 678.
- [21] J. W. G. Wildoer, L. C. Venema, A. G. Rinzler, R. E. Smalley, C. Dekker, *Nature* **1998**, *391*, 59.
- [22] S. Iijima, T. Ichihashi, *Nature* **1993**, *363*, 603.
- [23] M. S. C. Mazzoni, H. Chacham, *Appl. Phys. Lett.* **2000**, *76*, 1561.
- [24] W. Andreoni, *The chemical physics of fullerenes 10 (and 5) years later: the far-reaching impact of the discovery of C60*, Kluwer Academic Publishers, **1996**.
- [25] A. K. Geim, K. S. Novoselov, *Nat. Mater.* **2007**, *6*, 183.
- [26] K. S. Novoselov, A. K. Geim, S. V. Morozov, D. Jiang, M. I. Katsnelson, I. V. Grigorieva, S. V. Dubonos, A. A. Firsov, *Nature* **2005**, *438*, 197.
- [27] K. I. Bolotin, K. J. Sikes, Z. Jiang, M. Klima, G. Fudenberg, J. Hone, P. Kim, H. L. Stormer, *Solid State Commun.* **2008**, *146*, 351.
- [28] H. Wang, E. K. Hobbie, *Langmuir* **2003**, *19*, 3091.
- [29] N. H. Tai, M. K. Yeh, H. H. Liu, *Carbon* **2004**, *42*, 2774.
- [30] S. Stankovich, D. A. Dikin, G. H. B. Dommett, K. M. Kohlhaas, E. J. Zimney, E. A. Stach, R. D. Piner, S. T. Nguyen, R. S. Ruoff, *Nature* **2006**, *442*, 282.
- [31] H. B. Lee, A. V. Raghun, K. S. Yoon, H. M. Jeong, *Journal of Macromolecular Science Part B-Physics* **2010**, *49*, 802.
- [32] H. Javier Salavagione, G. Martinez, M. A. Gomez, *J. Mater. Chem.* **2009**, *19*, 5027.
- [33] R. Verdejo, M. M. Bernal, L. J. Romasanta, M. A. Lopez-Manchado, *J. Mater. Chem.* **2010**, *21*, 3301.
- [34] H. Kim, Y. Miura, C. W. Macosko, *Chem. Mater.* **2010**, *22*, 3441.

- [35] J. O. Aguilar, J. R. Bautista-Quijano, F. Aviles, *Express Polymer Letters* **2010**, *4*, 292.
- [36] J. Li, P. C. Ma, W. S. Chow, C. K. To, B. Z. Tang, J.-K. Kim, *Adv. Funct. Mater.* **2007**, *17*, 3207.
- [37] C. A. Martin, J. K. W. Sandler, M. S. P. Shaffer, M. K. Schwarz, W. Bauhofer, K. Schulte, A. H. Windle, *Compos. Sci. Technol.* **2004**, *64*, 2309.
- [38] J. J. Hernandez, M. C. Garcia-Gutierrez, A. Nogales, D. R. Rueda, M. Kwiatkowska, A. Szymczyk, Z. Roslaniec, A. Concheso, I. Guinea, T. A. Ezquerro, *Compos. Sci. Technol.* **2009**, *69*, 1867.
- [39] H.-B. Zhang, W.-G. Zheng, Q. Yan, Y. Yang, J.-W. Wang, Z.-H. Lu, G.-Y. Ji, Z.-Z. Yu, *Polymer* **2010**, *51*, 1191.
- [40] J. Liang, Y. Wang, Y. Huang, Y. Ma, Z. Liu, F. Cai, C. Zhang, H. Gao, Y. Chen, *Carbon* **2009**, *47*, 922.
- [41] O. Regev, P. N. B. El Kati, J. Loos, C. E. Koning, *Adv. Mater.* **2004**, *16*, 248.
- [42] H. J. Barraza, F. Pompeo, E. A. O'Rear, D. E. Resasco, *Nano Letters* **2002**, *2*, 797.
- [43] Q. H. Zhang, D. R. Lippits, S. Rastogi, *Macromolecules* **2006**, *39*, 658.
- [44] J. Yu, K. Lu, E. Sourty, N. Grossiord, C. E. Konine, J. Loos, *Carbon* **2007**, *45*, 2897.
- [45] N. Grossiord, J. Loos, C. E. Koning, *J. Mater. Chem.* **2005**, *15*, 2349.
- [46] J. C. Grunlan, A. R. Mehrabi, M. V. Bannon, J. L. Bahr, *Adv. Mater.* **2004**, *16*, 150.
- [47] A. Dufresne, M. Paillet, J. L. Putaux, R. Canet, F. Carmona, P. Delhaes, S. Cui, *J. Mater. Sci.* **2002**, *37*, 3915.
- [48] E. Tkalya, M. Ghislandi, A. Alekseev, C. Koning, J. Loos, *J. Mater. Chem.* **2010**, *20*, 3035.

Graphene: Preparation and properties

The chapter introduces the main routes utilized in this work for the preparation of graphene and discusses the particularities of each method. Techniques used for characterization of single sheet properties and its organization inside polymer composites are presented, with focus on atomic force microscopy and Raman spectroscopy.

A single-layer graphene is the strongest material ever measured, exhibiting an ultimate strength of 130 GPa and Young's modulus of 1 TPa, in addition to an extremely high surface area (theoretical limit: 2630 m²/g).^[1] It has a thermal conductivity of 5000 W/(m.K), which is more than twice the value of graphite (~2000 W/(m.K)) and comparable with the upper bound of the highest values reported for SWCNT bundles.^[2] An electrical conductivity of up to 600000 S/m was reported for a single graphene layer.^[3] The implementation of the huge potential of applications that graphene has, can only become reality if the development of simple and relatively inexpensive methods of producing this material in macroscopic quantities with the desired characteristics is achieved. Since the first method for isolating graphene based on the mechanical cleavage of graphite layers was developed, the efforts of many research groups have been focused on the development of more effective approaches to solve this problem and to design new technological approaches for the isolation and purification of graphene.

2.1 Mechanical exfoliation of graphite

2.1.1 Micro-mechanical cleavage or scotch tape method

The Nobel Prize winners, Geim and Novoselov,^[4] proved that a fresh surface of a layered crystal can be rubbed against another surface, resulting in a variety of flakes attached to that surface (the rubbing process can be described as similar to “drawing by chalk on a blackboard”). Single layers can always be found amongst the flakes (see Figure 2.1). Using dry etching in oxygen plasma, graphite mesas were prepared, cleaved off from highly-oriented pyrolytic graphite (HOPG) sheets by a photoresist substrate, and baked. Then, using scotch tape, flakes were repeatedly peeled off the mesas. Thin flakes left on the photoresist are released in acetone. When a silicon wafer was dipped in the solution and then washed in plenty of water and propanol, some flakes became captured on the wafer's surface.^[5] Using optical microscopy, the 2D crystallites became visible on top of the oxidized silicon wafer, because even a monolayer adds up sufficiently to the optical path of reflected light so that the interference color changes with respect to the one of a clear substrate (phase contrast).^[6,7]

In a similar approach, arrays of graphite micropillars were fabricated on a HOPG surface using micro-patterning followed by masked anisotropic oxygen plasma etching. Mounted graphite blocks were produced and used on a cantilever as the tip of an atomic force microscope (AFM) in order to transfer thin graphite samples onto a SiO_2 / Si substrate for subsequent device fabrication. By operating the AFM in contact mode with a load on the graphite mounted cantilever, very thin layers of HOPG were sheared off onto the substrate. This microscopic cleaving process can be controlled by tuning the normal force between the cantilever and the substrate.^[8,9]

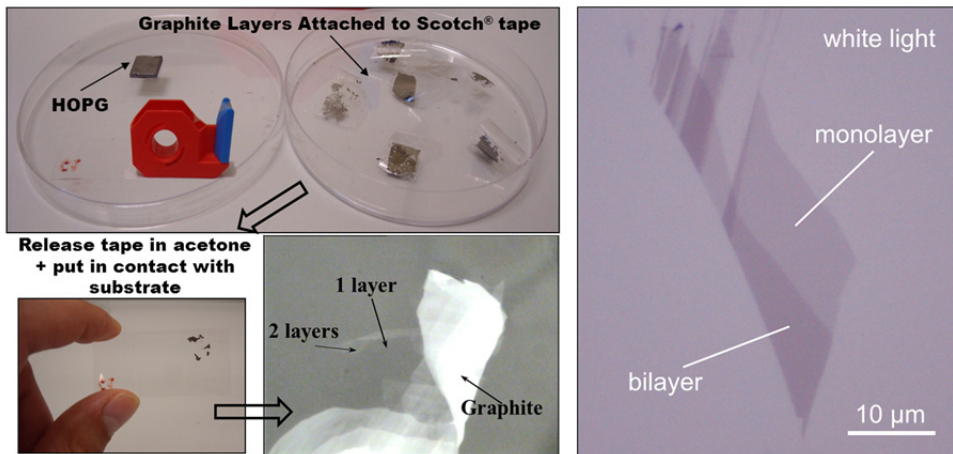


Figure 2.1 Scotch tape procedure used for the micro-mechanical cleavage of HOPG. Optical microscopy images show single and multi-layer graphene platelets deposited on glass (middle) and on SiO_2 / Si substrates (right).

The mechanical cleaving process allows one to obtain graphene sheets within the micrometer range. The main problem lies in their identification. The fraction of single layer samples in the conglomerate flake is relatively small and their identification using optical microscopy is challenging. Large scale production is also difficult with this method since it is almost impossible to produce single layer graphene on the gram scale. However, this method yields primarily defect free pure single layer graphene sheets, which are preferably used as reference for exploiting and characterizing their properties.

2.1.2 Liquid-phase sonication

Coleman and coworkers produced graphene dispersions, with concentrations up to 0.01 mg/ml, by exfoliation of graphite in organic solvents such as N-methyl-pyrrolidone (NMP).^[10] Long-term bath sonication treatment, followed by centrifugation to remove non-exfoliated graphite particles, resulted in a black homogeneous suspension of graphene flakes in the solvents.^[10,11] Characterization of the suspensions revealed the presence of defect- and oxide-free mono- and bilayer graphene flakes as well as multilayer structures.

Using water as solvent, Green et al. exfoliated graphite in sodium cholate (SC)/water solution applying horn sonication and density gradient ultracentrifugation to isolate graphene sheets with controlled thickness,^[12] resulting in stable graphene dispersions with graphene concentrations of 90 $\mu\text{g/ml}$. Lotya et al. presented a method to produce graphene dispersions, stabilized in water by the surfactant SC, using concentrations up to 0.3 mg/ml. The process uses low power sonication for long times (up to 400 h) followed by centrifugation to yield stable dispersions.^[13] Depending on the sonication and centrifugation time different concentrations of graphene sheets could be obtained. Transmission electron microscopy showed the dispersed phase to consist of small graphitic flakes. Free-standing films prepared with graphene/SC dispersions by vacuum filtration exhibited an electrical conductivity of 17500 S/m after annealing.

All processes described above use either high boiling point solvents or surfactants to successfully exfoliate graphite into graphene sheets, which can be detrimental to processing conditions or final properties of the nanocomposites. Alternatively, O'Neill et al. were able to identify low boiling point solvents and optimize conditions for stable graphene dispersions in chloroform, acetone and isopropanol. Depending on the preparation conditions, which include long-term and low-energy bath sonication and centrifugation, dispersions with a graphene concentration as high as 0.5 mg/ml could be obtained.^[14]

2.2 Oxidation and reduction

Since it was first prepared in the nineteenth century, graphite oxide has been mainly produced by the Staudenmaier^[13] and Hummers^[15,16] methods, which involve oxidation of graphite in the presence of strong acids and oxidants. The level of the oxidation can be

varied on the basis of the method applied, the reaction conditions and the precursor graphite used. The sp^2 -bonded carbon network of graphite is strongly disrupted and a significant fraction of this carbon network is bonded to hydroxyl groups or participates in epoxide groups (see Figure 2.2).^[17-20] Minor components of carboxylic acid or carbonyl groups are thought to populate the edges of the layers in graphite oxide (GO).

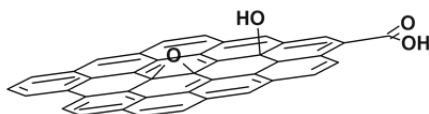


Figure 2.2 Proposed chemical structure of graphene oxide.^[19]

Graphite oxide thus consists of a layered structure of graphene oxide sheets that are strongly hydrophilic such that intercalation of water molecules between the layers readily occurs. Graphite oxide can be completely exfoliated to produce aqueous colloidal suspensions of graphene oxide sheets by simple sonication and by stirring the water/graphite oxide mixture for a sufficiently long time.^[17]

2.2.1 Chemical reduction of graphene oxide

Although oxidation of graphite generates electrically insulating materials, the reduction of graphene oxide by chemical methods, using reductants such as hydrazine, dimethylhydrazine, and hydroquinone has produced electrically conducting materials.^[17, 21-27] The reduction of an aqueous graphene oxide suspension by hydrazine resulted in agglomerated graphene-based nanosheets, and, when dried, in a black powder that is electrically conductive. Elemental analysis revealed the existence of a significant amount of oxygen, indicating that reduction of graphene oxide is not complete.

Homogeneous colloidal suspensions of electrically conducting reduced graphene oxide were produced by chemical reduction with dimethyl-hydrazine or hydrazine in the presence of either polymer or surfactant.^[24,28] The reduction of an aqueous suspension containing a mixture of graphene oxide sheets and poly(sodium 4-styrene sulfonate) (PSS) resulted in an aqueous black suspension of reduced graphene oxide sheets coated by the PSS.^[28] The reduction of isocyanate-modified graphene oxide in the presence of PS generated a suspension of reduced graphene oxide sheets in DMF.^[24]

Reduction of sodium dodecylbenzenesulfonate (SDBS)-wrapped graphene oxide with hydrazine and then its chemical modification with aryl diazonium salt produced SDBS-wrapped chemically modified graphene that was dispersible in DMF, N,N' -dimethylacetamide and NMP at concentrations up to 1 mg/ml.^[22]

A few methods for creating colloidal suspensions of graphene sheets without the help of stabilizers or surfactants have been reported. An aqueous suspension (0.5 mg/ml) of reduced graphene oxide sheets under basic conditions (pH 10) was described by Li and coworkers.^[29] The graphene oxide was reduced by hydrazine, and excess hydrazine was removed by dialysis. It was suggested that shifting the pH to 10 converts neutral carboxylic groups to negatively charged carboxylate groups, so that when the interior of the graphene oxide sheets is reduced by hydrazine, the negatively charged particles do not agglomerate.

2.2.2 Thermal reduction of graphene oxide (GO)

Thermally reduced graphene oxide can be produced by rapid heating of dry GO under inert gas and at high temperature.^[30-33] Heating GO in an inert environment at 1000 °C for 30 s leads to reduction and exfoliation of GO. Exfoliation takes place when the pressure, generated by the gas (CO_2) evolved due to the decomposition of the epoxy and hydroxyl sites of GO, exceeds the van der Waals forces that holds the graphene oxide sheets together. About 30% weight loss is associated with the decomposition of the oxygen groups and evaporation of water.^[32] The exfoliation leads to a volume expansion of 100-300 times producing very low bulk density graphene. Because of the structural defects caused by the loss of CO_2 , these sheets are highly wrinkled as shown in Figure 2.3.

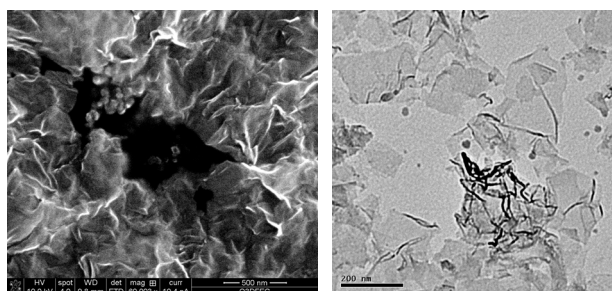


Figure 2.3 SEM image (left) and TEM image (right) of dry, as-produced thermally reduced graphene powder. The sheets are highly wrinkled, exhibiting a fluffy morphology.

The advantage of the thermal reduction method is the ability to produce chemically modified graphene sheets in large quantities. The same is true for the chemical reduction method, but thermal reduction has the advantage of not using a solvent during the reduction stage. It was reported that 80% of the sheets are single layers graphene with an average size of about 500 nm and a surface area of around 1700 m²/g, independent of the starting GO size.^[32] Reduced GO has a C/O ratio of about 10/1 compared to 2/1 for GO.^[30, 34] This ratio has been increased up to 660/1 through heat treatment at higher temperature (1500 °C) or for longer time.^[35] The sheets can be well dispersed in organic solvents such as N,N-dimethylformamide (DMF), tetrahydrofuran and chloroform. The thermal reduction step also leads to restoration of the electrical conductivity with reported values of 10 and 20 S/cm for a compacted film with density 0.3 g/cm³, compared to 6000 S/cm for defect-free single graphene sheets.^[31,34]

2.3 Chemical vapor deposition (CVD) and epitaxial grow

CVD of is one of the most common methods for obtaining CNTs on a macroscopic scale.^[36] It is based on the thermocatalytic decomposition of gaseous hydrocarbons on the surface of some metals which leads to the formation of various carbon nanostructures.^[37] An example of the successful use of CVD for the synthesis of graphene is the work of Kim et al. using a nickel substrate as catalyst.^[38] It was found that the average number of graphene layers and the coverage of the substrate are determined by the thickness of the nickel film and the duration of the growth process. Thus, the film synthesized within 7 minutes on a nickel substrate of 300 nm thickness contained predominantly two-layer flakes of graphene. AFM analysis, after graphene sheets were transferred to a desired substrate, indicate a bumpy surface structure of the graphene sheets.

Further efforts towards improving the CVD method for obtaining graphene sheets resulted in a significant increase in the size of the synthesized samples. Li et al. produced single-layer graphene sheets with a transverse size of about 1 cm. In this method graphene was grown on the copper foil of 25 micrometers thickness at 1000 °C in a stream of methane and hydrogen.^[39] The results of the measurements showed that the films obtained exhibit usually a continuous structure and contain mostly single-layer graphene. It was found that graphene growth on Cu is self-limited; growth that proceeded for more than 60

min yielded a similar structure to growth runs performed for ~10 min. These observations allows one to conclude that graphene is growing by a surface-catalyzed process, rather than by a precipitation process, as was reported by others for Ni.^[38,40,41] Monolayer graphene formation caused by surface segregation or surface adsorption of carbon was also observed on transition metals such as Ni and Co at elevated temperatures.^[42-44]

Bae and coworkers were able to increase the size of the graphene sheet up to 75 cm in the diagonal.^[45] They report the roll-to-roll production and wet-chemical doping of predominantly monolayer 30-inch graphene films grown by chemical vapor deposition onto flexible copper substrates. The films have sheet resistances as low as $\sim 125 \Omega \square^{-1}$ with 97.4% optical transmittance.

Another studied route to produce graphene platelets is their growing by thermal decomposition of SiC. Graphene multilayers are grown epitaxially on single crystal silicon carbide, producing single crystalline films down to approximately one graphene layer.^[46-49] The advantage of this approach is that the size of the synthesized sample can be comparable to the size of the original SiC crystal if the crystal is of a good quality. However, the large-scale structural quality is limited by the lack of continuity and uniformity of the grown film.^[50,51]

2.4 Techniques for evaluation of graphene and nanocomposites properties

Optical microscopy, SEM, AFM, TEM and Raman spectroscopy are techniques widely used to characterize graphene sheets and their polymer composites. Standard elemental analysis is applied to estimate the degree of oxidation of graphene oxide. X-ray photoelectron spectroscopy can determine the amount of oxygen on the graphene surface as well as identify the types of the bonds.

Although the identification of graphene sheets transferred to oxidized silicon wafer substrates can be obtained via optical microscopy, AFM is a highly effective way for the characterization of the graphene morphology, deposited on virtually any flat substrate. From the step height of graphene on the substrate, it is possible to estimate the number of graphene layers in the sheet. Due to the differences in tip attraction/repulsion between the insulating substrate and graphene it is unlikely to measure the theoretical thickness of 0.34 nm. Also, microscopic corrugations have been observed on all suspended^[52] and

supported^[53] graphene sheets studied so far. This rippling has been invoked to explain the thermodynamic stability of free-standing graphene sheets and many distinctive electronic and chemical properties of graphene have been attributed to the presence of these ripples.^[54,55] However, the fabrication and characterization of high-quality ultraflat graphene monolayers by making use of a mica support was reported as well.^[56]

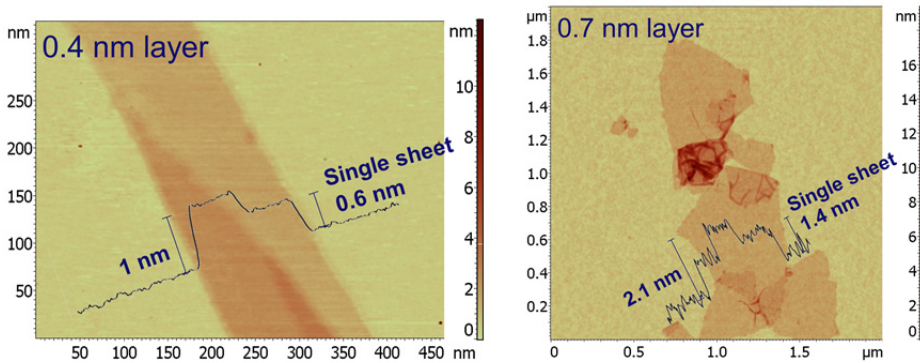


Figure 2.4 AFM tapping mode showing a 0.4 nm layer-step on graphene (right) prepared via micro-mechanical cleavage and deposited on mica substrate, and a 0.7 nm layer-step on graphene (right) prepared via chemical/oxidation, deposited on SiO₂.

In Figure 2.4 it is possible to see the differences in thickness and roughness measured on single layer graphene produced by micro-mechanical cleavage and oxidation/reduction processes. Typical thicknesses range from 0.4 to 1.0 nm for single layer graphene.^[57] Roughness of the substrate, folded or wrinkled sheets, together with adsorbed solvents, moisture or surfactants, can compromise the measurements.^[21,32,34]

The lateral size of graphene layers can be observed with TEM with atomic spatial resolution. In addition to that electron diffraction patterns can clearly differentiate single from bilayer sheets.^[52] High-resolution TEM (HR-TEM) can identify atomic bonds on functionalized sheets and atomistic defects.^[58] Infinite defect-free graphene sheets do not differ from each other. The real graphene platelets differ one from another not only in size but also in the boundary structure. These differences significantly affect the characteristics of graphene and in particular its electronic properties, e.g. it can exhibit either quasi-metallic or semiconducting behavior, depending on the atomic structure of their edges. Cutting a graphene sheet along a straight line produces two typical kinds of peripheral shapes called armchair and zigzag; the axial direction of these latter two differs by 30°.^[59]

Figure 2.5 illustrates the edge configuration of defects (holes) in graphene sheets. Studies showed long-term stability for zigzag configuration.^[60]

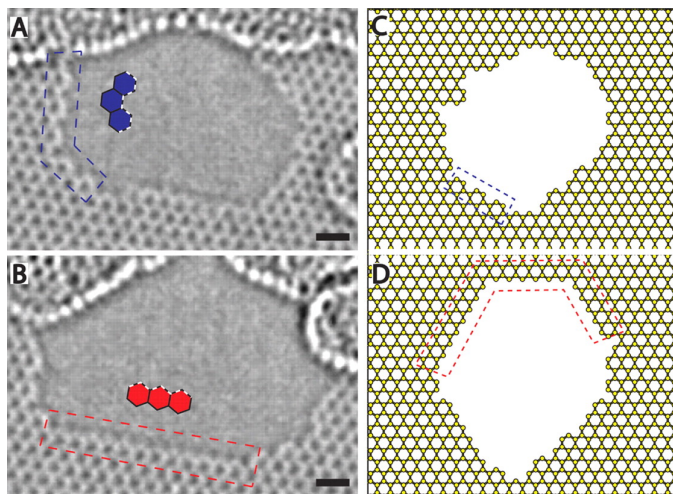


Figure 2.5 Edge configurations. Aberration-corrected TEM image of (A) an armchair and (B) zigzag configuration of carbon atoms at the edge of a hole in graphene. Examples of the emergence of long-range order in the simulation of hole growth are (C), with a 7-hexagon armchair segment at the edge of the simulated hole and (D), an extremely long (19 hexagon) zigzag edge interrupted by two 60° turns.^[60] "From ref. 60. Reprinted with permission from AAAS."

In graphene one of the most occurring types of defects are edge defects. As said above, the simplest edge structures are the armchair and the zigzag orientation. Raman spectroscopy is a sensitive tool to probe the nature of graphene edges. It was suggested^[61] that perfectly armchair or zigzag edges are routinely obtained when exfoliating graphene, even though they appear to follow defined directions on a large scale.

Throughout the nearly one century of Raman spectroscopy that has been used to study the science of sp^2 carbon materials, more and more fundamental aspects of their electronic and vibrational properties have been revealed.^[62] Raman spectra were first reported^[63] from single crystals of graphite and other graphitic materials, showing one single peak at 1575 cm^{-1} . For materials like commercial graphite, activated charcoal, lampblack, and vitreous carbon, another line is detected at 1355 cm^{-1} . The Raman intensity of this band is inversely proportional to the crystallite size and is caused by a breakdown of the k -selection rule.^[63] Raman fingerprints for single-, bilayer, and few-layer graphene reflect changes in the

electronic structure and electron-phonon interactions and allow unambiguous, high-throughput, nondestructive identification of graphene layers.^[34,64] In some samples, Raman mapping with circular polarization shows no significant dependence of the defect peak intensity on the macroscopic edge orientation. This indicates that edges can be mixed and disordered at least on the laser spot scale even though they follow well-defined crystallographic directions at a larger scale.^[61]

From the experimental side, near-field optics can now unravel Raman spectra with spatial resolution below the diffraction limit, a former limitation for Raman spectroscopy. The technique combined with a scanning probe microscopy setup (so-called apertureless near-field optical microscopy), and in particular combined with tip-enhanced Raman spectroscopy (TERS) and imaging/mapping (TERM), allows detection of features or defects with lateral resolution in the nanometer range. TERS uses a metallic (usually silver-/gold-coated AFM or STM) tip to enhance the Raman signals of molecules situated in its vicinity. It was demonstrated that TERS on carbon nanotubes samples provides high enhancement factors of the peak intensity. In case of SWCNT, TERS imaging with lateral resolution far better than 50 nm and enhancement factors for different vibrational modes of up to $\sim 10^5$ were obtained.^[65,66] Details of the technique and its applications for characterization of graphene sheets are described in Chapter 5 of this thesis.

SEM can give qualitative insight into the three-dimensional structure of graphene sheets and their organization inside a polymer matrix.^[30,67]

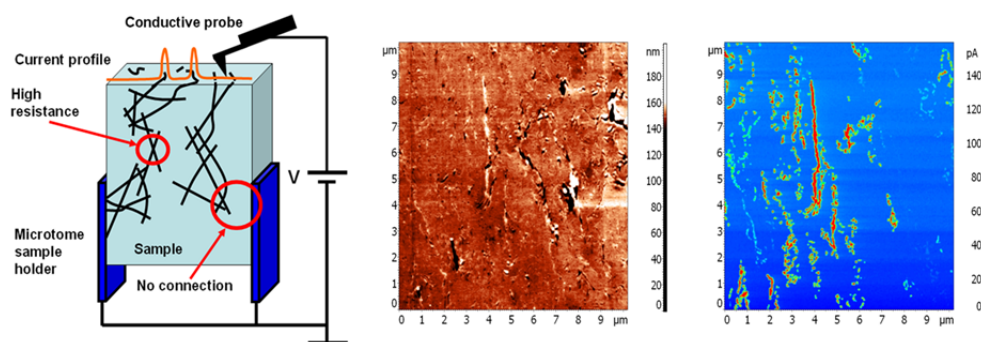


Figure 2.6 C-AFM technique setup (left) and images of the PS/graphene samples containing 1.9 wt.% graphene obtained in topography (middle), and as electrical current distribution image (right), showing the graphene platelets that are connected with the ground electrode.

The local organization of graphene sheets in conductive graphene/PS nanocomposite and their conductivity distribution was also analyzed in our group with nanometer resolution by means of conductive atomic force microscopy (C-AFM).^[68] Using a conductive AFM probe, in our case a gold-coated silicon tip, the local electrical conductivity can be measured at exactly the same area of the specimen subsequent to the topography and phase contrast imaging. The C-AFM tip measures the current throughout the volume of the nanocomposite specimen at a given voltage which is running via the graphene network to the ground contacts. Only platelets that are connected with the ground contacts can be monitored, and the observed differences in current are determined by the intra-network graphene junctions with highest resistivity. Graphene contributing to sub-networks without connection to the ground contacts show no current. In this way, a current distribution image is obtained and the conductive platelets can be distinguished from the insulating polymer matrix (see Figure 2.6, left). Figure 2.6 shows that most of the bright (white) areas, corresponding to graphene in the cross-section topographic image (middle), fit with the higher current level seen on the right mapping, indicating the presence of conductive pathways.

References

- [1] C. Lee, X. D. Wei, J. W. Kysar, J. Hone, *Science* **2008**, *321*, 385.
- [2] A. A. Balandin, S. Ghosh, W. Z. Bao, I. Calizo, D. Teweldebrhan, F. Miao, C. N. Lau, *Nano Lett.* **2008**, *8*, 902.
- [3] X. Du, I. Skachko, A. Barker, E. Y. Andrei, *Nat. Nanotechnol.* **2008**, *3*, 491.
- [4] K. S. Novoselov, D. Jiang, F. Schedin, T. J. Booth, V. V. Khotkevich, S. V. Morozov, A. K. Geim, *Proc. Natl. Acad. Sci. U. S. A.* **2005**, *102*, 10451.
- [5] K. S. Novoselov, A. K. Geim, S. V. Morozov, D. Jiang, Y. Zhang, S. V. Dubonos, I. V. Grigorieva, A. A. Firsov, *Science* **2004**, *306*, 666.
- [6] L. B. Gao, W. C. Ren, F. Li, H. M. Cheng, *ACS Nano* **2008**, *2*, 1625.
- [7] Z. H. Ni, H. M. Wang, J. Kasim, H. M. Fan, T. Yu, Y. H. Wu, Y. P. Feng, Z. X. Shen, *Nano Lett.* **2007**, *7*, 2758.
- [8] Y. B. Zhang, J. P. Small, W. V. Pontius, P. Kim, *Appl. Phys. Lett.* **2005**, *86*.
- [9] L. X. Li, R. P. Liu, Z. W. Chen, Q. Wang, M. Z. Ma, Q. Jing, G. Li, Y. Tian, *Carbon* **2006**, *44*, 1544.
- [10] Y. Hernandez, V. Nicolosi, M. Lotya, F. M. Blighe, Z. Y. Sun, S. De, I. T. McGovern, B. Holland, M. Byrne, Y. K. Gun'ko, J. J. Boland, P. Niraj, G.

- Duesberg, S. Krishnamurthy, R. Goodhue, J. Hutchison, V. Scardaci, A. C. Ferrari, J. N. Coleman, *Nat. Nanotechnol.* **2008**, *3*, 563.
- [11] U. Khan, A. O'Neill, M. Lotya, S. De, J. N. Coleman, *Small* **2010**, *6*, 864.
- [12] A. A. Green, M. C. Hersam, *Nano Lett.* **2009**, *9*, 4031.
- [13] M. Lotya, P. J. King, U. Khan, S. De, J. N. Coleman, *ACS Nano* **2010**, *4*, 3155.
- [14] A. O'Neill, U. Khan, P. N. Nirmalraj, J. Boland, J. N. Coleman, *J. Phys. Chem. C* **2011**, *115*, 5422.
- [15] L. Staudenmaier, *Ber. Deut. Chem. Ges.* **1898**, *31*.
- [16] W. S. Hummers, R. E. Offeman, *J. Am. Chem. Soc.* **1958**, *80*, 1339.
- [17] S. Park, R. S. Ruoff, *Nat. Nanotechnol.* **2009**, *4*, 217.
- [18] A. Lerf, H. Y. He, M. Forster, J. Klinowski, *J. Phys. Chem. B* **1998**, *102*, 4477.
- [19] H. Y. He, J. Klinowski, M. Forster, A. Lerf, *Chem. Phys. Lett.* **1998**, *287*, 53.
- [20] W. W. Cai, R. D. Piner, F. J. Stadermann, S. Park, M. A. Shaibat, Y. Ishii, D. X. Yang, A. Velamakanni, S. J. An, M. Stoller, J. H. An, D. M. Chen, R. S. Ruoff, *Science* **2008**, *321*, 1815.
- [21] S. Stankovich, D. A. Dikin, R. D. Piner, K. A. Kohlhaas, A. Kleinhammes, Y. Jia, Y. Wu, S. T. Nguyen, R. S. Ruoff, *Carbon* **2007**, *45*, 1558.
- [22] J. R. Lomeda, C. D. Doyle, D. V. Kosynkin, W. F. Hwang, J. M. Tour, *J. Am. Chem. Soc.* **2008**, *130*, 16201.
- [23] V. C. Tung, M. J. Allen, Y. Yang, R. B. Kaner, *Nat. Nanotechnol.* **2009**, *4*, 25.
- [24] S. Stankovich, D. A. Dikin, G. H. B. Dommett, K. M. Kohlhaas, E. J. Zimney, E. A. Stach, R. D. Piner, S. T. Nguyen, R. S. Ruoff, *Nature* **2006**, *442*, 282.
- [25] G. X. Wang, J. Yang, J. Park, X. L. Gou, B. Wang, H. Liu, J. Yao, *J. Phys. Chem. C* **2008**, *112*, 8192.
- [26] Y. Si, E. T. Samulski, *Nano Lett.* **2008**, *8*, 1679.
- [27] R. Muszynski, B. Seger, P. V. Kamat, *J. Phys. Chem. C* **2008**, *112*, 5263.
- [28] S. Stankovich, R. D. Piner, X. Q. Chen, N. Q. Wu, S. T. Nguyen, R. S. Ruoff, *J. Mater. Chem.* **2006**, *16*, 155.
- [29] D. Li, M. B. Muller, S. Gilje, R. B. Kaner, G. G. Wallace, *Nat. Nanotechnol.* **2008**, *3*, 101.
- [30] M. J. McAllister, J. L. Li, D. H. Adamson, H. C. Schniepp, A. A. Abdala, J. Liu, M. Herrera-Alonso, D. L. Milius, R. Car, R. K. Prud'homme, I. A. Aksay, *Chem. Mater.* **2007**, *19*, 4396.
- [31] R. K. Prudhomme, I. A. Aksay, D. Adamson, A. Abdala, R. K. Prud'Homme, H. R. K. Prud, Prudhomme R K; Aksay I a; Univ Princeton, **2007**.

- [32] H. C. Schniepp, J. L. Li, M. J. McAllister, H. Sai, M. Herrera-Alonso, D. H. Adamson, R. K. Prud'homme, R. Car, D. A. Saville, I. A. Aksay, *J. Phys. Chem. B* **2006**, *110*, 8535.
- [33] P. Steurer, R. Wissert, R. Thomann, R. Mulhaupt, *Macromol. Rapid Commun.* **2009**, *30*, 316.
- [34] H. Kim, A. A. Abdala, C. W. Macosko, *Macromolecules* **2010**, *43*, 6515.
- [35] I. A. Aksay, S. Korkut, D. L. Milius, R. K. Prudhomme, R. K. Prud'Homme, Aksay I a; Milius D L, **2009**.
- [36] G. Che, B. B. Lakshmi, C. R. Martin, E. R. Fisher, R. S. Ruoff, in *Chem. Mater.*, Vol. 10, **1998**, pp. 260.
- [37] I. M. I. A.V. Eletskii, A.A. Knizhnik, D.N. Krasikov, *Phys. Usp.* **2011**, *54*, 233.
- [38] K. S. Kim, Y. Zhao, H. Jang, S. Y. Lee, J. M. Kim, K. S. Kim, J. H. Ahn, P. Kim, J. Y. Choi, B. H. Hong, *Nature* **2009**, *457*, 706.
- [39] X. S. Li, W. W. Cai, J. H. An, S. Kim, J. Nah, D. X. Yang, R. Piner, A. Velamakanni, I. Jung, E. Tutuc, S. K. Banerjee, L. Colombo, R. S. Ruoff, *Science* **2009**, *324*, 1312.
- [40] Q. K. Yu, J. Lian, S. Siriponglert, H. Li, Y. P. Chen, S. S. Pei, *Appl. Phys. Lett.* **2008**, *93*.
- [41] A. Reina, X. T. Jia, J. Ho, D. Nezich, H. B. Son, V. Bulovic, M. S. Dresselhaus, J. Kong, *Nano Lett.* **2009**, *9*, 30.
- [42] M. Eizenberg, J. M. Blakely, *Surf. Sci.* **1979**, *82*, 228.
- [43] M. Eizenberg, J. M. Blakely, *J. Chem. Phys.* **1979**, *71*, 3467.
- [44] J. C. Hamilton, J. M. Blakely, *Surf. Sci.* **1980**, *91*, 199.
- [45] S. Bae, H. Kim, Y. Lee, X. F. Xu, J. S. Park, Y. Zheng, J. Balakrishnan, T. Lei, H. R. Kim, Y. I. Song, Y. J. Kim, K. S. Kim, B. Ozyilmaz, J. H. Ahn, B. H. Hong, S. Iijima, *Nat. Nanotechnol.* **2010**, *5*, 574.
- [46] A. K. Geim, K. S. Novoselov, *Nat. Mater.* **2007**, *6*, 183.
- [47] C. Berger, Z. M. Song, T. B. Li, X. B. Li, A. Y. Ogbazghi, R. Feng, Z. T. Dai, A. N. Marchenkov, E. H. Conrad, P. N. First, W. A. de Heer, *J. Phys. Chem. B* **2004**, *108*, 19912.
- [48] C. Berger, Z. M. Song, X. B. Li, X. S. Wu, N. Brown, C. Naud, D. Mayou, T. B. Li, J. Hass, A. N. Marchenkov, E. H. Conrad, P. N. First, W. A. de Heer, *Science* **2006**, *312*, 1191.
- [49] K. V. Emtsev, A. Bostwick, K. Horn, J. Jobst, G. L. Kellogg, L. Ley, J. L. McChesney, T. Ohta, S. A. Reshanov, J. Rohrl, E. Rotenberg, A. K. Schmid, D. Waldmann, H. B. Weber, T. Seyller, *Nat. Mater.* **2009**, *8*, 203.
- [50] J. Hass, R. Feng, T. Li, X. Li, Z. Zong, W. A. de Heer, P. N. First, E. H. Conrad, C. A. Jeffrey, C. Berger, *Appl. Phys. Lett.* **2006**, *89*.

- [51] H. Hibino, H. Kageshima, F. Maeda, M. Nagase, Y. Kobayashi, H. Yamaguchi, *Physical Review B* **2008**, *77*, 075413
- [52] J. C. Meyer, A. K. Geim, M. I. Katsnelson, K. S. Novoselov, T. J. Booth, S. Roth, *Nature* **2007**, *446*, 60.
- [53] U. Stoeberl, U. Wurstbauer, W. Wegscheider, D. Weiss, J. Eroms, *Appl. Phys. Lett.* **2008**, *93*.
- [54] A. Fasolino, J. H. Los, M. I. Katsnelson, *Nat. Mater.* **2007**, *6*, 858.
- [55] L. Liu, S. Ryu, M. R. Tomasik, E. Stolyarova, N. Jung, M. S. Hybertsen, M. L. Steigerwald, L. E. Brus, G. W. Flynn, *Nano Lett.* **2008**, *8*, 1965.
- [56] C. H. Lui, L. Liu, K. F. Mak, G. W. Flynn, T. F. Heinz, *Nature* **2009**, *462*, 339.
- [57] L.-X. Dong, Q. Chen, *Front. Mater. Sci. China* **2010**, *4*, 45.
- [58] K. A. Mkhoyan, A. W. Contryman, J. Silcox, D. A. Stewart, G. Eda, C. Mattevi, S. Miller, M. Chhowalla, *Nano Lett.* **2009**, *9*, 1058.
- [59] Fujita, *J. Phys. Soc. Japan* **1996**, *65*.
- [60] C. O. Girit, J. C. Meyer, R. Erni, M. D. Rossell, C. Kisielowski, L. Yang, C.-H. Park, M. F. Crommie, M. L. Cohen, S. G. Louie, A. Zettl, *Science* **2009**, *323*, 1705.
- [61] C. Casiraghi, A. Hartschuh, H. Qian, S. Piscanec, C. Georgi, A. Fasoli, K. S. Novoselov, D. M. Basko, A. C. Ferrari, *Nano Lett.* **2009**, *9*, 1433.
- [62] M. S. Dresselhaus, A. Jorio, M. Hofmann, G. Dresselhaus, R. Saito, *Nano Lett.* **2010**, *10*, 751.
- [63] F. Tuinstra, J. L. Koenig, *J. Chem. Phys.* **1970**, *53*, 1126.
- [64] A. C. Ferrari, J. C. Meyer, V. Scardaci, C. Casiraghi, M. Lazzeri, F. Mauri, S. Piscanec, D. Jiang, K. S. Novoselov, S. Roth, A. K. Geim, *Phys. Rev. Lett.* **2006**, *97*.
- [65] A. Hartschuh, E. J. Sanchez, X. S. Xie, L. Novotny, *Phys. Rev. Lett.* **2003**, *90*.
- [66] G. G. Hoffmann, G. de With, J. Loos, *Macromol. Symp.* **2008**, *265*, 1.
- [67] J. Loos, A. Alexeev, N. Grossiord, C. E. Koning, O. Regev, *Ultramicroscopy* **2005**, *104*, 160.
- [68] E. Tkalya, M. Ghislandi, A. Alekseev, C. Koning, J. Loos, *J. Mater. Chem.* **2010**, *20*, 3035.

Electrical conductivity of compacts of graphene, multi-wall carbon nanotubes, carbon black, and graphite powder

The electrical conductivity of different carbon materials (multi-walled carbon nanotubes, graphene, carbon black and graphite), widely used as fillers in polymeric matrices, was studied using compacts produced by a paper preparation process and by powder compression. Powder pressing assays show that the bulk conductivity depends not only on the intrinsic material properties but is also strongly affected by the number of particle contacts and the packing density. Conductivities at high pressure (5 MPa) for the graphene, nanotube and carbon black show lower values ($\sim 10^2$ S/m) as compared to graphite ($\sim 10^3$ S/m). For nanotube, graphene and graphite particles, the conductive behavior during compaction is governed by mechanical particle arrangement/deformation mechanisms while for carbon black this behavior is mainly governed by the increasing particle contact area. The materials resulting from the paper preparation process for carbon black and graphite showed similar conductivity values as for the compacts, indicating a limited effect of the surfactant on the conductivity. The paper preparation process for the large surface area nanotube and graphene particles induces a highly preferred in-plane orientation, thereby yielding largely the single particle intrinsic conductivity for the in-plane direction, with values in the order of 10^3 S/m.

Part of the results presented in this chapter was published:

B. Marinho, M. Ghislandi, E. Tkalya, C. E. Koning, G. de With, *Powder Technology*, **2012**.

3.1 Introduction

The discovery of graphitic nanoparticles with exceptional electrical transport properties, like high conductivity and high charge mobility, has incredibly broadened the range of potential applications of this class of materials, thus unleashing a revolution in the electronic device industry. Two of the most important members of this new generation of materials are undoubtedly carbon nanotubes and graphene.^[1-6]

Particularly in composite science and technology, current studies have shown that the incorporation of these two materials into polymeric matrices is capable of enhancing the electrical conductivity of polymers by several orders of magnitude without compromising other important features, such as the mechanical and optical properties.^[7,8]

Perhaps the biggest challenge to be faced at this stage is how to manipulate these nanoparticles in order to bring effectively their remarkable electrical properties onto the macroscopic level. Since the conductivity of a composite is directly related to the formation of a conductive network through the polymer matrix,^[9,10] its understanding depends, at least partly, on the knowledge of the electrical behavior of the nanoparticles agglomerates, here called bulk powder.

Traditionally, due to its simplicity and reproducibility for many systems, the electrical behavior of both metallic and non-metallic powders is characterized by monitoring the electrical conductivity of these powders under compression.^[11-16] This method was also employed recently to study the electrical resistivity of carbon microtube compacts as a function of filament diameter and graphitization technique.^[17]

Recent studies with filtered dispersions of carbon nanotubes produced highly oriented films in which some of the favorable intrinsic features of these nanomaterials, such as their electronic and thermal transport properties, are duly reflected. These films, known as buckypapers, consist of paper-like structures in which the nanoparticles are joined together by van der Waals interactions and present promising materials for investigating their properties macroscopically, not only for the nanotubes^[18] but also for graphene.^[19] Similar structures can be made from other carbon fillers and we refer to these generically as “papers” or if a specific carbon filler such as graphene is used as “graphene paper”.

The electrical conductivity of a bulk powder is generally lower than that of the individual particles, since the interface between the particles offers extra resistance to charge transport. The expected pressure-conductivity dependence for a particle compact is

shown in Figure 3.1. The application of pressure increases the conductivity basically by enlarging the contact area between the particles; some elastic and plastic deformation also may happen. In the final stage, which corresponds to the theoretical maximum degree of compaction (i.e. in principle 100% relative density), single particle conductivity is generally not reached, since the contact effects cannot be completely eliminated.^[20,21]

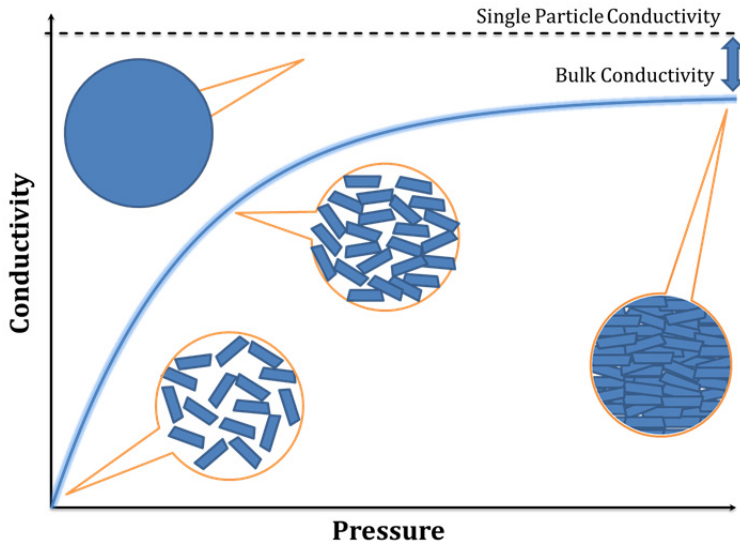


Figure 3.1 Schematic of the expected behavior of powder conductivity during compaction.

In this work, four different carbon fillers have been studied: multi-walled carbon nanotubes (MWCNTs), graphene, graphite and carbon black (CB). Except for CB, which consist of a mixture of sp^2 - and sp^3 -hybridized carbon atoms, all other materials are mainly formed from a sp^2 honeycomb network. Interpreting the conductivity of these materials is a challenging task. In literature their intrinsic conductivity was studied.^[2-7] The powder (bulk) and paper conductivity are measured, related to structure and intrinsic conductivity and their relevance in the field of composites processing technology is discussed.

3.2 Experimental

In order to study the electrical conductivity of carbon-based materials, two different processing conditions were applied. The first one consists of monitoring the electrical conductivity during the compaction of powders, whereas the second involves the preparation of paper films and measuring their conductivity. The conductivities of both compact and paper were studied as a function of the bulk density, defined by $\rho = m/Al$, where m is the mass of material, A is the area and l is the thickness of the specimen.

3.2.1 Materials

Purified long thin MWCNTs (*Nanocyl® 7000*, Nanocyl Belgium) were used. The tubes were produced according to the “Catalytic Carbon Vapor Deposition” method; carbon purity 90%. Graphene sheets (*SP-2 Bay Carbon*) used were obtained via graphite oxidation and a thermo-expansion process.^[22] XPS shows an amount of oxygen content around 15%, while TEM studies indicated at least 50% of single sheets.

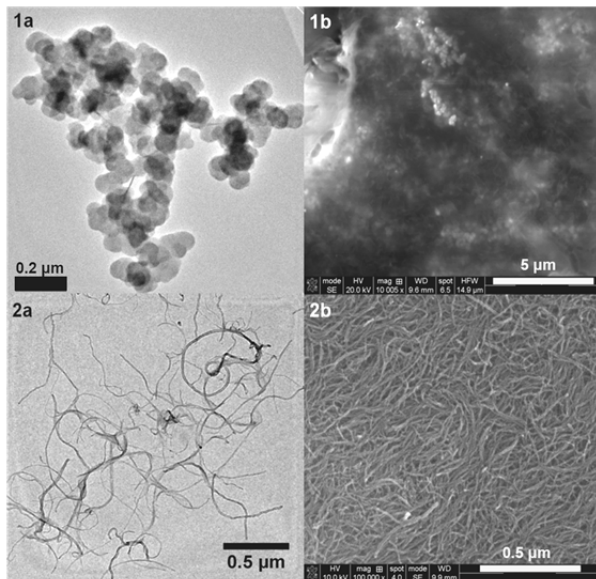


Figure 3.2 TEM images (left side) reveal the grape-like aggregation of CB spheres (1a) and a few multi-walled carbon nanotubes (2a). SEM images (right side) show the packing of CB in the paper-like structures (1b) and the boiled spaghetti organization of the tubes oriented in the surface direction (2b).

Electroconductive CB (*Ketjenblack® EC-600JD*, AkzoNobel) and synthetic graphite (*SP-2 Bay Carbon*, mesh size below 200), whose compaction behavior has already been extensively documented in literature^[11-16], were used for the sake of comparison and also to verify the reliability of the pressing device measurements. SEM and TEM characteristics are shown in Figure 3.2.

Nitrogen adsorption analysis (Micromeritics TriStar 3000) was employed for further morphological characterization of the powders. The samples were degassed for 12 h at 150 °C in vacuum. The surface area was calculated in accordance with the BET method.^[23]

3.2.2 Paper preparation

The aqueous filler dispersions were prepared with the surfactant polystyrene sodium sulfonate (PSS, Aldrich, $M_w = 70$ kg/mol). Initially, 0.08 g of filler was added to an 80 ml (100 ml flask) aqueous solution containing surfactant (PSS, ratio PSS/H₂O equal to 1/1). The dispersion was made via a sonication process, promoted by a horn sonicator (Sonic Vibracell VC750) with a cylindrical tip (10 mm end cap diameter) for 2 h. The output power was set to 20 W. For the purpose of controlling the temperature, the container with the mixture was immersed in a bath of ice during the sonication process. The quality of the dispersion was verified by monitoring the process via UV-Vis spectroscopy.^[24]

10 ml of the filler dispersion, prepared according to the previous procedure, was transferred into a filtration set-up containing a polyamide membrane with a pore size of 0.45 μm and then pressurized. As a result of the filler sedimentation, a smooth and black film was formed on the filter surface. In order to remove residual moisture, the films were dried at 90 °C under 200–400 mbar in a vacuum oven for 3 h.

The dc electrical resistance of the papers (and also of the powder compacts) for the in-plane (longitudinal) direction was measured via the four-point method. The electrical current was provided by a source-measure unit (Keithley 237), while the voltage was measured by an electrometer (Keithley 6517A). It should be emphasized that for each sample several values of the current were tested until the Ohmic range was established. For each value, six values of applied current I and their correspondent voltages V were registered and the resistance R was calculated from Ohm's law, i.e. from $R = V/I$. The

electrical contact between the sample and the equipment was done via four indented copper pins (3 cm length) pressed against four 1 cm long parallel silver paste lines painted on the surface of the paper, with an internal interval length l of 0.5 cm. The cross-section area A was obtained by multiplying the 1 cm long lines (corresponding to the width) with the thickness of the samples. The conductivity σ was then estimated according to $\sigma = l/AR$. For the measurements on the transversal direction the papers were cut (\varnothing 1.19 cm) and measured with the powder pressing setup according to procedure described in Section 3.2.3.

3.2.3 Powder pressing

The compression assays were performed in especially designed equipment, based on work described elsewhere,^[15] and schematically shown in Figure 3.3. The device consists of a thick isolating ceramic die (inner diameter 1.20 cm), vertically fixed on a heavy circular copper support containing a stationary piston (1.19 cm thick, 1 cm length) that closes the bottom of the cylinder. A close-fitting copper plunger (1.19 cm thick, 4 cm length), which is allowed to move down in the cylinder, closes the compression chamber. After filling the chamber with an accurately weighed amount of powder, the load applied on the piston was controlled by a universal testing machine (Lloyd EZ20), varying from 5 to 500 N, which resulted in a pressure range from 50 kPa to 5 MPa. Such a range, although apparently wide, proved to provide good electric contacts in the particle bed without damaging its structure.^[15]

The dc electrical resistance of the compressed powders (and also of the papers on the transversal direction) was measured via the four-point method. The electrical current was provided by a source-measure unit (Keithley 237), while the voltage was measured by an electrometer (Keithley 6517A). For each pressure, five values of the applied current and the corresponding voltages were registered and the resistance was calculated. The conductivity was then estimated according to $\sigma = l/AR$, where l represents the powder column height, obtained by the displacement of the piston and A is the cross-section area of the piston.

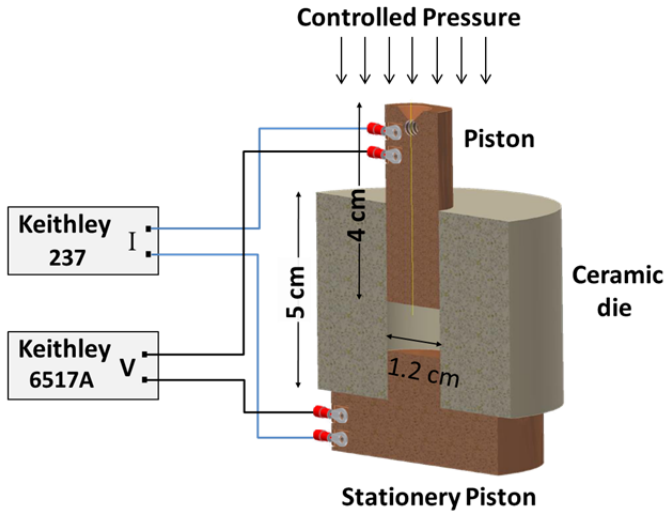


Figure 3.3 Schematic representation of the experimental setup involved in the measurement of the powder density and conductivity.

The electrical contact between the sample and the copper pistons was enhanced by polishing the two surfaces area of the metal exposed to the filler (1.13 cm^2) and direct pressing against the weighted amount of powder. No silver paint was necessary. The electrical resistivity of the apparatus itself (copper pistons in contact with each other plus cable contacts tightly screwed to the pistons) was verified and found to be lower than $10^{-6} \Omega \cdot \text{m}$, consequently not compromising the powder measurements. This measurement was done via a four-point method with the absence of powder; varying the pressure from 50 kPa to 5 MPa, with no change in resistance observed.

3.3 Results and discussion

3.3.1 Amount of powder for pressing

The amount of powder used to fill the die plays an essential role in the success of a compression experiment. Indeed a certain minimum number of particles are required in order to achieve representative results. Moreover, small amounts of material are more

susceptible to edge effects like particle orientation, since the proportion of material in contact with the piston and chamber walls is relatively high. On the other hand, a too large amount of material causes a less homogeneous pressure distribution, which unavoidably leads to density gradients, directly affecting the reliability of the experiment.^[15] Therefore, it is indispensable to determine a proper range of mass for each material before interpretation of the acquired data can be done reliably. Hence, preliminary pressing essays with different amounts of powder were performed and compared.

For small quantities of powder, the conductivity is extremely variable, suggesting that the previously discussed low-amount effects are present. From a certain value of the initial powder column height, though, the conductivity during compaction is no longer strongly dependent on the amount of material for every pressure, which means that the “homogeneity” conditions are met. In a certain range after this point, the conductivity measured proved to be insensitive to the amount of powder used. Hence a column height range where the conductivity value is stable was used in the measurements. This value is higher for graphite and CB (more than 6 mm) than for MWCNTs and graphene (about 3 mm), suggesting that for graphite and CB a smaller number of contacts is present as compared to MWCNTs and graphene. Based on this, the amount of powder material and initial column height selected for analyses were respectively: graphite, 0.75 g ± 0.001 and 9.9 mm ± 0.1; CB, 0.5 g ± 0.001 and 12.6 mm ± 0.1; MWCNTs 0.1 g ± 0.001 and 13.4 mm ± 0.1; Graphene, 0.1 g ± 0.001 and 16.8 mm ± 0.1.

3.3.2 Density versus pressure

Figure 3.4 shows the density as a function of pressure (ρ - P curve). The data shown are the average of three measurements, the results of which differ by no more than 3%.

As can be seen, the different fillers show similar densification–pressure behavior, namely a bi-linear dependence on the logarithmic pressure, as has been often noticed in the ceramic literature.^[25] This behavior can be interpreted as follows: The morphology of the carbon powders consists of agglomerates, built up from many primary particles. After filling the die, a loosely packed compact results with large voids between the agglomerates. In the low pressure region, densification is due mainly to rearrangement and fragmentation of relatively weak agglomerates controlled by particle–particle friction; no significant

change in internal agglomerate structure is expected. This behavior is represented by the first linear portion of each curve in Figure 3.4. At pressures exceeding a transition point, however, densification is mainly a result of compression (elastic/plastic deformation) of the agglomerates; the process is controlled by forces between the primary particles within the agglomerates. Densification will increase as a result of rearrangement and reduction of intra-agglomerate primary-particle distances (second linear portion of curves in Figure 3.4).

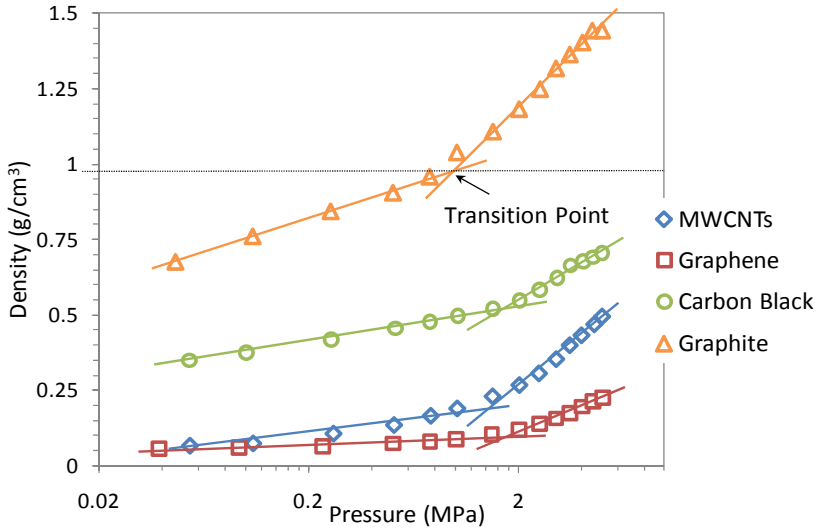


Figure 3.4 Density as a function of pressure (ρ - P curve) for the various powder compacts. Data are the average of 3 experiments with values varying less than 3%.

One of the few simple approaches, if not the only one, that takes these two processes explicitly into account is proposed by Cooper and Eaton.^[26] According to these authors, because of disordered packing of particles there is a distribution of the pressures necessary to fill the pores. A probabilistic approach to the problem therefore is desirable. The normalized volume fraction $V^* = (V_0 - V)/(V_0 - V_\infty)$, where V represents the actual volume and V_0 and V_∞ the initial and final volume, respectively, is a function of pressure that takes account to the several variables factors that determines the likelihood of holes being filled. Lacking detailed knowledge of these factors and assuming general statistical considerations, one may select a simple, which can be easily integrated, first-order kinetics for V^* in the reciprocal pressure for the filling of pores with one same size. That is $dV^* = -bV^*d(1/P)$ or $V^* = \exp(-b/P)$; a small value of the coefficient b , with units of pressure,

indicates an easier filling of pores. Generally however, we have a range of pore size and the effects of separate sizes add to $V^* = \sum a_i \exp(-b_i/P)$. To utilize the previous expressions for the compaction from individual processes, it is necessary to define fractional coefficients, where a_i defines the fraction of pores with characteristic b_i . The authors^[26] have considered only two classes of pores, the large pore distribution between the agglomerates and the small pore distribution between the particles within the agglomerate. Hence, their final relation reads

$$V^* = V_l^* + V_s^* = a_l e^{-b_l/P} + a_s e^{-b_s/P} \quad (3.1)$$

where a_l (a_s) and b_l (b_s) are constants related to large (small) pore contribution. The dimensionless coefficients a_l and a_s , indicate the fraction of theoretical compaction that would be achieved at infinite pressure by each particular process. Eq. (3.1) was used to fit the experimental data for the different carbon fillers and results are shown in Table 3.1.

Table 3.1 Fit parameters for volume fraction calculation.

<i>Filler</i>	a_l	b_l (MPa)	a_s	b_s (MPa)	RMSD
MWCNTs	0.749	0.130	0.275	1.537	0.012
Graphene	0.337	0.113	0.788	1.785	0.011
Carbon	0.440	0.089	0.465	2.845	0.010
Graphite	0.513	0.070	0.485	1.606	0.006

To illustrate the fit, Figure 3.5 shows the curves as obtained experimentally (V^*_{exp}) and as fitted (V^*_{calc}) for MWCNTs, the filler with the highest root mean square deviation (RMSD). V_l^* and V_s^* stand for volume fraction related to large and small pore contributions, respectively. Overall, the values for the RMSDs indicate an excellent fit with a maximum difference less than 5% and an average difference of about 1%. According to the Cooper-Eaton approach $a_l + a_s$ equals 1 when compaction can be completely described in terms of two separate processes, a condition reasonably well fulfilled for all materials (see

Table 3.1). Finally, we note that the transition point, as indicated in Table 3.3 for the data of Figure 3.4, corresponds with the pressure P_t where $dV_l^*/dP = dV_s^*/dP$ holds. For MWCNTs $P_t \cong 1.5$ MPa.

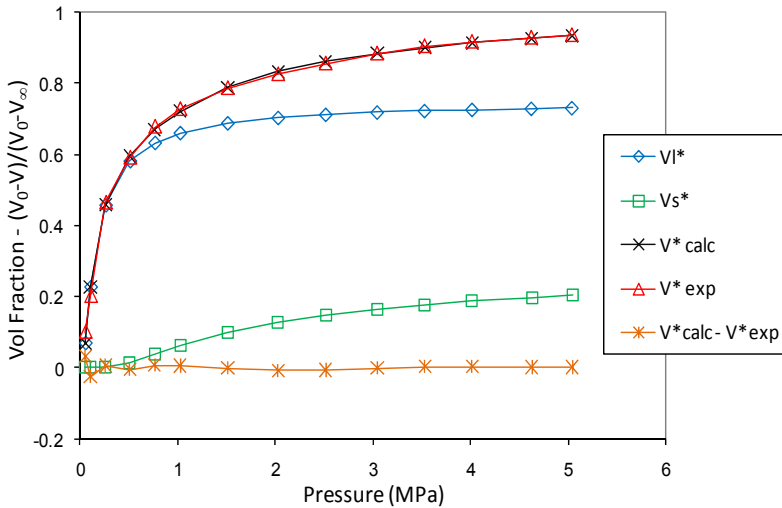


Figure 3.5 Normalized volume fraction as a function of pressure for MWCNTs using the Cooper-Eaton approach.

3.3.3 Conductivity versus pressure

Conductivity versus pressure data are shown in Figure 3.6. The data represent an average of three measurements, the results of which differ not more than 3%, indicating good reproducibility. A comparison of powder and paper conductivity is given in Table 3.2, together with data on specific surface area and intrinsic conductivity.

Surprisingly, the highly conductive single particles such as MWCNTs and graphene, when pressed together, exhibit lower conductivity values than graphite (see Table 3.2). Also the two processing methods, i.e. powder pressing and paper, generate different conductivity values (see Table 3.2).

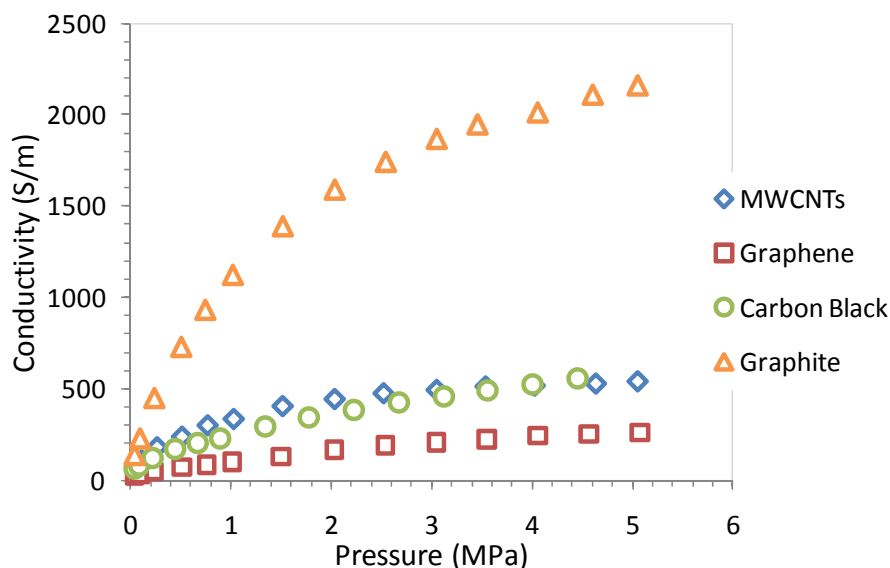


Figure 3.6 Electrical conductivity behavior of the different carbon powders as a function of pressure. For each material the data points represent an average of at least 3 identical assays differing not more than 3%.

Clearly the constriction of the current flow due to contact spots plays a major role when comparing the bulk conductivity of different powders. As expected, for none of the carbon materials the single particle conductivity was reached for the bulk materials, due to the impossibility of annulling the contact resistance effect. Interestingly, the conductivity of a single particle of carbon black differs by only a factor of 2, as compared with the conductivity obtained by powder pressing.

CB as used in this work can be considered as spherical agglomerates and hence the same kind of contacts in both powder and paper are expected. Indeed, the CB paper conductivity only shows a slightly lower conductivity value as compared to the powder pressed at the same density. A similar remark can be made for graphite, although here the difference is somewhat larger. Since the density is the same, this small decrease is probably caused by the remaining amount of surfactant. For nanotubes and graphene this difference reaches up to 5 and 6 orders of magnitude, respectively. This indicates that the contact resistance influence is far more pronounced for the nanoparticles (MWCNTs, graphene) than for the microparticles (graphite, carbon black) based structures.

Table 3.2 Material and compact characteristics.

<i>Filler</i>	<i>BET Surface Area (m²/g)</i>	<i>Conductivity (S/m)</i>			
		<i>Powder Compact at 5 MPa</i>	<i>Paper</i>	<i>Isolated Single Particle Conductivity</i>	<i>Filler contribution limit from compact*</i>
MWCNTs	272	5.43×10^2	5×10^3	10^6 - 10^7 ^a	10.3×10^3
Graphene	180	2.62×10^2	1.4×10^3	10^7 - 10^8 ^[2]	10.9×10^3
CB	56.9	5.58×10^2	9×10^1	10^3 ^[14]	8.8×10^3
Graphite	3.08	2.12×10^3	1.2×10^3	10^5 ^{[27]#}	13.8×10^3

* Estimation based on model.^[17] # Highly variable depending on source.

An increasing conductivity with increasing particle diameter was also observed for carbon filaments^[17] and has been attributed, among other reasons^[17], to the decreasing effect of contact resistance with increasing particle size. Due to the much higher surface area of the nanoparticles, as confirmed by BET, the number of contacts is much higher as compared to the microparticles for the same amount of material in the same volume. Table 3.2 also shows a simple calculation for the expected conductivity of the fillers in the compact utilizing a model described in literature^[17] based on the rule of mixtures and assuming a random geometric configuration of the fillers during compaction in 3D space. The contribution of filler conductivity σ_f in a compact is represented by $\sigma_f = 3\pi\sigma/2V_f^*$, where $3\pi/2$ is the geometric factor, σ is the powder compact conductivity at a pressure of 5 MPa and V_f^* the volume fraction of fillers at the same pressure. This equation represents the expected conductivity of the particles in the compacts assuming no contact resistance, and was used to estimate the high conductivity limits of carbon filaments from compacts. It provides a good indication of the achievable conductivity for the fillers, taking into account the different density states they present.

^a Nanocyl Company: <http://www.nanocyl.com/en/CNT-Expertise-Centre/Carbon-Nanotubes>

The conductivity and specific surface area do not show a straightforward relation, as others parameters like particle shape, interfacial forces between particles, electron transport mechanism and packing density, are also factors that influence the bulk conductivity. For the nanoparticles, although the paper density was not achieved for the powder compacts, the huge discrepancies as observed between the powder and the paper values suggest some preferred particle orientation, probably caused by their anisometric shape, as discussed in Section 3.3.5.

3.3.4 Conductivity versus density

Some further information can be extracted from the conductivity versus density behavior. We discuss first the results for CB and thereafter the other results. The variation of the conductivity σ of CB with the density is displayed in Figure 3.7.

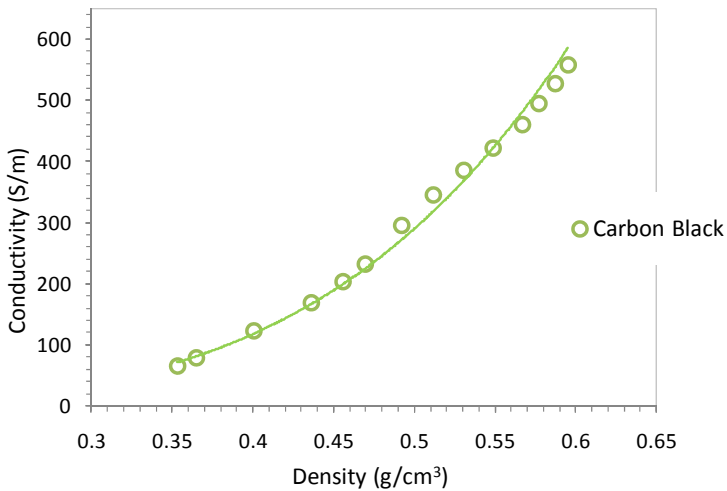


Figure 3.7 Conductivity σ of CB as a function of density ρ . The line represents the fit with $\sigma \approx \rho^4$ using the Kendall approach.

Due to its grape-like structure, packing of CB is often considered as an isotropic packing of spheres. Conductivity depends on the contact diameter between grains, and this can be calculated from the van der Waals attractive forces, knowing the size and elastic modulus of the particles.^[14,28] There is also a strong dependence on particle volume

fraction ϕ and this has been modeled by a ϕ^4 relation,^[29] resulting from a generalization of equations as derived for equal-sized spheres packed in various lattice types.^[30] This reasoning led to^[14]

$$\sigma = 40.6\sigma_*\phi^4 \left[\frac{\Gamma(1-\nu^2)}{ED} \right]^{1/3} \quad (3.2)$$

for the electrical conductivity σ , with D the particle diameter, E the Young's modulus, ν Poisson's ratio, σ_* the single particle conductivity, 40.6 a constant related to packing, and Γ the interface energy of the contact surface between the particles. This equation was successfully used to fit conductivity versus density for CB^[14] as well as Ti₄O₇, TiN and TiB₂^[28] powders.

Regression of experimental data according to Eq. (3.2) results in $\sigma = 4768\rho^{4.0}$, with a correlation coefficient of 0.995. From the fit results using the reference values for CB $E = 24 \text{ GPa}$ ^[14], $\nu = 0.3$, $\sigma_* = 4000 \text{ S/m}$ ^[14], $\rho = 0.80 \text{ g/cm}^3$ ^[15] and estimating $D = 100 \text{ nm}$ from SEM images (fig 3.1), the interface energy was found to be 4.6 mJ/m^2 . This value is in reasonable agreement with the 6 mJ/m^2 obtained by Kendall,^[14] taking into account that the results are sensitive to small changes in conductivity and density and are carried out on different equipments and probably using different CB powders.^[12,15]

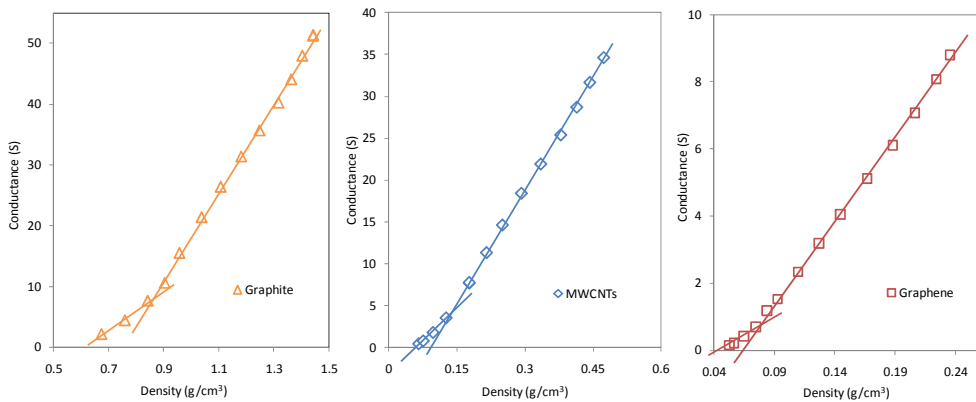


Figure 3.8 Conductance of the various powders as a function of density.

Note that the particle size as estimated from the specific surface area, 130 nm, differs slightly from the SEM estimate, 100 nm. This is probably due to the experimental uncertainty for the SEM measurements due to the limited number of particles analyzed.

Also note that for CB there is no clear transition point in the ρ - σ curve, like it was observed for the ρ - P curve. This indicates that the conductive behavior is not directly influenced by the mechanisms controlling compaction, i.e. initial rearrangement/fragmentation followed by elastic/plastic deformation of the agglomerates. Good conductive contacts are established in the initial low density regime even before deformation. This might be related to local plastic deformation at the contact points long before overall plastic deformation takes place, as shown by the ρ - P curve.

For the other materials, a plot of conductance G versus density ρ suggests a bi-linear relationship (Figure 3.8). For these materials with anisometric particles one can clearly identify a transition point (Table 3.3), as described before, being interpreted as agglomerate rearrangement/fragmentation for the low density, and elastic/plastic deformation for the high density part. These two mechanisms have a direct influence on the conductance behavior of these particles.

Table 3.3 Density transition points according to mechanical and electrical characterization.

Filler	Density Transition Points(g/cm ³)		Fit parameters for Holm equation		
	ρ - P curve (Figure 3.4)	G - ρ curve (Figure 3.8)	α	β	RMSD
Graphite	0.97	0.87	1182.4	0.38	43.47
MWCNTs	0.19	0.14	348.6	0.29	15.43
Graphene	0.10	0.08	108.5	0.57	6.62

An interesting point observed for all three materials is a small shift of the transition points to lower density values, when we compare values extracted from the ρ - P curve (Figure 3.3) and values extracted from the ρ - G curve (Figure 3.8), respectively (Table 3.3). This shift indicates that good contact or a higher number of electrical contacts starts to form a bit before the starting of the deformation/fracture regime. The assumption that good contact can be established already during rearrangement can rationalize this shift.

Holm^[20] proposed a relation between conductivity σ and pressure P based on an increasing contact area between particles upon increasing the pressure, which reads:

$$\sigma = \alpha P^\beta \quad (3.3)$$

with α and β constants. The value for β is predicted to be 0.5 for elastic contact and 0.33 for plastic contact. This equation was used to fit the experimental data shown in Figure 3.4 above the transition point and the results are also given in Table 3.3. The low values for the RMSDs (maximum difference below 10% and average difference below 1%) indicate the good fits. While the β -value for graphene is close to 0.5, the β -values for graphite and MWCNTs are closer to 0.33, indicating the difference in deformation behavior. Interestingly, the behavior of the CB could also be fitted well with the Holm equation. The β -value of about 0.5 indicates primarily elastic contact, in agreement with Kendall.

3.3.5 Orientation dependence

In order to detect preferred particle orientation, the conductivity of both the powder compacts and papers were measured for the surface (in-plane) direction and also for the transverse (through-the-sample) direction (see Figure 3.9). The in-plane conductivity was measured following the procedure described in section 3.3.2 and the transverse one directly in the pressing device. The compacts of MWCNTs and graphene result from pressing these powders into tablets at 5 MPa during 2 h. Three samples of each material were produced, with a variation in conductivity lower than 3% for the transverse direction and lower than 10% for the in-plane direction.

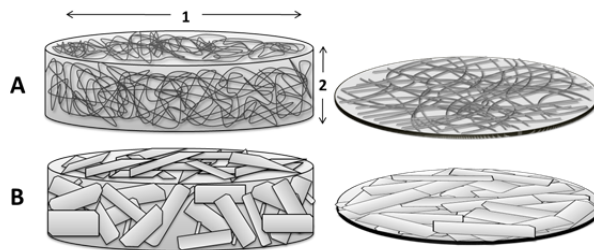


Figure 3.9 Carbon nanotubes (A) and graphene sheets (B) organized into compacts (left) and papers (right). Conductivity was measured for the in-plane (1) and transverse (2) directions.

The papers of MWCNTs and graphene were prepared according to the procedure described in Section 3.2.2 after which the filter membrane was removed. Three samples (10 mg each) were prepared from each material, with a variation of less than 10% in conductivity for the in-plane measurement direction and less than 5% for the transverse one. The results obtained are shown in Table 3.4. The in-plane (σ_{\parallel}) and transverse (σ_{\perp}) conductivities are similar for the powder compacts, whereas for the papers a huge difference (four to five orders of magnitude) in conductivity was observed. The average areal density was found 0.0024 g/cm² for graphene paper and 0.0027 g/cm² for MWCNTs paper; the average thickness t is shown in Table 3.4.

Table 3.4 Thickness, average in-plane and transverse conductivities for powder compacts and papers of MWCNTs and graphene.

Filler	Type	t (mm)	σ_{\parallel} (S/m)	σ_{\perp} (S/m)
MWCNTs	Compact	1.32	3.4×10^2	5×10^2
	Paper	0.045	5×10^3	1.4×10^{-2}
Graphene	Compact	1.10	1.3×10^2	2.7×10^2
	Paper	0.03	1.4×10^3	1.6×10^{-1}

Even high mechanical loading was not able to alter significantly the random character of the particle arrangements in the powder compacts. It was thus assumed that the carbon nanotubes still find themselves entangled in a “boiled spaghetti-like” structure, and that graphene sheets, besides disoriented, are mostly folded. On the other hand, the huge difference between the conductivity for the in-plane and transverse directions for the papers suggests that a high in-plane orientation of the particles is achieved during paper formation. Dispersion plus sonication promotes the exfoliation to individual particles, which are initially aggregated in bundles, and therefore the alignment of the nanotubes and the unfolding of the graphene sheets. The slow process of vacuum filtration gives the individual particles time to sediment and organize, forming a well-oriented film. This was also visualized by SEM analyses of the graphene fillers, as shown in Figure 3.10.

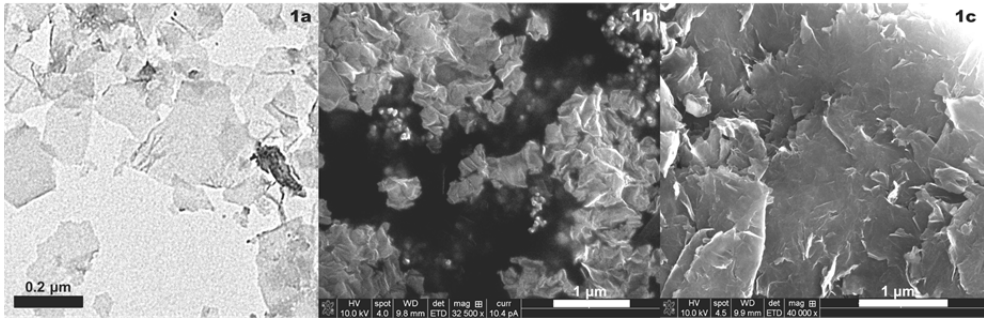


Figure 3.10 TEM image of isolated folded and unfolded graphene sheets after exfoliation/dispersion (8a), SEM image showing the highly entangled structure of wrapped graphene platelets, as observed in both powder and compacts (8b), and SEM surface image of in-plane oriented graphene platelets in paper-like structures (8c).

It has to be noted that since the papers are around 300 times thinner than their corresponding compacts, direct comparison is not straightforward. Apart from the relative ease of sedimentation/organization for the papers, a thicker sample usually contains less orientated particles since displacement/reorientation of particles during compaction is more hampered. Finally, in spite of the consistent conductivity–pressure behavior as observed for the compacts, density gradients may play a role.

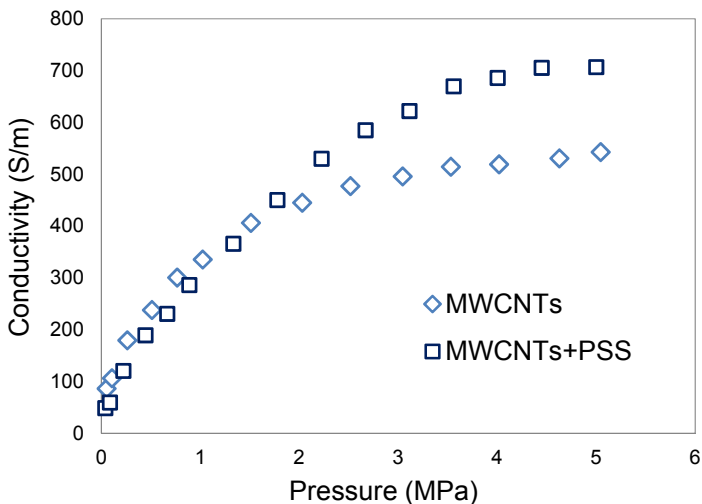


Figure 3.11 Electrical conductivity behavior of MWCNTs powders, with and without surfactant present, as a function of pressure. For each material the data points represent an average of at least 3 identical assays differing not more than 3%.

It was already noted that the influence of the surfactant, adsorbed on the filler and possibly hampering electronic transport, was negligible for compacts of the spherical CB particles. It is impossible to produce proper papers from aqueous nanofiller dispersions without the use of surfactants, as they are required to realize stable dispersions in water and proper filtering in order to obtain homogeneous paper films. Alternatively, we measured the conductivity during powder compaction using a powder with the same surfactant/filler ratio as used for the paper preparation and compared the results with results obtained for pure MWCNTs. The curves, shown in Figure 3.11, confirm that a difference of around 25% is measured at higher pressures, which is negligible as compared to the orders of magnitude difference observed for the other systems studied.

3.4 Conclusions

We studied four forms of carbonaceous materials: MWCNTs, graphene, graphite and CB. The differences in their electrical behavior, as observed using powder compaction and paper formation, reflect their distinct morphologies.

With powder compaction for all the materials, the bulk conductivity depends basically on the packing density. In a first pressing stage, the density is controlled by rearrangement and fragmentation of agglomerates, followed by a second regime where the elastic and plastic deformation determines the density. The conductive behavior is directly governed by these two mechanisms for the materials with anisometric particles, i.e. graphite, MWCNTs and graphene. For carbon black the relation is not straight forward and good conductive contacts are already formed at relative low density, below 0.5 g/cm^3 , before overall deformation.

In the case of MWCNTs and graphene, on top of the packing density influence described above, the orientation of the fillers proved to influence the bulk conductivity behavior significantly. For these materials, which consist of anisometric nanoparticles with high surface area, powder pressing conductivity curves showed unexpected low values, almost ten times lower as compared to graphite, probably due to the high number of particle contacts, which diminish the overall bulk conductivity measured on a macroscopic scale. On the other hand, papers produced with these materials largely preserved their intrinsic conductive properties for the in-plane direction, reaching a maximum of around

5×10^3 S/m for the MWCNTs. This processing method is therefore useful for the sake of comparison when developing new synthesis routes for carbon-based composites. Comparison of results for powder compacts with and without using surfactant, necessary to obtain good papers, showed that the influence of the surfactant on the conductivity is negligible.

The fact that (relatively) high bulk conductivity can be reached with (relatively) low intrinsic conductivity materials using random structures as in powder compacts, indicates that optimal processing is of the utmost importance. The successful fitting achieved for powder pressing assays shows that this method can clarify the influence of different compaction mechanisms on the final conductivity. Its high reproducibility, in addition to its simplicity and low cost, make powder pressing suitable for processing control of filler production.

References

- [1] Y. Gogotsi, *Nanomaterials handbook*, CRC/Taylor & Francis, **2006**.
- [2] J.-H. Chen, C. Jang, S. Xiao, M. Ishigami, M. S. Fuhrer, *Nat. Nanotechnol.* **2008**, 3, 206.
- [3] A. K. Geim, *Science* **2009**, 324, 1530.
- [4] C. Li, E. T. Thostenson, T.-W. Chou, *Compos. Sci. Technol.* **2008**, 68, 1227.
- [5] K. S. Novoselov, A. K. Geim, S. V. Morozov, D. Jiang, Y. Zhang, S. V. Dubonos, I. V. Grigorieva, A. A. Firsov, *Science* **2004**, 306, 666.
- [6] S. Iijima, *Nature* **1991**, 354, 56.
- [7] M. Moniruzzaman, K. Winey, *Macromolecules* **2006**, 39, 5194.
- [8] S. Stankovich, D. A. Dikin, G. H. B. Dommett, K. M. Kohlhaas, E. J. Zimney, E. A. Stach, R. D. Piner, S. T. Nguyen, R. S. Ruoff, *Nature* **2006**, 442, 282.
- [9] E. Tkalya, M. Ghislandi, A. Alekseev, C. Koning, J. Loos, *J. Mater. Chem.* **2010**, 20, 3035.
- [10] J. Yu, K. Lu, E. Sourty, N. Grossiord, C. E. Konine, J. Loos, *Carbon* **2007**, 45, 2897.
- [11] T. Noda, H. Kato, T. Takasu, A. Okura, M. Inagaki, *Bull. Chem. Soc. Jpn.* **1966**, 39, 829.
- [12] K. J. Euler, R. Kirchhof, H. Metzendorf, *J. Mater. Chem.* **1979**, 4, 611.

- [13] A. Espinola, P. M. Miguel, M. R. Salles, A. R. Pinto, *Carbon* **1986**, *24*, 337.
- [14] K. Kendall, *J. Phys. D: Appl. Phys* **1990**, *23*, 1329.
- [15] A. Celzard, J. F. Mareche, F. Payot, G. Furdin, *Carbon* **2002**, *40*, 2801.
- [16] X. P. Shui, D. D. L. Chung, *J. Mater. Sci.* **2000**, *35*, 1773.
- [17] X. P. Shui, D. D. L. Chung, *Carbon* **2001**, *39*, 1717.
- [18] M. Endo, H. Muramatsu, T. Hayashi, Y. A. Kim, M. Terrones, N. S. Dresselhaus, *Nature* **2005**, *433*, 476.
- [19] D. A. Dikin, S. Stankovich, E. J. Zimney, R. D. Piner, G. H. B. Dommett, G. Evmenenko, S. T. Nguyen, R. S. Ruoff, *Nature* **2007**, *448*, 457.
- [20] R. Holm, *Electric contacts: theory and applications*, Springer, **1999**.
- [21] K. V. Braunovic M, Myshkin N. , *Electrical Contacts: Fundamentals, Application and Technology*, CRC Press, **2007**.
- [22] M. J. McAllister, J.-L. Li, D. H. Adamson, H. C. Schniepp, A. A. Abdala, J. Liu, M. Herrera-Alonso, D. L. Milius, R. Car, R. K. Prud'homme, I. A. Aksay, *Chem. Mater.* **2007**, *19*, 4396.
- [23] P. C. Hiemenz, R. Rajagopalan, *Principles of colloid and surface chemistry*, Marcel Dekker, **1997**.
- [24] N. Grossiord, J. Loos, O. Regev, C. E. Koning, *Chem. Mater.* **2006**, *18*, 1089.
- [25] M. A. C. G. van de Graaf, J. H. H. ter Maat, A. J. Burggraaf, *Ceramic Powders*, Elsevier **1983**, 783.
- [26] A. R. Cooper, L. E. Eaton, *J. Am. Ceram. Soc.* **1962**, *45*, 97.
- [27] D. E. Gray, *American Institute of Physics handbook* McGraw-Hill, **1972**.
- [28] K. Kendall, *Powder Technol.* **1990**, *62*, 147.
- [29] K. Kendall, N. M. Alford, J. D. Birchall, *Proceedings of the Royal Society of London Series a-Mathematical Physical and Engineering Sciences* **1987**, *412*, 269.
- [30] B. J. Briscoe, M. J. Adams, *Tribology in particulate technology*, A. Hilger, **1987**.

Electrical conductivities of carbon powder nanofillers and their latex-based polymer composites

The electrical conductivity of graphene, multi-wall carbon nanotubes, carbon black nanopowders and graphite powder, characterized using paper-like films and by means of powder compression, is compared with the percolation threshold and final conductivity of polypropylene (PP) composites. The latex technology concept is used for the incorporation of the carbon fillers in the polymer. The fillers are first dispersed in water (assisted by surfactants) using ultra-sonication, subsequently mixed with PP latex, then freeze-dried and, finally, hot-pressed into composite tablets. PP composites produced in this work showed well-dispersed fillers inside the polymer, with percolation thresholds as low as 0.3 wt.%. The maximum conductivity obtained for the composites is approximately ~ 1 S/m, not reaching the high value of $\sim 10^3$ S/m, which are obtained for graphene and nanotube-based paper films or graphite compacts.

This chapter is based on:

M. Ghislandi, E. Tkalya, B. Marinho, C. E. Koning, G. de With, *Composites: Part A*, **2012** (submitted)

4.1 Introduction

Recent discoveries in the field of “graphitic” nanoparticles, in particular carbon nanotubes and graphene, have allowed the development of materials with exceptional electrical and mechanical properties.^[1-6] Graphite, the most abundant and stable form of carbon, exhibits properties which can be substantially enhanced by exfoliation of its layered structure into single or multilayer sheets.^[6,7] Carbon black, a common and well-studied nanofiller, also belongs to this class of carbonaceous materials, and is widely applied for electronic and reinforcement purposes.^[8,9] The above mentioned nano-scale powders are commonly incorporated into polymeric matrices to provide enhanced electrical, mechanical and thermal properties.^[10,11]

As mentioned in Chapter 3, since the conductive performance of a composite is directly related to the formation of a conducting network through the polymer matrix,^[12, 13] its understanding depends critically, on the knowledge of the electrical behavior of the agglomerated nanoparticles, e.g. in the form of a bulk powder or a paper film. Paper-like structures, known as “buckypapers”, in which the nanoparticles are joined together by van der Waals interactions, present promising materials for macroscopic investigations of their conductive properties, not only for the nanotubes^[14] but also for graphene.^[15] Similar structures can be made from other carbon fillers and we refer to these from now on as “buckypapers” or simply “papers”.

Conduction in carbon allotrope filled polymers (composites) results primarily either from the strong electric field effect between the conductive particles or from direct physical (Ohmic) contact. In the first case, processes such as tunneling, field emission and space charge limited transport need to be considered. In the latter case, when carbon particles are in direct contact, a continuous conducting network forms and the dependence between the current and voltage is of the Ohmic type.^[16] In composites of a non-conducting polymer with a conducting filler material, the conductivity often increases many orders of magnitude when the filler concentration becomes higher than a critical value, referred to as the percolation threshold. Above the percolation threshold, a continuous conducting path through the polymer exists.^[17-19]

For manufacturing of composites, latex technology has already been applied, e.g. for the incorporation of carbon nanotubes into a polymer matrix,^[12,20] or graphene in polystyrene.^[13] The latex approach facilitates the incorporation of nanofillers via liquid

phase mixing into any kind of highly viscous polymer which can be synthesized by emulsion polymerization or similar processes. This yields highly dispersed filler composites, that often have a low (~1 wt.% of filler content) electrical percolation threshold.^[21]

In this work, three different carbon nanofillers have been studied: multi-walled carbon nanotubes (MWCNTs), graphene, and carbon black (CB). Graphite was also used as reference filler for comparison. In order to study the electrical conductivity of the raw powders, two different characterization methods were used. The first one consists of monitoring the electrical conductivity during the compression of powders, whereas the second involves the preparation of paper films and subsequent electrical characterization. The relevance for the field of nanocomposites processing technology is discussed by comparing the powder and papers conductivities with the final conductivity and percolation threshold of the composite produced with these carbon fillers.

4.2 Experimental

4.2.1 Materials

MWCNTs, graphene, carbon black and synthetic graphite were the same as used and described in chapter 3. Sodium dodecylbenzenesulfonate (SDBS) (Aldrich, technical grade) surfactant was used as received. The latex was an anionic aqueous emulsion of maleic anhydride-modified polypropylene (PP) homopolymer Priex®801, containing 31-33 wt.% of solids. All dispersion experiments were carried out with distilled water.

4.2.2 Characterization

UV-Vis absorption spectra were recorded with a Hewlett-Packard 8453 spectrometer operating between 200 and 1100 nm. Samples were taken regularly during the sonicating process and diluted by a certain factor, resulting in certain filler contents that were suitable for UV-Vis measurements. As control (blank), the SDBS solution was diluted by the same factor and was measured under the same conditions as the samples themselves.

TEM images of the fillers were taken using a Technai 20 (Sphera, Fei Co.). The microscope was operated at 200 kV, with a LaB₆ filament, and a bottom mounted 1024 x 1024 Gatan CCD camera. A carbon-coated gold grid was used for deposition of samples. Composite films were also imaged using a XL30 ESEM (Fei Co.) equipped with a field emission electron source. High vacuum conditions were applied and a secondary electron detector was used for image acquisition. No additional sample treatment was applied before surface scanning.

4.2.3 Powder pressing

The compression assays were performed according to the method detailed in Chapter 3, Section 3.2.3, of this thesis.

4.2.4 Paper film and composite processing

CB and MWCNTs dispersions were prepared by mixing 0.06 g of each filler with 60 ml of an aqueous SDBS solution in a round flask (SDBS/filler ratio of 2/1) and subsequently sonicating the suspension for 50 min.^[12] Graphite and graphene filler dispersions were prepared identically, except for an increase sonication time to 2 h for further exfoliation of these fillers. All sonication processes were carried out with a horn sonicator (Sonic Vibracell VC750) with a cylindrical tip (13 mm end cap diameter). The output power was fixed at 25 W, thus delivering energy of 1300–1400 J/min. The flask was placed in an ice bath in order to prevent a temperature rise during sonication.

For paper film preparation, 10 ml of each filler dispersion was transferred into a filtration set up containing a polyamide membrane (pore size of 0.45 μm). The dispersion was then connected to a vacuum pump for pressurization. As a result of the filler's sedimentation, a smooth and black film was formed on the filter surface. In order to remove residual moisture, the films were dried at 90 °C in a vacuum (200–400 mbar) oven for 3 h.

For composite preparation, each dispersion was mixed with PP latex by stirring, to a final filler content between 0.1 wt.% and 10 wt.%. Each mixture was then frozen in liquid nitrogen for several minutes and the aqueous solvent was removed with a Christ Alpha 2–4 freeze dryer operated at 0.2 mbar and -50 °C for 48 h. The resulting composite powders were heated quickly to 140 °C and then for 20 min until 163 °C between Teflon sheets,

using a Collin Press 300G. Subsequently the heated material was compression molded into films of 0.5 to 1 mm thickness at 100 bar for 3 minutes, and then cooled at room temperature in air. Prior to final compression, the composite was degassed via 3 consecutive fast compressions for 20 seconds at 50 bar.

The electrical conductivity of paper and composites were measured using a standard four-point method. Parallel contact lines (on which the electrodes are placed) with 1 cm in length and with a 1 cm interval were drawn with conductive-silver paint (Fluka) on the composite film, and all conductivity measurements were performed at room temperature with a Keithley 6512 programmable electrometer. For each sample, conductivity data represent the average value of 10 consecutive measurements.

4.3 Results and Discussion

An initial morphological characterization of the nanofillers was carried out by TEM (Figure 4.1). The isolated round CB particles, on average 50 nm in diameter, agglomerate into grape like structures (Figure 4.1-a). The as-received MWCNTs are stacked in bundles, which can be exfoliated (Figure 4.1-b) to isolated tubes, which are 20-25 nm in diameter and several micrometers in length. The graphene sheets have an average surface area below $1 \mu\text{m}^2$ and are sometimes folded or stacked together. The folding and stacking are most likely a consequence of the manufacturing process by fast thermal expansion combined with drying phenomena during TEM sample preparation.

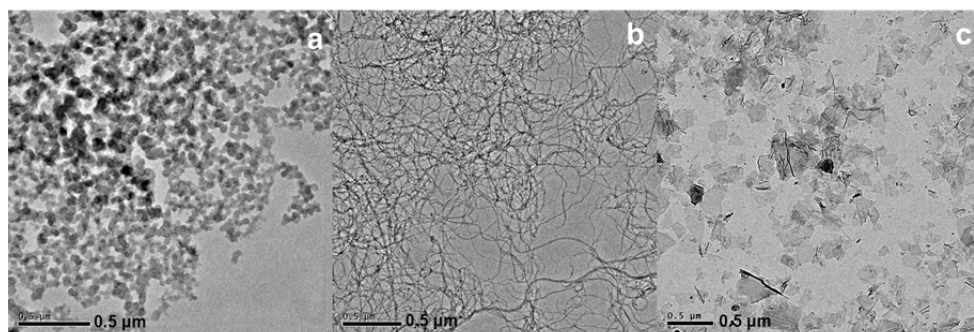


Figure 4.1 TEM images showing (a) the grape-like aggregates of CB spheres, (b) exfoliated multi-walled carbon nanotubes and (c) dispersed single and stacked graphene sheets.

4.3.1 Powder and paper conductivities

The amount of powder used to fill the die, together with detailed density vs. pressure and conductivity vs. density behaviors of the powders used in this work, were discussed in Chapter 3. A comparison of powder and paper conductivity values is also given in Chapter 3, Table 3.2, together with data on specific surface area and intrinsic single particle conductivity.

The conductivities of both powder and buckypaper are plotted (Figure 4.2) as a function of the bulk density ρ , $\rho = m/V$, where m is the mass of material, and V is the volume of the chamber at a certain pressure. As can be seen, the different fillers find themselves in different stages of compression, hampering direct conductivity comparison.

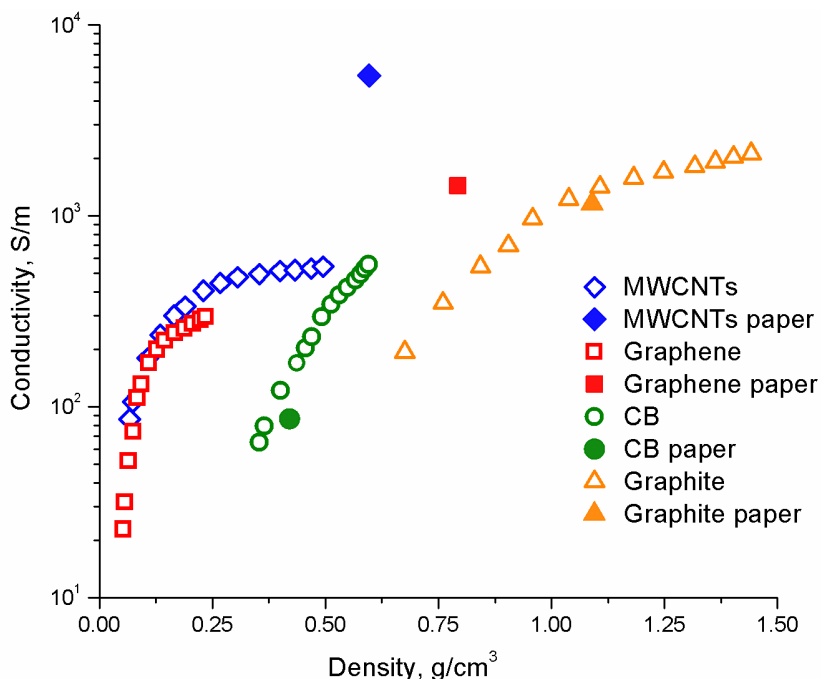


Figure 4.2 Electrical conductivity behavior of the different carbon powders as a function of density and conductivity value of paper-like structures. For each material the data points represent an average of at least 3 identical assays differing not more than 3%.

For graphite and carbon black, the buckypaper conductivity value practically fits in the powder curve. CB as employed in this work can be considered as an agglomerate of

primary spheres, and hence identical contacts in both powder and buckypaper are expected. At the same density, the slightly lower conductivity value obtained for CB buckypaper, in comparison with CB power compression curve is most likely caused by SDBS retained from film preparation. Nevertheless, the influence of SDBS is insignificant, considering the conductivity standard variations. In the case of MWCNTs and graphene, the buckypaper density was not achieved by the powder pressing even at maximum pressing load. Henceforth, large discrepancies are observed between the powder curves and the buckypaper values, which suggests that filler particles are preferentially oriented in papers on account of the paper preparation method combined with shape anisotropy of particles.

4.3.2 Polymer composite processing, conductivity and percolation threshold

In order to obtain the optimum dispersion conditions, the UV-Vis absorbance spectrum was monitored as a function of sonication time (Figure 4.3).

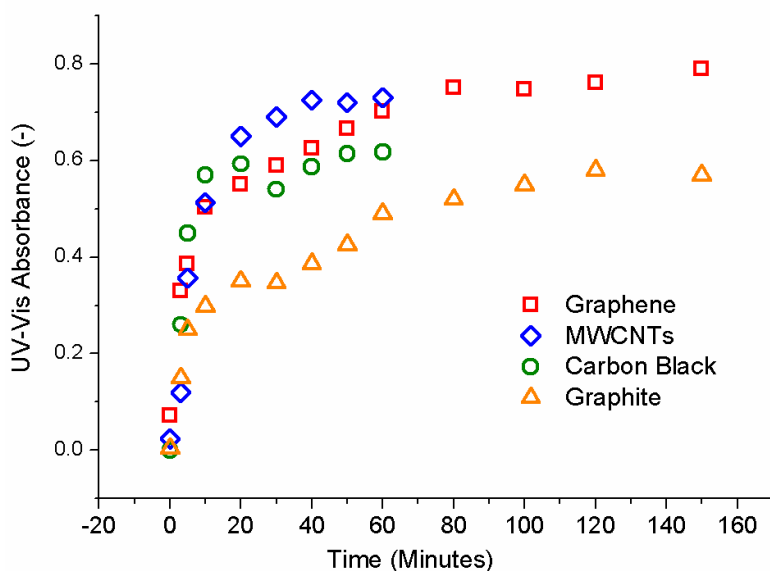


Figure 4.3 UV-Vis monitoring of the exfoliation process in water over time. Evolution of the height of the peak located around 268 nm for all aqueous 0.1 wt.% filler solutions (diluted 150 times).

For MWCNTs and CB, the maximum exfoliation seemed to be established faster, with the maximum absorbance reaching a plateau before 60 min of operation. The sonication

time was then set to 50 min, in agreement with studies reported previously by our group.^[12] For graphene and graphite, we noticed that a longer time was necessary for a maximum exfoliation, so a sonication time of 120 min was considered satisfactory for these two systems. It has to be pointed out that, even at longer sonication times, the maximum absorbance obtained for graphite is lower than for all other suspensions, indicating a poorer dispersibility of graphite in the water/SDBS system. The stability of graphite dispersion was also lower as compared to the others, showing settling after a few hours at rest. For graphene, MWCNTs, and CB the dispersions remained stable, without any visual settling, for up to a month. This factor, among others, might have an influence on the final organization of the filler inside the polymer matrix and, consequently, on the percolation threshold. We still considered it worth working with graphite for comparison.

SEM measurements obtained by charge contrast imaging confirm a homogeneously dispersed organization of the nanofillers inside the polymer matrix (Figure 4.4). Because of the differences in charge transport between the conductive fillers and the polymer matrix, the secondary electron emission is higher at the filler location. This results in the contrast between the filler network (bright) and the polymer matrix (dark). The poor charge contrast achieved for the CB composites images is a result of nano-dimensional and well-dispersed agglomerates. Graphene and nanotubes have at least one dimension in the micrometer range, allowing more efficient charge emission and consequently charge contrast.

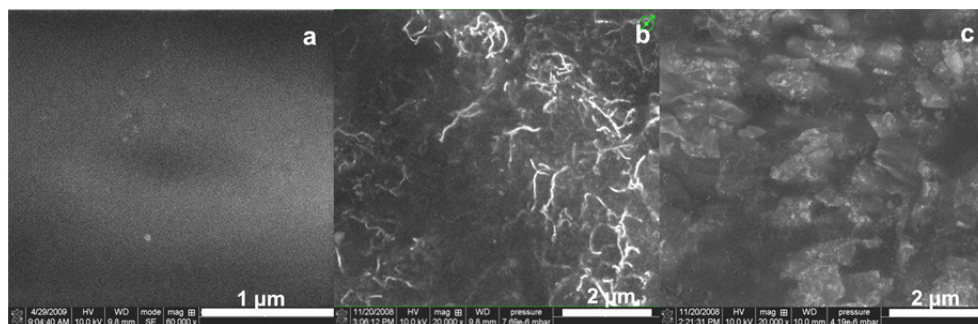


Figure 4.4 SEM images of (a) PP composite with barely visible CB at 5 wt.%, (b) the organization of the tubes inside the PP polymer composites and (c) the structure of partially wrapped graphene platelets inside the PP polymer matrix.

Figure 4.5 shows a comparison of the conductive percolation threshold and final conductivity obtained for the different composites. All the filler dispersions were mixed

with PP latex and processed following the same procedure. The maximum conductivity values are below 2 S/m, for all the samples. These values are much lower than the ones obtained for paper-like structures or powder compacts. As verified for powder compacts and paper samples, the conductivity is limited by filler-filler inter-particle contact resistance, with the addition of possible polymer/SDBS-filler contact resistance in the case of composites. If we apply the same voltage range for the composite samples (< 10 V) as used for conductivity measurements of paper films, we may induce an excessive current density passing through the fillers, causing power dissipation in the form of heat. For some composites samples, specially the most conductive ones, we observed initial burning or melting during conductivity measurements at current levels exceeding 10 mA.

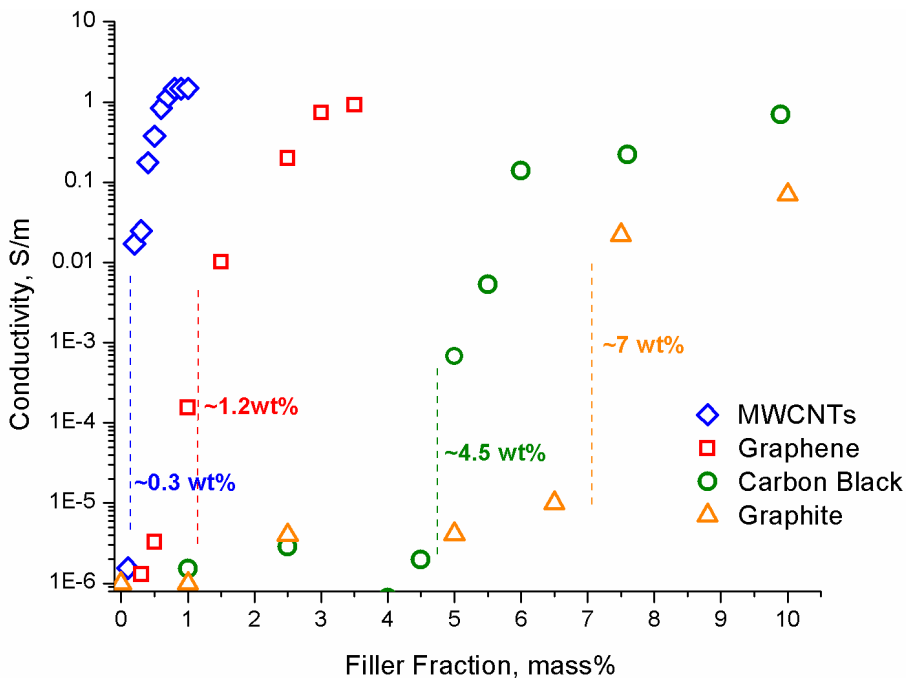


Figure 4.5 Percolation threshold of carbon composites prepared via latex technology. Electrical conductivity as a function of filler mass concentration. Values represent an average of 10 measurements; standard deviations are below 10%.

The amount of effective charge carriers (fillers) contributing to the overall conductivity (σ) is much lower for the composites (due to the much lower filler content in the same corresponding volume) than for powder compacts or paper films. If we consider e.g.

nanotubes composites with 1 wt.% of filler content, assuming that all the fillers are connected and contribute to the overall conductivity, we still have a total density of material, which effectively contributes to conductivity, 100 times lower than the intrinsic density attributed to the MWCNTs composite ($\sim 1 \text{ g/cm}^3$) at this filler content. This means that an effective density of $\sim 0.01 \text{ g/cm}^3$ for these composites is still much lower than the ones measured for powder compacts or paper films, hindering any direct comparison.

Table 4.1 Difference in conductivities for powder compacts and composites (above percolation threshold) at the same estimated effective density.

Filler type	Composite filler content (wt.%)	Effective composite ρ (g/cm^3)	Composite σ_{com} from Figure 4.2 (S/m)	Powder σ_{pow} at same ρ (S/m)	Factor $\sigma_{\text{com}}/\sigma_{\text{pow}}$ at same ρ
Graphite	7.5	0.075	0.07	0.01	0.2
	10.0	0.104	0.12	0.05	0.4
CB	5.0	0.047	0.00	0.01	15.0
	5.5	0.052	0.01	0.02	3.0
	6.0	0.057	0.14	0.02	0.2
	7.6	0.074	0.22	0.07	0.3
	9.9	0.098	0.70	0.24	0.3
MWCNTs	0.4	0.004	0.18	1.40	7.9
	0.5	0.005	0.38	1.92	5.1
	0.6	0.005	0.84	2.49	2.9
	0.7	0.006	1.16	3.10	2.6
	0.8	0.007	1.46	3.75	2.5
	0.9	0.008	1.42	4.44	3.1
	1.0	0.009	1.48	5.24	3.5
Graphene	1.5	0.014	0.01	0.26	25.8
	2.5	0.023	0.20	1.42	7.1
	3.0	0.028	0.74	2.77	3.7
	3.5	0.033	0.92	4.36	4.7

A bold extrapolation of the compact powder curves from Figure 4.2 was conducted in order to compare, at the same effective density (ρ), the conductivity with values obtained for composites. Using power equation trendlines to fit the initial part of each powder curve, and extrapolating the curve to extremely low density values, we can estimate the conductivity, for the same effective density range as obtained for composites. The formula used to estimate the effective density of the composite is simple. We multiplied, for each mixture, the volume fraction of the filler (vol.%), which we assume to effectively

contribute to the overall conductivity, by the real density of the filler. Hence, we have an effective density which can be directly compared with the results obtained for powder compact extrapolation curves. In Table 4.1 we verify that most of the extrapolated conductivities, obtained for powders at same densities as calculated for composites, satisfactorily match, with less than one order of magnitude difference, the low conductivities measured for the composites above the percolation threshold. Higher discrepancies were observed when comparing conductivities of composites that were still within the conductivity percolation range transition, namely the CB composites at 5 wt.% and graphene composite at 1.5 wt.%.

Interesting remarks can be made comparing powder compacts/papers and composites conductivities at the same (effective) density. First, the conductivity values for composites above the percolation threshold are in agreement with results obtained for powder compacts. This is a clear sign that for composites at low filler contents (1-5 wt.%) it is impossible to reach the high conductivities as obtained for powders in Figure 4.2, due to huge mismatch of effective densities. However, it is still possible to increase the ultimate composite conductivity by increasing the amount of filler content, following the trend observed for powders in fig 4.2. Of course this increase is gradual above the percolation, e.g., according to estimates, around 50 wt.% of graphene filler would be necessary to reach a conductivity of ~ 100 S/m in the final composite. We need to point out that this amount of filler content would have severe consequences in the state of filler dispersion and the mechanical properties of the composites prepared via latex technology. Second, as observed for powder compacts, composites with MWCNTs and graphene filler reach high conductivity values at much lower filler contents than CB or graphite composites. However, as for powders, the maximum conductivity might be limited for the former nanofillers composites by the impossibility of reaching high filler densities, also inside the composites.

We presume that the conductivities obtained for MWCNTs and graphene buckypapers would be difficult to reach for the composites, even at high filler loadings, also due to filler orientation issues. Composites are at least 10 times thicker than paper films, and exhibit a much lower filler concentration, so the fillers might orient in different planes, separated by the PP matrix, not touching each other. Annealing of the samples after powder pressing, allowing filler movements through the planes, was reported to improve the final

conductivity of carbon based composites.^[22-24] In this work, no difference in conductivity was observed for any composite after annealing at 100 °C for 5 h.

Overall, a much lower percolation threshold is observed for the nanocomposites of graphene and MWCNTs when compared to graphene and CB percolations. The higher surface areas and aspect ratios allow these composites to form a conductive network at much lower filler contents. It is important to mention that the state of dispersion during the preparation phase plays an important role. The successful exfoliation of the MWCNTs and homogeneous dispersion in the PP polymer using latex technology was confirmed, with composites exhibiting a percolation as low as 0.3 wt.%, a value that is lower than previous results reported using polystyrene (PS) latex.^[12] For graphene, the purity and dimensions (size and thickness) of the starting filler may influence this property. A percolation threshold as low as 0.9%, with a final conductivity of 15 S/m, was already reported,^[13] using similar preparation methods but different graphene and latex (PS) sources. The advantage of graphene over nanotubes may be the possible reduction of the percolation threshold by optimizations of filler properties (dimensions, purity, dispersibility) and processing conditions, added to potential lower production costs and superior gas barrier properties.

For the studied CB and graphite, the percolation threshold is much higher as compared to MWCNTs and graphene. The low surface area associated to low dispersibility in water may have shifted the percolation threshold to 4.5% for CB and at least 7% for graphite. Still these percolations are considerably lower than in other processing technologies.^[21] New techniques of long-term exfoliation of graphite, in water and organic solvents, using different surfactants have shown improved dispersibility^[25] with the drawback of low maximum concentration and reduced filler dimensions.

It is important to point out that the PP latex used in this work is semi-crystalline, so the effect of the filler or the cooling rate could alter the crystallinity of the polymer matrix and consequently have some influence on the conductivity of the composite. We kept the processing conditions identical for all the samples and assumed that any filler- induced nucleation, if present, was similar for all composites studied, not influencing significantly the conductivity comparison. A more detailed study on the crystallization behavior of PP/MWCNTs nanocomposites is presented elsewhere^[26] and was not the focus of this work.

4.4 Conclusions

MWCNTs, graphene, CB and graphite bulk powders exhibit different packing densities during compression and henceforth different macroscopic conductivities, even at high pressing loads up to 5 MPa. Moreover, powder compact conductivities never reach the intrinsic single particle conductivity value. For the nanoparticles graphene and MWCNTS, due to the much higher surface area and number of contacts in compacts, this difference reaches up to 5 and 6 orders of magnitude, respectively.

Well exfoliated water/SDBS/filler dispersions were produced with graphene, and MWCNTs; a CB dispersion presented a slightly lower exfoliation than the former two, whereas the dispersions obtained with graphite were poor and less stable than all the others. Smooth paper-like films, produced with graphene and MWCNTs dispersions, yielded macroscopic conductivity values ($\sim 10^3$ S/m) approximately one order of magnitude higher than those of powder compacts ($\sim 10^2$ S/m at 5 MPa), indicating that, for the former, even with the presence of surfactant, filler orientation, due to controlled dispersion and settling under pressure, helps to increase the apparent density and final conductivity of the bulk material.

Carbonaceous nanofiller/polypropylene composites exhibiting really low conductivity percolation thresholds were successfully produced using a latex technology process. A homogeneous distribution of the nanofillers inside the polymer matrix was confirmed by SEM. The conductivity measured for the composites show maximum values around 1 S/m, a value which is three orders of magnitude lower than the conductivity obtained for paper films (graphene and MWCNTs) or powder compacts (graphite). This maximum conductivity may be greatly limited by the amount and nature of conducting contact spots; most probably the contact resistance is increased by the presence of isolating polymer/SBDS covering the fillers. The amount of conductive paths per unit volume that effectively contribute to the overall conductivity is also much lower for the composites (due to the much lower filler content in the same corresponding volume) as compared to the amount of conductive paths in the powder compacts and paper samples. Nevertheless, the conductivity values for composites above the percolation threshold are in agreement with results obtained for powder compacts. This leads to a clear sign that for composites at low filler contents (1-5 wt.%) it is impossible to reach the high conductivities obtained for powders compacts, due to huge mismatch of effective densities of conductive fillers.

References

- [1] Y. Gogotsi, *Nanomaterials handbook*, CRC/Taylor & Francis, **2006**.
- [2] C. Li, E. T. Thostenson, T.-W. Chou, *Compos. Sci. Technol.* **2008**, *68*, 1227.
- [3] A. K. Geim, *Science* **2009**, *324*, 1530.
- [4] J.-H. Chen, C. Jang, S. Xiao, M. Ishigami, M. S. Fuhrer, *Nat. Nanotechnol.* **2008**, *3*, 206.
- [5] S. Iijima, *Nature* **1991**, *354*, 56.
- [6] K. S. Novoselov, A. K. Geim, S. V. Morozov, D. Jiang, Y. Zhang, S. V. Dubonos, I. V. Grigorieva, A. A. Firsov, *Science* **2004**, *306*, 666.
- [7] R. R. Nair, P. Blake, A. N. Grigorenko, K. S. Novoselov, T. J. Booth, T. Stauber, N. M. R. Peres, A. K. Geim, *Science* **2008**, *320*, 1308.
- [8] M. C. Lonergan, E. J. Severin, B. J. Doleman, S. A. Beaber, R. H. Grubb, N. S. Lewis, *Chem. Mater.* **1996**, *8*, 2298.
- [9] J. B. Donnet, in *Compos. Sci. Technol.*, Vol. 63, **2003**, pp. 1085.
- [10] M. Moniruzzaman, K. Winey, *Macromolecules* **2006**, *39*, 5194.
- [11] S. Stankovich, D. A. Dikin, G. H. B. Dommett, K. M. Kohlhaas, E. J. Zimney, E. A. Stach, R. D. Piner, S. T. Nguyen, R. S. Ruoff, *Nature* **2006**, *442*, 282.
- [12] J. Yu, K. Lu, E. Sourty, N. Grossiord, C. E. Koning, J. Loos, *Carbon* **2007**, *45*, 2897.
- [13] E. Tkalya, M. Ghislandi, A. Alekseev, C. Koning, J. Loos, *J. Mater. Chem.* **2010**, *20*, 3035.
- [14] M. Endo, H. Muramatsu, T. Hayashi, Y. A. Kim, M. Terrones, N. S. Dresselhaus, *Nature* **2005**, *433*, 476.
- [15] D. A. Dikin, S. Stankovich, E. J. Zimney, R. D. Piner, G. H. B. Dommett, G. Evmenenko, S. T. Nguyen, R. S. Ruoff, *Nature* **2007**, *448*, 457.
- [16] J. M. Margolis, *Conductive polymers and plastics*, Chapman and Hall, **1989**.
- [17] A. Bunde, S. Havlin, *Fractals and disordered systems*, Springer, **1996**.
- [18] S. Dietrich, A. Amnon, *Introduction to percolation theory*, Taylor & Francis, **1994**.
- [19] R. Viswanathan, M. B. Heaney, *Phys. Rev. Lett.* **1995**, *75*, 4433.
- [20] O. Regev, P. N. B. ElKati, J. Loos, C. E. Koning, *Advanced Materials* **2004**, *16*, 248.
- [21] N. Grossiord, J. Loos, C. E. Koning, *J. Mater. Chem.* **2005**, *15*, 2349.
- [22] S. H. Foulger, *J. Appl. Polym. Sci.* **1999**, *72*, 1573.
- [23] H. Deng, T. Skipa, R. Zhang, D. Lellinger, E. Bilotti, I. Alig, T. Peijs, *Polymer* **2009**, *50*, 3747.
- [24] H. Deng, E. Bilotti, R. Zhang, J. Loos, T. Peijs, *Synth. Met.* **2009**, *160*, 337.
- [25] A. O'Neill, U. Khan, P. N. Nirmalraj, J. Boland, J. N. Coleman, *J. Phys. Chem. C* **2011**, *115*, 5422.
- [26] H. E. Miltner, N. Grossiord, K. Lu, J. Loos, C. E. Koning, B. Van Mele, *Macromolecules* **2008**, *41*, 5753.

Tip-enhanced Raman spectroscopy and mapping of graphene sheets

Single graphene sheets, few graphene layers and bulk graphite, obtained via both micro-mechanical cleavage of highly oriented pyrolytic graphite and carbon vapor deposition methods, were deposited on a thin glass substrate without the use of any chemical treatment. Micro-Raman spectroscopy, tip-enhanced Raman spectroscopy (TERS) and tip-enhanced Raman spectroscopy mapping (TERM) were used for the characterization of the graphene layers. In particular TERM allows for the investigation of individual graphene sheets with high Raman signal enhancement factors and allows for imaging of local defects with nanometer resolution. Enhancement up to 560% of the graphene Raman bands intensity was obtained using TERS. TERM (with resolution better than 100 nm) showed an increase in the number of structural defects (D band) on the edges of both graphene and graphite regions.

Part of this chapter was accepted for publication:

M. Ghislandi, G. Hoffmann, E. Tkalya, L. Xue, G. de With, *Applied Spectroscopy Reviews* **2012**.

5.1 Introduction

Graphene has been first described by Geim and Novoselov as monocrystalline graphitic films, which are a few atomic layers thick but are nonetheless of remarkably high quality, stable under ambient conditions, and metallic in nature.^[1,2] The films were found by the authors to be a two-dimensional semimetal with a tiny overlap between the valence and conductance bands. Due to the possibility of producing these allotropes of carbon in large quantities, making it feasible to use them for numerous applications,^[3-6] it has become increasingly important to analyze these materials and to establish structure/property relations on the nanometer length scale.^[3]

Only recently the two-dimensional graphene sheets were produced by “simply” removing sheet after sheet from graphite to obtain a single graphene layer. Micro-mechanical cleavage (MC)^[1] and carbon vapor deposition (CVD)^[7,8] have been reported since then as common preparation routes in order to achieve graphene platelets; a great deal of attention is paid to this form of carbon because of its extraordinary functional properties, and potentially low production costs.^[2,7,9-12]

The conventional Raman spectrum of graphene and graphene layers has been studied in great detail by Ferrari et al.^[13,14] Graphene shows a Raman spectrum similar to that of graphite, where the differences observed mirror the missing interaction between the layers. The 2D peak (second order) changes in shape, width, and position for an increasing number of layers, reflecting the change in the electron bands via a double resonant Raman process. The so called G peak exhibits slight shifts in position and a great decrease in the ratio of the G/2D peak intensities.

Raman spectroscopy, and in particular micro-Raman,^[15] surface-enhanced Raman spectroscopy (SERS)^[16-18] and the recently introduced tip-enhanced Raman spectroscopy (TERS)^[19-23] are characterization techniques that are able to provide chemical as well as functional information on these class of carbon materials.^[24] The latter one, TERS, is a characterization technique combining the power of Raman spectroscopy to reveal chemical composition and molecular structure with the ultra-high spatial resolution of scanning probe microscopy (SPM). Theoretically, TERS allows spectroscopic analysis of any kind of macromolecular material (as well as inorganic materials like Si) with nanometer resolution, merely depending on probe quality. Only recently tip-enhanced Raman mapping (TERM) was demonstrated with lateral resolution far better than 50 nm and made it

possible to identify e.g. local defects along one individual single wall carbon nanotube. The group of Novotny and Hartschuh^[20,25,26] realized a resolution of 15 nm while reaching an intensity enhancement of four, whereas our group resolved about 30 nm while enhancing the G-line 256 times.^[24]

The potential of TERS is enormous: TERS on biological macromolecules such as proteins and ribonucleic acids^[27] as well as on various organic dyes^[28,29] has been demonstrated and resulted in spectra intensities that are enhanced by several orders of magnitude as compared to conventional confocal Raman spectroscopy. From theoretical considerations even sub-nanometer spatial resolution should be possible by tuning the interaction between tip and sample. Experimental obstacles like tip production^[30] and tip melting still hamper these achievements.

SERS was proven to be effective for enhancing the graphene Raman signal.^[17] In the present study we show for the first time enhanced Raman spectra using TERS and TERM results obtained from graphene.

5.2 Experimental

A general view of the multi-purpose scanning near-field optical spectrometer NTEGRA-SPECTRATM (NT-MDT) is shown in Figure 5.1. Its back-scattering geometry-based configuration for analyzing a specimen on transparent substrates allows us to record: atomic force or shear force microscopy (AFM/SFM) images (topography, phase contrast, etc.), confocal optical images, confocal far-field Raman and fluorescence spectra and images, and tip-enhanced near-field Raman spectra and images/mapping (fluorescence enhancement/quenching). A linearly-polarized laser beam from a He-Ne laser operating at 632.8 nm ($E = 1.96$ eV, TEM₀₀) enters the spectrometer through a single-mode optical fiber. The laser output passing through the plasma line filter is expanded and converted to a mode with a given polarization (linear, circular, radial, azimuthal). After it is reflected by the edge-filter, the beam goes into the inverted optical microscope (Olympus IX70) through a beam-splitter cube (10/90) and a pinhole. A 100x oil immersion objective (Olympus, n.a. = 1.3, refractive index of oil $n = 1.516$) focuses the laser beam into a spot with a diameter of less than 300 nm, with a final power at the sample of about 2 mW.

The tip is positioned into one of the two longitudinal lobes near rims of the diffraction-limited laser spot to locally enhance the electromagnetic field beneath its apex. This system allows one to lock the tip position inside the laser spot to maintain optimum illumination conditions. A near-field Raman image is established by raster scanning the sample with a xy-scan stage equipped with a close-loop operation system. The scattered and/or reflected light is collected with the same objective and directed back to the spectrometer through the pinhole. An additional Kaiser notch-filter is installed into the optical path to suppress the Rayleigh scattering. Confocal and spectral modes of the light transmitted by the beam-splitter cube are detected by a photomultiplier (Hamamatsu, PMT943-02) and a thermoelectrically cooled charge-coupled (CCD) detector (ANDOR, DV420), respectively. All Raman spectra can be recorded within a spectral range of 150–3500 cm^{-1} . A 200 lines/mm grating provides a spectral resolution of better than 15 cm^{-1} . The pinhole size used with the 100x oil immersion objective was equal to 60 μm .

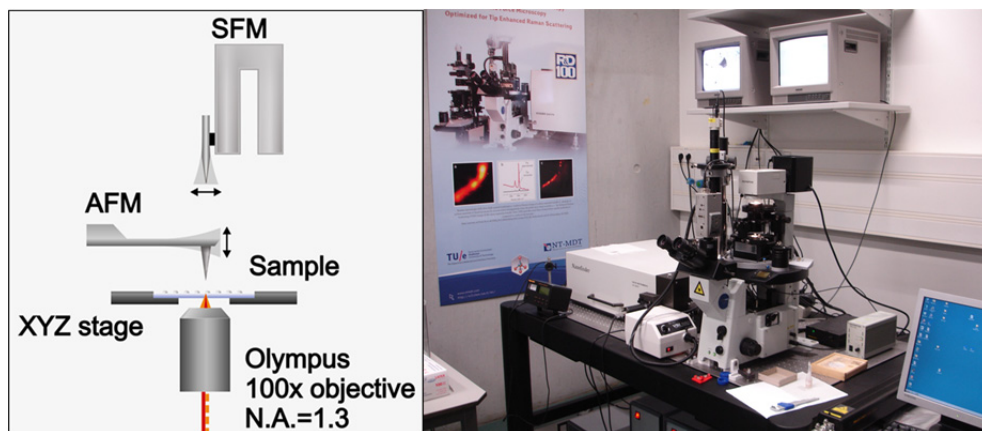


Figure 5.1 (left) Schematic optical setup of the TERS instrument used and (right) picture of the TERS equipment.

Mechanically cleaved graphene was obtained from HOPG ZYH supplied from NT-MDT Company. Flakes were removed from bulk graphite piece by attaching them to a normal transparent Scotch[®] adhesive tape. After removing the tape, macroscopically homogeneous layers remained attached to it. The tape was then placed in acetone for 1 h in order to release the glueing interaction between tape and graphite sheets. Graphene sheets (10x10 mm^2) produced via the CVD[™] method were purchased from Graphene

Laboratories. The films were grown directly on a Ni film deposited on an oxidized silicon wafer.

A thin (0.17 mm) glass substrate 50x24 mm² was cleaned with a UV-Ozone cleaning system from Novascan[®] for 20 min at room temperature for the removal of molecular organic contamination. Both cleaved graphene on tape and CVD graphene on nickel were carefully transferred^[7] onto the cleaned glass by the use of a thermal release tape (Graphene Laboratories Inc.); after a quick removal of the tape, some thin graphite flakes were visible and the transparent graphene could be identified by Raman spectroscopy.

5.3 Results and Discussion

The two most intense Raman bands for graphite are the G peak at $\sim 1570\text{ cm}^{-1}$ and the 2D peak at $\sim 2680\text{ cm}^{-1}$. The G band is a tangential shear mode of carbon atoms that corresponds to the stretching mode in the graphite plane. The G peak is due to the doubly degenerate zone center E_{2g} mode.^[14] The 2D band has nothing to do with the G peak, but is a second-order process from two-zone boundary phonons. It is an intrinsic property of graphite, and present even in defect-free structures. Since zone-boundary phonons do not satisfy the fundamental Raman selection rule, they are not seen in first order Raman spectra of defect-free graphite. Such phonons give rise to a peak at $\sim 1350\text{ cm}^{-1}$ in graphite containing defects, usually called the D peak.^[13]

The spectra in Figure 5.2 show a significant change in shape and intensity of the 2D peak of graphene compared to bulk graphite. The 2D peak in bulk graphite presents a shoulder at roughly 1/4 height and a main peak at half height of the G peak. We measure a single, sharp 2D peak in graphene, roughly 5 times more intense than the G peak. On the inset, it is possible to see the evolution of the 2D band as a function of number of layers analyzed. These bands immediately indicate that a bilayer has a much broader and up-shifted 2D band with respect to graphene. The G peak intensity of a single graphene layer is about 4 times lower and the G position is $\sim 5\text{ cm}^{-1}$ higher compared to bulk graphite. Figure 5.2 shows that no D peak is observed in the spectrum. This proves the absence of a significant number of defects.

With a conventional Raman spectroscopy setup a large area of graphite/graphene surface is analyzed at the same time and the average amount and type of defects can be

calculated. However, in order to learn more about the local defect distribution in individual graphene sheets and optimizing procedures for their functionalization, TERS was utilized.

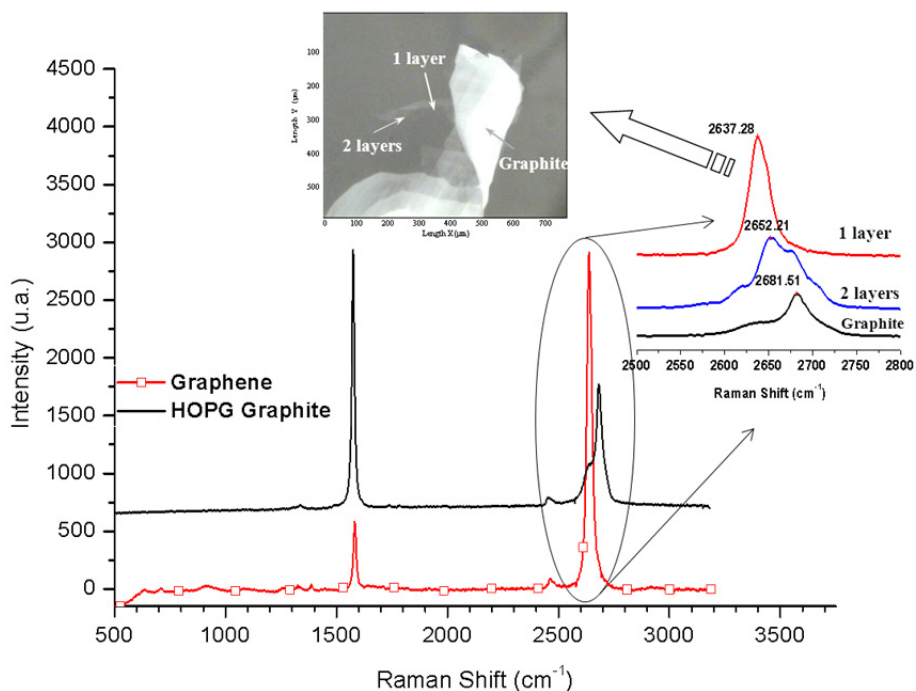


Figure 5.2 Confocal Raman spectra of graphite and graphene areas for 632.8 nm laser excitation. The zoom over the 2D peaks clearly shows the distinct curve shape and shift on Raman position for different number of graphene layers. The optical Image indicates the spots where Raman spectra were measured.

Based on the concept of evanescent waves existing in the near-field (<100 nm) optical measurements beyond the diffraction limit are possible for attaining ultra-high resolution in optical spectroscopy. A practical implementation of that has become possible by combining optical spectroscopy and scanning probe microscopy (SPM), often referred to as apertureless near-field optical microscopy, and in particular, as TERS. The crucial role in TERS is played by the SPM tip as a nanoscopic scatterer and/or lighting source. In the first case, the tip disturbs a confined non-radiating electromagnetic field in the proximity of a nanometer-sized specimen and converts it to a radiating one, which can be then detected by standard diffraction-limited optics. In the second case, a tip localizes and enhances the

scattered optical radiation over the incident radiation due to the coupled excitation of free electrons and the electromagnetic field present (called localized surface plasmon) in the metal of the tip. The latter is caused by the fact that metals, due to their small skin effect, provide the highest enhancement and scattering efficiency. An additional contribution to the field enhancement, known as the quasi-static lightning rod effect, stems from a purely geometrical factor of the tip resulting in a quasi-singularity of the electromagnetic field near its apex. The material composition of the tip, its geometry and the polarization state of the incident light in the local excitation-based scheme are of the greatest importance for efficient enhancements.

For our experiments we used gold tips etched from a 0.2 mm gold wire in our laboratory following procedure used by Ren et al.^[31] To obtain a measure of the sharpness and quality of the resulting tip we mapped the reflection of the laser light from the tip using a photomultiplier while moving the tip in two dimensions using the scanner of the shear force head. In fig 5.3 we show scanning electron microscopy images (a and b) and the resulting scan of a tip (c). Though the scan does not necessarily show a one-to-one correspondence to the shape of the tip, they clearly show the nice symmetry of the tip by the detection of diffraction rings and a tip radius below 60 nm. This indicates a resolution of around 25 nm or roughly half of tip radius.

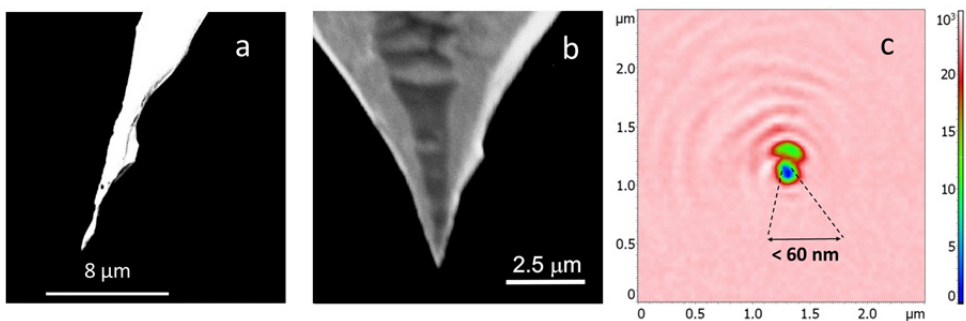


Figure 5.3 Scanning electron microscopy and reflectivity mapping of gold tips.

Spectroscopic imaging of mechanically cleaved (MC) graphene/graphite was obtained by accumulation of local Raman data using TERM. Figure 5.4 shows an optical microscopy image and tip-enhanced Raman topographical scans of graphite/graphene samples that were taken with the self-made gold SFM tip for the tip-on operation mode (in

this mode the tip is close to the sample surface and active in the near field). More details on the experiments performed can be found elsewhere.^[24]

We can compare the intensity of the 2D peak region (2630-2675 cm^{-1}), and also the shift position of these peaks. It is possible to identify clearly defined areas corresponding to graphene using TERM (black dot in Figure 5.4 right). This is due to a better lateral resolution promoted by this technique.^[32]

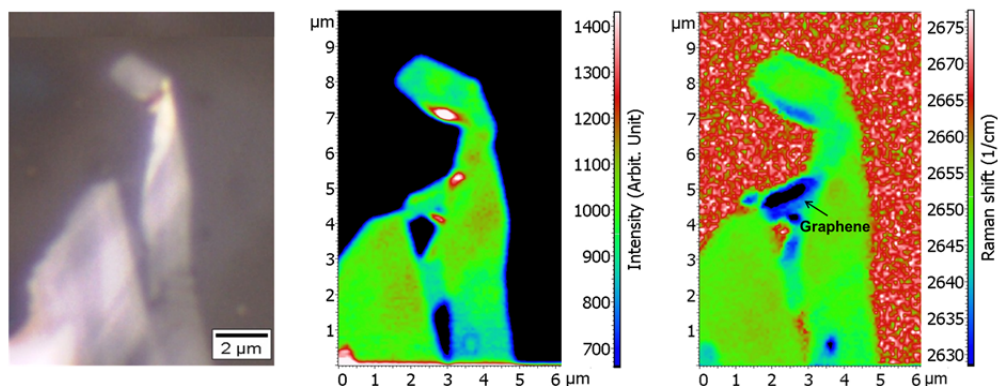


Figure 5.4 Optical Microscopy image (left), Tip-Enhanced Raman Mapping showing 2D peak Intensity (middle) and 2D Shift position (right).

In the region where graphene was found, two single Raman spectrum were acquired (10 seconds of acquisition time), comparing tip-on mode and tip-off (in this mode SPM tip is far away from the sample surface) mode (Figure 5.5). An enhancement of more than 400% was verified for the G and 2D bands and an enhancement of more than 500% was obtained for the D band using TERS. While the displacement vectors of the vibrations of graphene lie in the molecule's plane, some of the displacement vectors of the graphene layers with defects do not. With a tip that only emits photons polarized at a right angle to the graphene plane it should not be possible to excite Raman lines at all, but of course tips are far from ideally shaped, especially during mapping procedure. Enhancement is then possible if the displacement vectors have components parallel to the polarization of the exciting electromagnetic field.

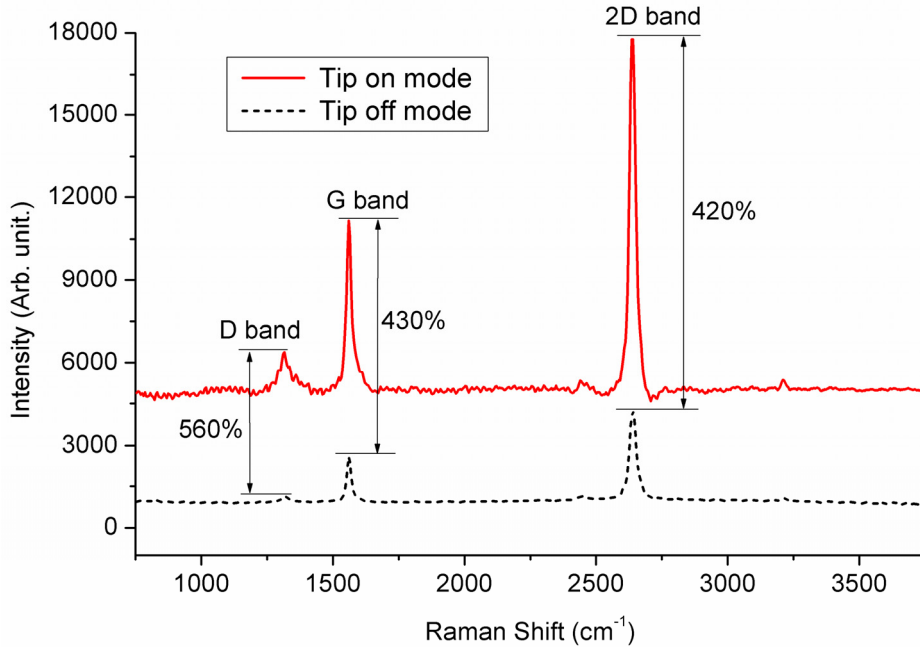


Figure 5.5 Single Raman spectrum of graphene, using TERS (tip-on mode, red line) and confocal Raman (tip-off mode, dashed black line).

A much higher enhancement factor was already obtained by our group^[31] using the same setup for carbon nanotubes. This technique was used in order to obtain Raman images of carbon nanotubes with high spatial resolution mediated by local enhancement of the incident and scattered fields. It is generally believed that the main vector component of the enhanced field is oriented normally to the surface, although it was already observed that the near field Raman intensity was not sensitive to the polarization direction of the incident laser beam relative to the nanotube axis, showing that the enhanced field is radially symmetric with respect to the tip axis.^[20]

If the enhanced field is polarized along the long axis of the tip, there should be no enhancement for graphene at all, as all the vibrations of graphene are only in the plane of the graphene sheet. To take a closer look at these vibrations, we have done density functional theory calculations on a small graphene model. These calculations on the B3LYP/6-31G* level (Gaussian09)^[33] were done on a perfect graphene model (Figure 5.6 c, d) and a graphene model with a defect obtained by H₂ addition (Figure 5.6 a, b). Whereas the perfect model only shows vibrations with a dipole transition moment vector in the plane

of the molecule (e.g. vibration calculated at 1628 cm^{-1}), we can find vibrations with a dipole transition moment vector out of the plane of the molecule for the defected graphene (e.g. vibration calculated at 1651 cm^{-1}), which means vibrations with components of the dipole transition moment vector parallel to the axis of the enhancing tip. The same holds for the vector of change in polarizability, which fits well to our experimental observation in which the D band is more enhanced than the G peak. Enhancement of the G peak (with lower efficiency) can be attributed to the fact that the conditions of the experiment are not ideal: the angle of the tip with the graphene plane is not exactly 90° , and the tip does not only enhance the field along its axis but also at angles of a few degrees.

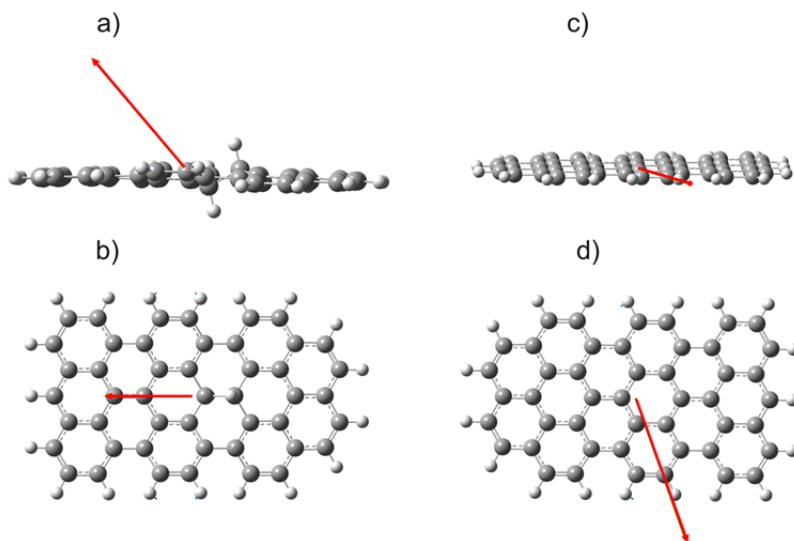


Figure 5.6 Vibrations of a defect-containing, by H_2 addition, (a, b) and a perfect (c, d) graphene model. a, c: side view, b, d: top view. Vectors of the dipole transition moment shown by the arrows.

The spatial resolution of our TERM is not as good as it could be and the reason for this is illustrated in Figure 5.7. Our TERM consists of two components: the far field contribution and the near field contribution. A sharp step (blue line) on the sample can be seen with a resolution of 30 nm in the near field image, whereas in the far field image (green line) the same step can be observed with a resolution of only 300 nm. If the enhancement then is about 4, the resolution of a sharp step is around 100 nm by

combination of the two images (shown in red). On the other hand, if one obtains an enhancement of 200, as in the case of single-walled carbon nanotubes, the far field contribution can be neglected.

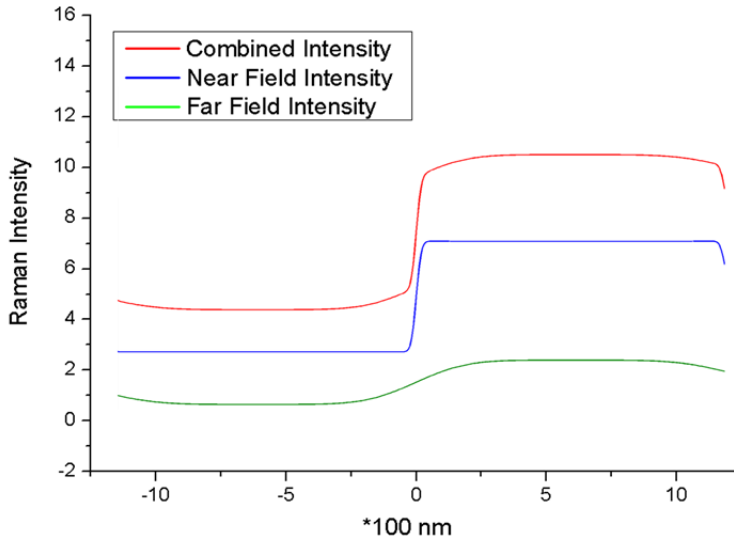


Figure 5.7 Resolution of Raman mappings (lower: near field, middle: far field, upper: both contributions together).

The samples of graphene grown by CVD were also analyzed and show a similar TERS enhancement as the ones obtained by MC. For the CVD samples, a graphene spot was identified via confocal Raman in a $10 \mu\text{m}^2$ scanning area (Figure 5.8-a) and an AFM phase (Figure 5.8-b) image showed that the monolayer was grown on the flat surface region over the substrate, surrounded by rougher thicker graphite region. A more localized ($2 \mu\text{m}^2$) TERM analysis was then conducted in order to identify with nanometer resolution specific features of the graphene Raman spectra according to their position on the sheet. In detail, it is possible to see the evolution of the D, G, and 2D bands in a straight line crossing the graphene/graphite border (Figure 5.8-d).

Commonly as-prepared graphene does not have enough structural defects for the D peak to be seen,^[13] which is indicative of the high crystallinity of graphene obtained by the production process (MC or CVD). In this case, the D peak is only present at the edges,^[13] since they act as defects, allowing elastic backscattering of electrons even in an otherwise

defect-free sample. Raman spectroscopy of graphene edges was already investigated by Casiraghi et al.^[34] The $I(D)$ to $I(G)$ peak ratio strongly depends on polarization, relative position of the laser spot with respect to the edge, and the amount of edge disorder. In some samples Raman mapping with circular polarization shows no significant dependence of the D peak intensity on the macroscopic edge orientation. This indicates that edges can be mixed and disordered at least on the laser spot scale even though they follow well-defined crystallographic directions at a larger scale.^[34]

In Figures 5.8-c and 5.8-d, when going from the outside (point 1), which corresponds to a thicker graphite region according to Raman analysis, to the inside (point 4) of the single layer graphene sheet, the intensity of the defect peak $I(D)$, around 1350 cm^{-1} , increases, reaches a maximum and then decreases. On the other hand, $I(G)$, around 1570 cm^{-1} , increases moving from inside to outside the flake. This is expected, since the spectra outside (red area of Figure 5.8-d or blue area of Figure 5.8-c) indicate graphite and the Raman intensity of the allowed peak is proportional to the volume of the sample. Consequently the intensity I of point 1 was normalized for comparison.

Monitoring the 2D peak, there is a clear transition from graphite to graphene. The peak is broad (with a shoulder) and has a low intensity. If compared to the G peak for point 1, it gets sharper and shifts to lower wavenumbers when the stage moves to point 4, which corresponds to one layer graphene. The D peak interestingly behaves in a different way as compared to the G and 2D peaks, because its intensity is proportional to the amount of defects which, neglecting structural disorder, can be assumed to be proportional to the edge length under the laser spot, as discussed above. Thus, the maximum $I(D)$ should be measured when the diameter of the laser beam crosses the edges.

With respect to the amount of layers on the interface, Saito et al.^[23] proposed a relation using the change of intensity of the Raman band of silicon (when using silicon tips) generated from the near-field probe for the calculation of number of layers. In our study we limit ourselves to showing for the first time direct TERM of the 2D peak and compare, with nanometer resolution, the full spectra at the interface section. An estimation of the higher TERS resolution using a slice through the intensity image gives a spatial resolution far better than 60 nm for the present experimental setup.

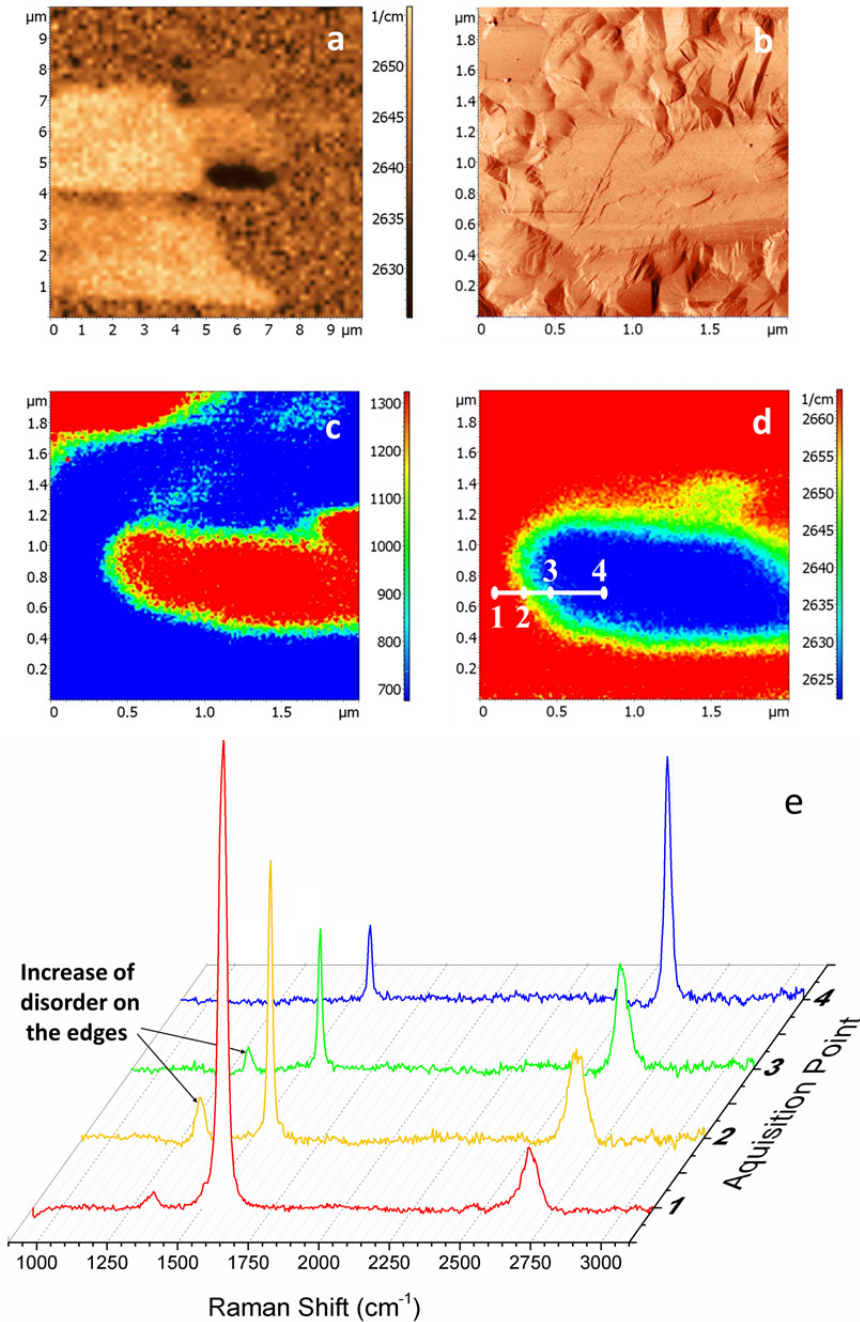


Figure 5.8 (a) Confocal Raman mapping of graphene (black dot)/graphite grown by CVD, (b) AFM phase image of graphene (flat region) area identified by Raman, (c) TERM mapping showing intensity of 2D band for the selected area, (d) TERM mapping showing shift position of 2D band and (e) Raman spectra corresponding to points selected in (d).

5.4 Conclusions

Single graphene sheets, a few stacked graphene layers and bulk graphite were successfully deposited on a thin glass substrate, without the use of any chemical treatment, which can lead to contamination and damaging of the molecular structure of the specimens.

Raman spectroscopy combined with a scanning probe microscopy setup, so-called apertureless near-field optical microscopy, and in particular tip-enhanced Raman spectroscopy and mapping (TERS and TERM), allows detection of structural defects with lateral resolution in the nanometer range. We have demonstrated for the first time direct enhancement of more than 400% for the D, G, and 2D bands of graphene using TERS. TERM on graphite/graphene samples grown by CVD shows the different Raman properties in the center and at the edges of the platelets, confirming (with resolution better than 100 nm) an increase in the D band on the edges of both graphene and graphite areas.

References

- [1] K. S. Novoselov, A. K. Geim, S. V. Morozov, D. Jiang, Y. Zhang, S. V. Dubonos, I. V. Grigorieva, A. A. Firsov, *Science* **2004**, *306*, 666.
- [2] A. K. Geim, K. S. Novoselov, *Nat. Mater.* **2007**, *6*, 183.
- [3] A. H. Castro Neto, F. Guinea, N. M. R. Peres, K. S. Novoselov, A. K. Geim, *Reviews of Modern Physics* **2009**, *81*, 109.
- [4] G. Eda, G. Fanchini, M. Chhowalla, *Nat. Nanotechnol.* **2008**, *3*, 270.
- [5] E. Tkalya, M. Ghislandi, A. Alekseev, C. Koning, J. Loos, *J. Mater. Chem.* **2010**, *20*, 3035.
- [6] S. Stankovich, D. A. Dikin, G. H. B. Dommett, K. M. Kohlhaas, E. J. Zimney, E. A. Stach, R. D. Piner, S. T. Nguyen, R. S. Ruoff, *Nature* **2006**, *442*, 282.
- [7] K. S. Kim, Y. Zhao, H. Jang, S. Y. Lee, J. M. Kim, K. S. Kim, J.-H. Ahn, P. Kim, J.-Y. Choi, B. H. Hong, *Nature* **2009**, *457*, 706.
- [8] X. Li, W. Cai, J. An, S. Kim, J. Nah, D. Yang, R. Piner, A. Velamakanni, I. Jung, E. Tutuc, S. K. Banerjee, L. Colombo, R. S. Ruoff, *Science* **2009**, *324*, 1312.
- [9] Y. B. Zhang, J. P. Small, W. V. Pontius, P. Kim, *Appl. Phys. Lett.* **2005**, *86*, 3.
- [10] X. L. Wang, *Phys. Rev. Lett.* **2008**, *100*.

- [11] T. Ramanathan, A. A. Abdala, S. Stankovich, D. A. Dikin, M. Herrera-Alonso, R. D. Piner, D. H. Adamson, H. C. Schniepp, X. Chen, R. S. Ruoff, S. T. Nguyen, I. A. Aksay, R. K. Prud'homme, L. C. Brinson, *Nat. Nanotechnol.* **2008**, *3*, 327.
- [12] A. Reina, X. T. Jia, J. Ho, D. Nezich, H. B. Son, V. Bulovic, M. S. Dresselhaus, J. Kong, *Nano Lett.* **2009**, *9*, 30.
- [13] A. C. Ferrari, J. C. Meyer, V. Scardaci, C. Casiraghi, M. Lazzeri, F. Mauri, S. Piscanec, D. Jiang, K. S. Novoselov, S. Roth, A. K. Geim, *Phys. Rev. Lett.* **2006**, *97*, 4.
- [14] A. C. Ferrari, *Solid State Commun.* **2007**, *143*, 47.
- [15] I. R. Lewis, P. R. Griffiths, *Appl. Spectrosc.* **1996**, *50*, A12.
- [16] R. K. Chang, B. L. Laube, *Crc Critical Reviews in Solid State and Materials Sciences* **1984**, *12*, 1.
- [17] F. Schedin, E. Lidorikis, A. Lombardo, V. G. Kravets, A. K. Geim, A. N. Grigorenko, K. S. Novoselov, A. C. Ferrari, *ACS Nano* **2010**, *4*, 5617.
- [18] G. Goncalves, P. Marques, C. M. Granadeiro, H. I. S. Nogueira, M. K. Singh, J. Gracio, *Chem. Mater.* **2009**, *21*, 4796.
- [19] R. M. Stockle, Y. D. Suh, V. Deckert, R. Zenobi, *Chem. Phys. Lett.* **2000**, *318*, 131.
- [20] A. Hartschuh, E. J. Sanchez, X. S. Xie, L. Novotny, *Phys. Rev. Lett.* **2003**, *90*, 4.
- [21] L. G. Cancado, A. Hartschuh, L. Novotny, *J. Raman Spectrosc.* **2009**, *40*, 1420.
- [22] K. L. A. Chan, S. G. Kazarian, *Nanotechnology* **2011**, *22*, 175701.
- [23] Y. Saito, P. Verma, K. Masui, Y. Inouye, S. Kawata, *J. Raman Spectrosc.* **2009**, *40*, 1434.
- [24] S. S. Kharintsev, G. G. Hoffmann, P. S. Dorozhkin, G. de With, J. Loos, *Nanotechnology* **2007**, *18*, 315502.
- [25] E. J. Sanchez, L. Novotny, X. S. Xie, *Phys. Rev. Lett.* **1999**, *82*, 4014.
- [26] L. Novotny, S. J. Stranick, in *Annu. Rev. Phys. Chem.*, Vol. 57, **2006**, pp. 303.
- [27] E. Bailo, V. Deckert, *Angewandte Chemie-International Edition* **2008**, *47*, 1658.
- [28] B. Pettinger, *Mol. Phys.* **2010**, *108*, 2039.
- [29] D. Zeisel, B. Dutoit, V. Deckert, T. Roth, R. Zenobi, *Anal. Chem.* **1997**, *69*, 749.
- [30] S. S. Kharintsev, A. I. Noskov, G. G. Hoffmann, J. Loos, *Nanotechnology* **2010**, *22*, 025202.
- [31] B. Ren, G. Picardi, B. Pettinger, *Rev. Sci. Instrum.* **2004**, *75*, 837.

- [32] S. S. Kharintsev, G. G. Hoffmann, J. Loos, G. de With, P. S. Dorozhkin, M. K. Salakhov, *Journal of Experimental and Theoretical Physics* **2007**, *105*, 909.
- [33] M. J. Frisch, G. W. Trucks, H. B. Schlegel, G. E. Scuseria, M. A. Robb, J. R. Cheeseman, G. Scalmani, V. Barone, B. Mennucci, G. A. Petersson, H. Nakatsuji, M. Caricato, X. Li, H. P. Hratchian, A. F. Izmaylov, J. Bloino, G. Zheng, J. L. Sonnenberg, M. Hada, M. Ehara, K. Toyota, R. Fukuda, J. Hasegawa, M. Ishida, T. Nakajima, Y. Honda, O. Kitao, H. Nakai, T. Vreven, J. Montgomery, J. A., J. E. Peralta, F. Ogliaro, M. Bearpark, J. J. Heyd, E. Brothers, K. N. Kudin, V. N. Staroverov, R. Kobayashi, J. Normand, K. Raghavachari, A. Rendell, J. C. Burant, S. S. Iyengar, J. Tomasi, M. Cossi, N. Rega, N. J. Millam, M. Klene, J. E. Knox, J. B. Cross, V. Bakken, C. Adamo, J. Jaramillo, R. Gomperts, R. E. Stratmann, O. Yazyev, A. J. Austin, R. Cammi, C. Pomelli, J. W. Ochterski, R. L. Martin, K. Morokuma, V. G. Zakrzewski, G. A. Voth, P. Salvador, J. J. Dannenberg, S. Dapprich, A. D. Daniels, Ö. Farkas, J. B. Foresman, J. V. Ortiz, J. Cioslowski, D. J. Fox, Revision B.01 ed., Gaussian Inc, Wallingford, **2009**.
- [34] C. Casiraghi, A. Hartschuh, H. Qian, S. Pisanec, C. Georgi, A. Fasoli, K. S. Novoselov, D. M. Basko, A. C. Ferrari, *Nano Lett.* **2009**, *9*, 1433.

Investigating the preparation routes to aqueous graphene dispersions and their influence on electrical conductivity of polymer composites

Graphene was produced from graphite powder using the three best known water-based conversion approaches. The first two are based on chemical oxidation methods, only differing in the reduction process, either by the use of hydrazine or by thermal expansion, respectively. The third one is based on long-term ultrasonic exfoliation. Water/surfactant solutions were prepared with these three nanofillers and latex technology was applied for the preparation of conductive graphene/polystyrene composites with well-dispersed graphene platelets. The samples were characterized with respect to filler properties and morphology, and their influences on electrical conductive properties of the composites were compared. Microscopic studies showed that both reduction processes lead to agglomeration/wrinkling of the nanoplatelets, even though they yield composites with high conductivity and low percolation threshold. Although mechanical ultrasound exfoliation of graphite produces less defective multi-layer graphene, these platelets have a smaller lateral size and their composites exhibit a higher percolation threshold.

This chapter has been submitted for publication:

M. Ghislandi, E. Tkalya, A. Alekseev, C. E. Koning, G. de With, *Nanotechnology*, **2012**.

6.1 Introduction

The new rising star of nanofillers, graphene, with its combination of extraordinary physical and electrical properties plus the ability to be dispersed in various polymer matrices, has enabled the manufacturing of a new class of polymer composites.^[1,2] Various methods to obtain graphene have been reported, since it was first mechanically isolated from graphite by Novoselov et al.,^[3] facilitating its production on large scales. The growing of graphene sheets from substrates^[4,5] and, in particular, the controlled deposition from carbon vapor^[6,7] have been recently described in literature as techniques that enable the production of single graphene layers in large 2D dimensions.^[8] These materials find potential applications mainly in nanoelectronic devices.^[9-12]

The chemical synthesis of graphene using graphite, graphite oxide (GO) or other graphite derivatives as starting materials have also been studied. The conversion of graphite into GO via Hummers^[13] or similar methods is an initial stage for graphene preparation. The water soluble GO can be reduced with the use of chemicals^[14,15] (*ORchem*) or by quick thermal expansion^[16] (*ORtherm*) to form graphene. Recently, the long-term (e.g. more than 200 h) simple mechanical exfoliation (sonication) of graphite dispersed in polar solvents, as well as in water/surfactant systems, were reported as methods that yield single and multilayer graphene platelets at relatively high concentrations.^[17-19] The chosen conversion techniques^[20] can not only be up-scaled but also provide graphene with improved processability and, potentially, new functionality. The preparation of highly conductive paper-like graphene has been reported, yielding conductivities ranging from 10^3 to 10^4 S/m for the above chemical exfoliation approaches.^[19,21,22] The exfoliated dispersions are most suitable for the preparation of polymer composites with enhanced mechanical and electrical properties.^[1,23,24]

In this work, we produce graphene dispersed in water starting from graphite following the two main chemical conversion approaches (*ORchem* and *ORtherm*) and one physical conversion, using long-term ultrasonic exfoliation (*Sonic*). Subsequently, graphene/polystyrene (PS) composites are prepared by the well-known latex technology. The latex concept enables the homogeneous incorporation of nanofillers into any kind of highly viscous polymer matrix, e.g. PS synthesized by emulsion polymerization or similar processes.^[24-27] In the following, a detailed comparison of the three chosen techniques with

respect to filler morphology and conductive properties of the respective nanocomposites is presented.

6.2 Experimental

6.2.1 Chemicals and polymer latex

Sodium dodecyl sulfate (SDS) (90%, Merck), sodium carbonate (99%, Aldrich), sodium peroxodisulfate (SPS) (90%, Merck), poly(sodium 4-styrene sulfonate) (PSS) (Aldrich, M_w 70 kg/mol) and sodium cholate (SC) (99%, Aldrich) were used as received. Styrene (99%, Merck) was passed over an inhibitor remover column prior to use. SP-2 graphite (Bay Carbon) powder was used as obtained.

PS latex was synthesized via conventional free radical emulsion polymerization. The reactor was charged with: styrene (252 g), SDS (26 g, 0.09 mol), sodium carbonate (0.7 g, 6.6 mmol), and H₂O (712.2 g). The reaction mixture was degassed by purging with argon for 30 min. A solution of SPS (0.45 g, 1.9 mmol) in H₂O (10 g) was also degassed. The reaction was started upon the introduction of the initiator solution and was performed at 70 °C with an impeller speed of 400 rpm for 1 hour. The average latex particle size, as determined by dynamic light scattering, was 90 nm. Size exclusion chromatography analysis showed M_n , M_w and PDI values of 495 kg/mol, 944 kg/mol, and 1.9, respectively.

6.2.2 Preparation of graphene via chemical oxidation/reduction treatment

In the first approach, graphene, designated *ORchem*, was synthesized via oxidation of SP-2 graphite using the Hummers method^[13] and subsequent sonication of graphene oxide (GO), followed by reduction with hydrazine in the presence of a ten-fold excess of PSS (wt./wt. GO). The entire procedure is described in detail by Stankovich et al.^[14] After the synthesis, the graphene was filtered off with a polyamide membrane filter, which also removes excess of PSS, and dried under vacuum. The product was then re-dispersed in water (1 mg/ml) by a 40 minutes sonication treatment (Sonics Vibracell VC750 horn sonicator with a 10 mm diameter tip) at 20 W during cooling in an ice-bath to maintain or even to lower the solution temperature.

6.2.3 Preparation of graphene via chemical oxidation and thermal reduction treatment

Graphene (designated *ORtherm*) was obtained via initial preparation of GO from graphite using the Staudenmaier method^[28] followed by a thermo-expansion process. The thermal expansion process consists of a quick exposure of dry GO to a pre-heated tubular furnace at 1025 °C. A detailed description of this process is given by McAllister et al.^[16] Aqueous exfoliated graphene dispersions (1 mg/ml) were then prepared with the use of SC or PSS surfactants. Both polymers resulted in well-exfoliated and stable dispersions using a 1:1 graphene/surfactant wt.% ratio. Energy for exfoliation was supplied by sonication following procedure described above (20 W for 40 min).

6.2.4 Preparation of graphene sonicated in solution

In the third approach, graphene (designated *Sonic*) was prepared following the method described by Coleman's group.^[17,19] Graphite exfoliation was carried out in SC/water solution using low power ultra-sonication (Bransonic[®] 1510E, ~16 W) for long times (up to 400 h) followed by centrifugation (2000 rpm for 1 h).

6.2.5 Composites processing

The compounding procedures for the three different graphene dispersions were identical. Each dispersion was mixed with PS latex, frozen in liquid nitrogen for several minutes, and subsequently freeze dried (Christ Alpha 2–4 freeze dryer operated at 0.2 mbar and -50 °C for 24 h). The resulting composite powders were heated quickly to 150 °C and then for 20 min until 180 °C between Teflon sheets, using a Collin Press 300G. Subsequently the heated material was compression molded into films of 0.5 to 1 mm thickness at 100 bar for 2 minutes.

6.2.6 Characterization

UV–Vis absorption spectra were recorded with a Hewlett–Packard 8453 spectrometer operating between 200 and 1100 nm. Small sample volumes of the surfactant/graphene

dispersions were taken after the sonication processes and diluted with water by shaking, resulting in a graphene concentration of 0.0125 mg/ml for all samples. As control experiment the original SC/PSS solutions were diluted and analyzed as above.

A LABRAM confocal Raman spectroscope equipped with an optical microscope was utilized. Samples were irradiated with a red laser (632.8 nm) supplied by Melles Griot.

Atomic force microscopy (AFM) characterization of graphene was performed with a NT-MDT NTEGRA operated in tapping mode using silicon tips NSG11 (NT-MDT). We deposited our graphene/graphite dispersions onto freshly cleaved mica substrates by spraying a pipette-held droplet (~10 μ L) with a burst of compressed air. The samples were rinsed with water/alcohol solution for removal of surfactant. The conductive AFM (C-AFM) measurements on composites cross-sections were performed by an NTEGRA Tomo (NT-MDT Co.). The device is a combination of a microtome EM UC6-NT (Leica) and an SPM measuring head. This design allows for alternate microtome cutting and SPM measurements of the sample block-face. The local current measurements were performed in C-AFM mode with a gold-coated silicon cantilever NSC36/Cr-Au (Micomash). The sample was electrically connected to a grounded holder; and a bias of 2 V was applied.^[29]

The electrical conductivity was measured using the standard four-point method. Parallel contact lines, with 1 cm in length and with a 1 cm interval, were drawn on the composite film with conductive-silver paint (Fluka). All conductivity measurements were performed at room temperature with a Keithley 6512 programmable electrometer. For each sample, conductivity data represent the average over 10 consecutive measurements in a voltage range from 0 to 10 V and at frequencies between 50 and 60 Hz.

6.3 Results and Discussion

6.3.1 Graphene powder and dispersion analyses

Raman spectra (Figure 6.1 a) were first investigated in order to determine the “quality” of the exfoliated graphene. It is well known that Raman spectroscopy is suitable not only for determination of the number of layers, but also for detecting the presence of structural defects.^[30, 31] Thin films were produced from all three graphene dispersions by drop casting. For each film we measured Raman spectra at multiple locations. The spectra for the

untreated graphite powder and the micro-mechanically cleaved graphene reference are shown for comparison.

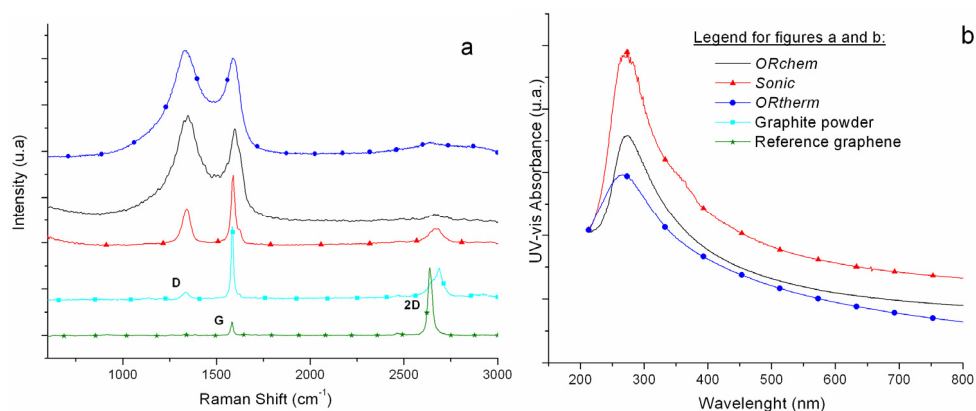


Figure 6.1 (a) Average Raman spectra of the graphenes prepared plus raw graphite powder and mechanically cleaved graphene used as references, and (b) UV-Vis spectra of the three dispersions used for composite manufacturing.

For *ORchem* and *ORtherm* graphene, the prominent D peak (absent in mechanically cleaved graphene and graphite powder references) is attributed to the presence of sp^3 carbon vibrations in the basal carbon plane. Several forms of defects, which could include residual carboxylic acids, epoxides, or ketones, may well cause lattice distortions, accounting for the increased D band intensity. The intensity of the 2D peak of the *ORchem* and *ORtherm* samples with respect to the D and G peaks is very small, most likely due to the discussed structural disorder. On account of the low intensity and broadness, we only report here a small shift for the 2D peaks to lower wavenumbers as compared to the untreated graphite sample. The absence of any prominent shoulder on the 2D peak indicates that only graphene having a few layers are present in solution. More in-depth analyses are presented elsewhere.^[32]

The introduction of edge defects in graphene dispersions submitted only to long-term sonication (*Sonic*) is unavoidable, as large crystallites are cut into smaller flakes during processing. However, the D band observed for *Sonic* flakes (see Figure 6.1 a) is both narrower and less intense as in *ORchem* and *ORtherm* samples, strongly suggesting that the former graphene contains less defects.^[17] Overall for sonic flakes, the 2D band displays a

non-graphite-like character. The spectra were consistent with flakes having a few graphene layers. As mentioned before for *ORchem* and *ORtherm* samples, the also non-homogeneous and low 2D band intensity of sonic flakes prevents a more detailed conclusion.

By UV-Vis analysis the highest absorbance, i.e. the best dispersion, was measured for the *Sonic* samples, followed by the *ORchem* samples (Figure 6.1 b). The selection of surfactants for each dispersion method was based on the best performing combinations (surfactant+method) as learned from previous reports.^[19,23,33] We would like to stress that a good dispersion with high absorbance measured by UV-Vis doesn't necessarily mean that it has a large number of single layer graphene platelets. It should be more seen as an indication that a large amount of small particles are present, which remain suspended and absorb radiation. Although all sample dispersions were visually stable, black colored and without any signs of settling in the short term (1 week), the only dispersion without any trace of settling in the long-term (6 months) was the *Sonic* sample.

AFM was extensively applied to determine the sheet thickness, morphological features and lateral dimensions of the graphene samples. Right after chemical oxidation, the first step for preparation of *ORchem* and *ORtherm* graphene, the formation of a great majority of 1 nm thick GO platelets was confirmed.^[14,24] The oxidation process yielded almost 100% of GO with a thickness of around 1 nm and surface areas between 1 and 3 μm^2 .

AFM analyses of the chemically treated graphene after reduction are shown in Figure 6.2. A wrinkling of the platelets is visible (see black arrows in Figure 6.2 c and f). This wrinkling is clearly more severe for the *ORtherm* graphene, probably because of the fast "explosion" that the GO is submitted to during reduction. It was also observed that sheet agglomeration and a decreasing sheet surface area may be a result of the chemical reduction process. The decreasing sheet size is just indicative as the folding/agglomeration of graphene prevents to obtain reliable statistical data. Measurements of the sheet thickness on flat areas indicated mostly monolayers or a few layers of graphene stacked together. Thicknesses were between 1-3 nm for more than 90% of the *ORchem* sheets and for more than 75% of the *ORtherm* sheets (see Figure 6.2 b and e). The roughness of exfoliated graphene is higher than the mechanically cleaved graphene reference prepared via the scotch tape method,^[3] probably due to defects, un-removed functional groups, or surfactants on treated surfaces.

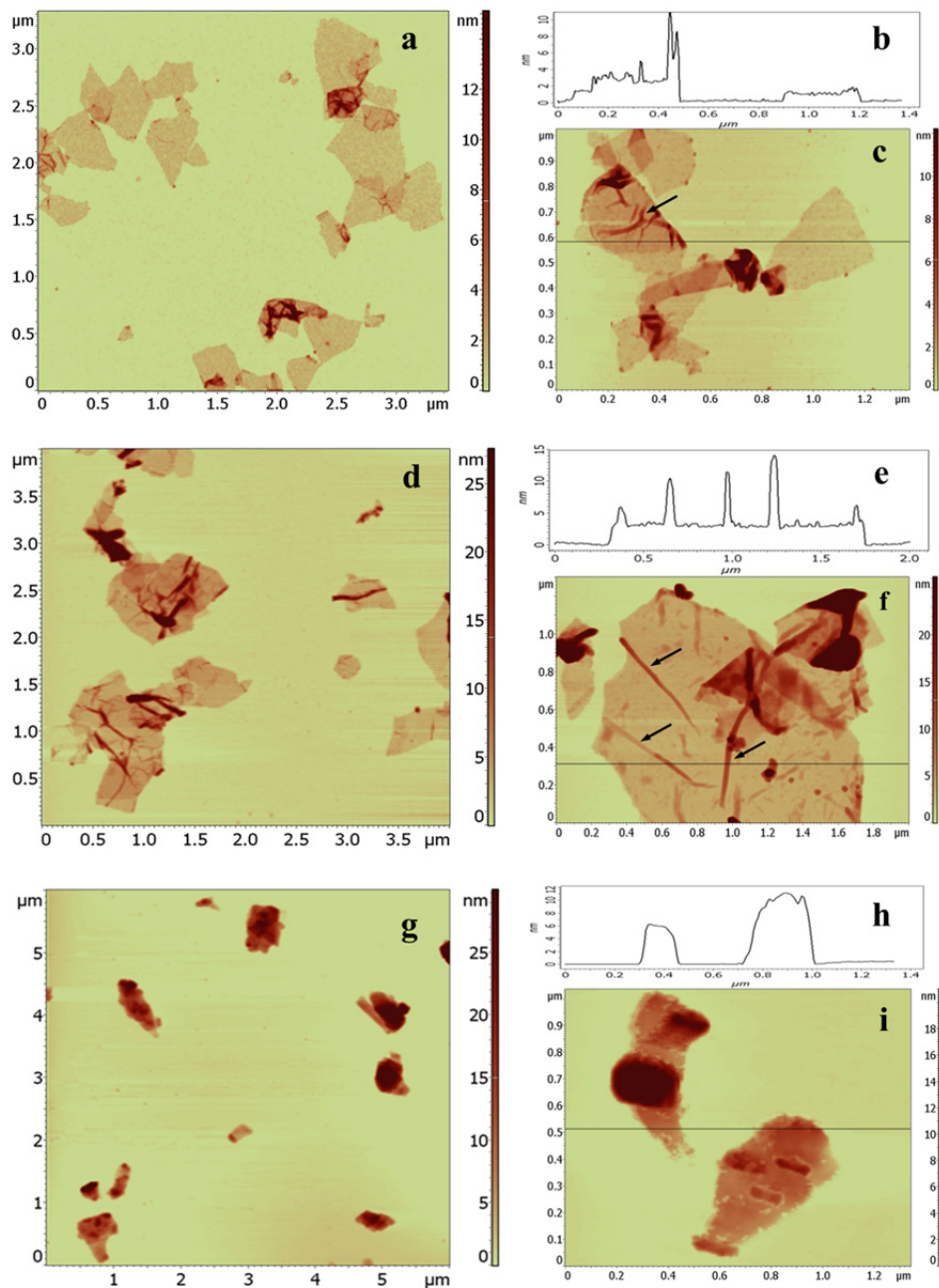


Figure 6.2 AFM topography tapping mode of graphene: a and c - oxidized/reduced chemically (*ORchem*), d and f - oxidized/reduced thermally (*ORtherm*), and g and i - sonicated in solution (*Sonic*). Images b, e, and h show the thicknesses profile of chosen sheets which in average represent *ORchem*, *ORtherm*, and *Sonic* samples, respectively. Arrows indicate wrinkling/folding of the sheets.

AFM analysis of non-oxidized (*Sonic*) graphene submitted only to long-term mechanical sonication shows, on average, thicker and smaller platelets. In contrast to previous studies,^[17,19] a great majority (> 90%) of small multi-layer graphene particles are present, exhibiting a thickness between 5 and 25 nm (see Figure 6.2 h). Some traces of more than 100 nm thick graphite flakes were also found, but discarded from further analysis. Obviously, for more than 5 nm thick flakes, no wrinkling was observed. The average surface areas were below 1 μm^2 . In summary, the *Sonic* approach provides smaller multi-layer graphene platelets as compared to the two oxidation/reduction methods. Nevertheless, *Sonic* dispersions show a much better long term-stability after centrifugation, without visible settling of particles.

6.3.2 PS/graphene composite analysis

The three different graphene dispersions were mixed with polystyrene (PS) latex and manually stirred, followed by freeze-drying and compression molding, resulting in composite tablets with thicknesses ranging from 0.5 to 1.0 mm. The composite processing was identical for all dispersions. Finally, the electrical conductivity of the nanocomposites was measured as a function of the nanofiller content (Figure 6.3). The composites exhibit a conductivity percolation threshold when the filler content is increased to form a continuous conductive path. The percolation threshold depends critically on the dispersion state, the nature of the contacts which defines the electron transport mechanism, and filler content, type, and dimensions.

For the *ORchem* samples, at a concentration of ~0.9 wt.% the conductivity increases dramatically and reaches 15 S/m at 1.5 to 2 wt.%. This value is, to the best of our knowledge, the highest value measured for graphene/PS nanocomposites with graphene loadings below 10 wt.%. For the remaining two approaches, percolation occurs at loadings of ~2 wt.% for the *ORtherm* and ~4.5 wt.% for the *Sonic* composites, respectively. Here, the maximum conductivity was measured to be 10 S/m (*ORtherm*) and 1 S/m (*Sonic*), respectively. *ORtherm* graphene/PS composites, prepared from the same optimized dispersions and stabilized with PSS or SC surfactants, show similar degrees of exfoliation, exhibit almost identical percolation threshold curves (~2 wt.%) and show the same final conductivity values (~10 S/m). Therefore, the choice of SC or PSS does not significantly influence the final conductivity and percolation in the final composites. However, we

cannot deny the importance of the choice of the surfactant for a proper initial exfoliation in water.

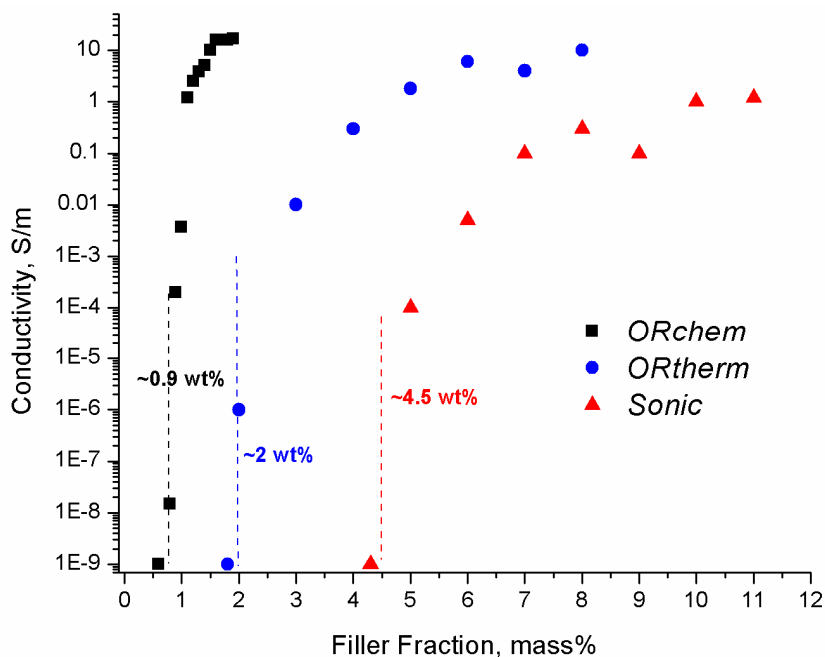


Figure 6.3 Electrical conductivity of graphene/PS composites as a function of graphene weight fraction. Values represent an average of 10 measurements for each sample; standard deviations are below 10%.

Based on Raman and UV-Vis alone, one would expect the lowest percolation threshold for the *Sonic* composites, as they presented the least structural damage during exfoliation and the most stable suspensions (highest UV-Vis absorption and long-term stability). This was not observed in the actual conductivity measurements; therefore, conductivity is not only determined by defect density in the exfoliated graphite or the stability of the dispersion. Here, we speculate that an attractive force between graphene sheets is necessary for network formation, i.e. less stable suspensions may be favorable. Also others reported^[33] that PS/graphene nanocomposites prepared from PS latex and aqueous graphene dispersions with relatively low stability and relatively low degrees of exfoliation exhibit lower percolation thresholds when compared to PS composites based on more stable dispersions with higher degrees of graphene exfoliation. Theoretical predictions,

inserting the degree of polydispersity to calculate percolation thresholds of the nanocomposites, confirmed this trend.^[33]

A nano-scale view of the conductive network is provided by conductive atomic force microscopy. The C-AFM tip measures the current throughout the volume of the nanocomposites specimen at a given voltage, which is transported via the graphene network to the ground contact. That means that only platelets that are grounded are monitored. Observed differences in current are determined by the path length and the intra-network graphene junctions, which may have a different resistivity.^[29] Graphene sheets forming sub-networks without ground connection show no current. In this way, C-AFM provides a current distribution image from which the conductive network can be distinguished from the insulating polymer/filler matrix. In Figure 6.4, the red/green brighter colored areas (which correspond to graphene in a cross-section topographic image) show non-zero current levels, indicating the presence of conductive pathways. The *ORchem* composites show a high number of conductive paths at 2 wt.% filler contents.

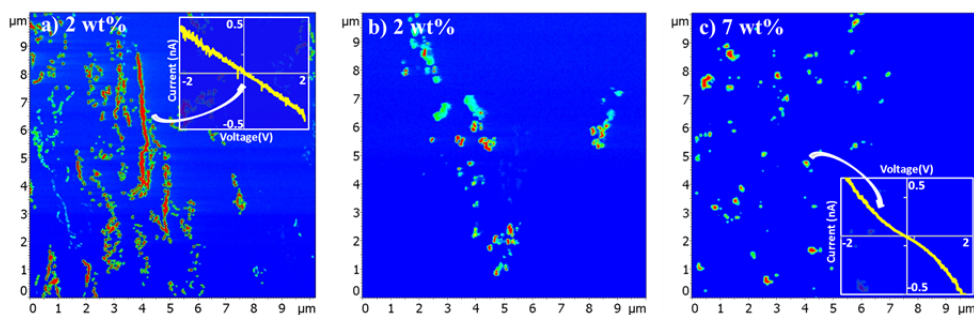


Figure 6.4 C-AFM of the composites cross section areas for the three graphene used. (a) *ORchem* (inset linear $I-V$ curve), (b) *ORtherm* and (c) *Sonic* (inset exponential-like $I-V$ curve) composites. Green/red spots correspond to graphene paths which contribute to conductivity through the sample.

In addition, a current vs. voltage ($I-V$) curve was measured at different points from at least 5 graphene clusters. When analyzing the various $I-V$ curves, corresponding to each of the different composites, we observed differences in the curve shapes. Most notably, $I-V$ curves obtained from *ORchem* composites show a linear $I-V$ relation (inset in Figure 6.4 a) for most graphene clusters, indicating predominantly Ohmic contacts between graphene sheets. For the other two samples we observe the conventional exponential-like $I-V$ curve

relation. This latter behavior is associated to tunneling electron transport,^[34-36] due to non-perfect contacts and the presence of surfactant or polymers in between the graphene sheets. AFM and SEM analyses show that *ORchem* graphene platelets are larger, thinner and less wrinkled than the other two graphene types. This would allow a larger direct contact area between the platelets, considering that the same filler weight concentration is present. A more detailed investigation on this topic is ongoing in our group.

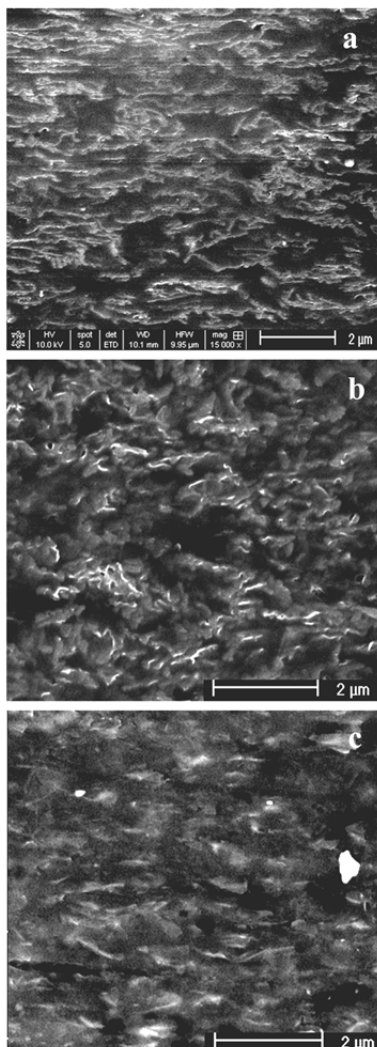


Figure 6.5 SEM analysis of composites: (a) *ORchem* , 2 wt.% of filler loading, (b) *ORtherm.*, 2 wt.% of filler loading, (c) *Sonic*, 2 wt. % of filler loading. Bright charging features correspond to the conductive graphene fillers inside the isolating PS polymer.

Figure 6.5 shows charge contrast SEM images of composite cross-sections as presented in Figure 6.4. Besides a more or less dark background, referring to the non-conductive matrix, bright areas are visible, which represent the graphene sheets. Because of the differences in charge transport between graphene and the polymer matrix, the secondary electron emission is higher at the graphene location. This results in the contrast between the graphene network (bright) and the polymer matrix (dark).^[37] Therefore, by using charge contrast imaging at high acceleration voltage we are able to gain representative information on the organization of a conductive network of graphene sheets in a polymer matrix. We could again notice the presence of more elongated filler arrangements for the *ORchem* material. It is also possible to identify the wrinkled and agglomerated graphene structures (the not so bright features in the background of Figure 6.5b) for the *ORtherm* composites. For the *Sonic* composites we can only observe non-defined bulk pieces of filler material along the cross-section area instead of platelets. Overall, in all samples the graphene filler was homogeneously distributed within the matrix.

6.4 Conclusions

Graphene, produced via difference water-based methods, was successfully used for the manufacturing of conductive graphene/PS nanocomposites, using latex technology.

With respect to graphene production, Raman analyses confirmed that oxidation/reduction methods introduce structural distortions/defects to the basal plane of graphene. Less damage was noticed for graphite which was submitted only to long-term sonication. Dispersions produced with graphene using this latter approach showed also higher long-term stability. AFM showed that the GO reduction techniques used in this work yield thin graphene platelets and, as a consequence, also induce wrinkling/agglomeration and possible size reduction of the platelets, especially for the *ORtherm* samples. Nevertheless, the thickness of the majority of the sheets was between 1 and 3 nm, corresponding to a single or only a few layers of graphene. The *Sonic* graphene was thicker, indicating multi-layer graphene (5 to 25 nm) and the average size was smaller. As these samples are much thicker, no wrinkling was observed.

The conductivities of the *ORchem* nanocomposites (by both four point and local current measurements) reveal high values up to 15 S/m and a low percolation threshold (0.9

wt.%). By the use of latex technology, well-dispersed graphene sheets in PS matrix were obtained and visualized using charge contrast SEM. SEM and C-AFM illustrate the different graphene shapes, even inside the polymer, depending on the filler production method. Interestingly, differences in electronic transport behavior were observed, which suggest mostly direct contact transport for *ORchem* graphene in contrast to tunneling for mostly of the *ORtherm* and *Sonic* graphene conductive paths. *ORtherm* composites produced with both PSS and SC surfactant exhibited almost identical percolation thresholds and final conductivities, indicating negligible influence of the surfactant, at the final stage, on these properties. However, surfactants have an important role during initial dispersion in water. Utilizing our dispersions, optimized with ionic surfactants and ultra-sonication, and same composite processing conditions, we conclude that the conductive properties of the final composites mainly depend on the initial morphological characteristics of the produced graphene and its self-organization inside the polymer matrix. The characteristics may have an important influence also on the type of electronic transport behavior through the composite.

References

- [1] J. R. Potts, D. R. Dreyer, C. W. Bielawski, R. S. Ruoff, *Polymer* **2010**, *52*, 5.
- [2] H. Kim, A. A. Abdala, C. W. Macosko, *Macromolecules* **2010**, *43*, 6515.
- [3] K. S. Novoselov, A. K. Geim, S. V. Morozov, D. Jiang, Y. Zhang, S. V. Dubonos, I. V. Grigorieva, A. A. Firsov, *Science* **2004**, *306*, 666.
- [4] C. Berger, Z. M. Song, T. B. Li, X. B. Li, A. Y. Ogbazghi, R. Feng, Z. T. Dai, A. N. Marchenkov, E. H. Conrad, P. N. First, W. A. de Heer, *J. Phys. Chem. B* **2004**, *108*, 19912.
- [5] W. A. de Heer, C. Berger, X. S. Wu, P. N. First, E. H. Conrad, X. B. Li, T. B. Li, M. Sprinkle, J. Hass, M. L. Sadowski, M. Potemski, G. Martinez, *Solid State Commun.* **2007**, *143*, 92.
- [6] K. S. Kim, Y. Zhao, H. Jang, S. Y. Lee, J. M. Kim, K. S. Kim, J. H. Ahn, P. Kim, J. Y. Choi, B. H. Hong, *Nature* **2009**, *457*, 706.
- [7] X. S. Li, W. W. Cai, J. H. An, S. Kim, J. Nah, D. X. Yang, R. Piner, A. Velamakanni, I. Jung, E. Tutuc, S. K. Banerjee, L. Colombo, R. S. Ruoff, *Science* **2009**, *324*, 1312.

- [8] A. Reina, X. T. Jia, J. Ho, D. Nezich, H. B. Son, V. Bulovic, M. S. Dresselhaus, J. Kong, *Nano Lett.* **2009**, *9*, 30.
- [9] G. Eda, G. Fanchini, M. Chhowalla, *Nat. Nanotechnol.* **2008**, *3*, 270.
- [10] R. R. Nair, P. Blake, A. N. Grigorenko, K. S. Novoselov, T. J. Booth, T. Stauber, N. M. R. Peres, A. K. Geim, *Science* **2008**, *320*, 1308.
- [11] X. L. W. X. L. Wang, *Phys. Rev. Lett.* **2008**, *100*, 4.
- [12] C. Berger, Z. M. Song, X. B. Li, X. S. Wu, N. Brown, C. Naud, D. Mayou, T. B. Li, J. Hass, A. N. Marchenkov, E. H. Conrad, P. N. First, W. A. de Heer, *Science* **2006**, *312*, 1191.
- [13] W. S. Hummers, R. E. Offeman, *J. Am. Chem. Soc.* **1958**, *80*, 1339.
- [14] S. Stankovich, D. A. Dikin, R. D. Piner, K. A. Kohlhaas, A. Kleinhammes, Y. Jia, Y. Wu, S. T. Nguyen, R. S. Ruoff, *Carbon* **2007**, *45*, 1558.
- [15] D. Li, M. B. Muller, S. Gilje, R. B. Kaner, G. G. Wallace, *Nat. Nanotechnol.* **2008**, *3*, 101.
- [16] M. J. McAllister, J. L. Li, D. H. Adamson, H. C. Schniepp, A. A. Abdala, J. Liu, M. Herrera-Alonso, D. L. Milius, R. Car, R. K. Prud'homme, I. A. Aksay, *Chem. Mater.* **2007**, *19*, 4396.
- [17] M. Lotya, Y. Hernandez, P. J. King, R. J. Smith, V. Nicolosi, L. S. Karlsson, F. M. Blighe, S. De, Z. M. Wang, I. T. McGovern, G. S. Duesberg, J. N. Coleman, *J. Am. Chem. Soc.* **2009**, *131*, 3611.
- [18] Y. Hernandez, V. Nicolosi, M. Lotya, F. M. Blighe, Z. Y. Sun, S. De, I. T. McGovern, B. Holland, M. Byrne, Y. K. Gun'ko, J. J. Boland, P. Niraj, G. Duesberg, S. Krishnamurthy, R. Goodhue, J. Hutchison, V. Scardaci, A. C. Ferrari, J. N. Coleman, *Nat. Nanotechnol.* **2008**, *3*, 563.
- [19] M. Lotya, P. J. King, U. Khan, S. De, J. N. Coleman, *ACS Nano* **2010**, *4*, 3155.
- [20] H. Bai, C. Li, G. Q. Shi, *Adv. Mater.* **2011**, *23*, 1089.
- [21] H. Chen, M. B. Muller, K. J. Gilmore, G. G. Wallace, D. Li, *Adv. Mater.* **2008**, *20*, 3557.
- [22] S. De, P. J. King, M. Lotya, A. O'Neill, E. M. Doherty, Y. Hernandez, G. S. Duesberg, J. N. Coleman, *Small* **2008**, *6*, 458.
- [23] S. Stankovich, D. A. Dikin, G. H. B. Dommett, K. M. Kohlhaas, E. J. Zimney, E. A. Stach, R. D. Piner, S. T. Nguyen, R. S. Ruoff, *Nature* **2006**, *442*, 282.
- [24] E. Tkalya, M. Ghislandi, A. Alekseev, C. Koning, J. Loos, *J. Mater. Chem.* **2010**, *20*, 3035.
- [25] O. Regev, P. N. B. El Kati, J. Loos, C. E. Koning, *Adv. Mater.* **2004**, *16*, 248.

- [26] N. Grossiord, J. Loos, C. E. Koning, *J. Mater. Chem.* **2005**, *15*, 2349.
- [27] J. R. Yu, K. B. Lu, E. Sourty, N. Grossiord, C. E. Koning, J. C. Loos, *Carbon* **2007**, *45*, 2897.
- [28] L. Staudenmaier, *Berichte der deutschen chemischen Gesellschaft* **1898**, *31*, 1481.
- [29] A. Alekseev, D. Chen, E. E. Tkalya, M. G. Ghislandi, J. Syurik, O. Ageev, G. d. With, *Adv. Funct. Mater.* **2012**, *22*, 1311.
- [30] A. C. Ferrari, J. C. Meyer, V. Scardaci, C. Casiraghi, M. Lazzeri, F. Mauri, S. Piscanec, D. Jiang, K. S. Novoselov, S. Roth, A. K. Geim, *Phys. Rev. Lett.* **2006**, *97*, 4.
- [31] A. C. Ferrari, *Solid State Commun.* **2007**, *143*, 47.
- [32] D. Yang, A. Velamakanni, G. Bozoklu, S. Park, M. Stoller, R. D. Piner, S. Stankovich, I. Jung, D. A. Field, C. A. Ventrice, R. S. Ruoff, *Carbon* **2009**, *47*, 145.
- [33] E. Tkalya, *Graphene-based polymer nanocomposites*, PhD thesis, Technische Universiteit Eindhoven (Eindhoven), **2012**.
- [34] A. Trionfi, D. A. Scrymgeour, J. W. P. Hsu, M. J. Arlen, D. Tomlin, J. D. Jacobs, D. H. Wang, L. S. Tan, R. A. Vaia, *J. Appl. Phys.* **2008**, *104*, 6.
- [35] S. Ansari, E. P. Giannelis, *J. Polym. Sci., Part B: Polym. Phys.* **2009**, *47*, 888.
- [36] C. Gau, C. Y. Kuo, H. S. Ko, *Nanotechnology* **2009**, *20*, 6.
- [37] J. Loos, A. Alexeev, N. Grossiord, C. E. Koning, O. Regev, *Ultramicroscopy* **2005**, *104*, 160.

High performance graphene and MWCNTs-based PS/PPO composites via organic solvent dispersion

The concept of liquid-phase dispersion, inspired on the latex technology, was applied for the preparation of well-dispersed suspensions of multi-wall carbon nanotubes and graphene in chloroform, using long-time ultra-sonication, without the use of surfactants. The dispersions with pre-defined filler concentration (0.5 mg/ml) were monitored via UV-Vis until the achievement of optimum exfoliation (6 h). The mixture of the filler suspensions with a PS/PPO solution, both using chloroform as solvent, subsequent drying and hot pressing, yielded for most of the samples a visually homogeneous and shiny black composite tablet. The well-dispersed organization of the fillers inside the polymer matrix, visualized with scanning electron microscopy, resulted in ultimate conductivities and percolation thresholds of 57 S/m and 0.2 wt.% for nanotubes composites, and 0.9 S/m and ~1 wt.% for graphene composites, respectively. Dynamic mechanical analysis showed that an increase in the storage moduli of the PS/PPO matrix could be gradually obtained by the insertion of fillers, e.g. reaching ~30% of enhancement by the addition of 3 wt.% of graphene filler. The same trend in improvement, at lower augmentation, was observed for the corresponding nanotubes-based composites.

7.1 Introduction

Polystyrene (PS) and poly(2,6-dimethyl-1,4-phenylene oxide) (PPO) constitute one of the most studied and explored polymer blend systems. It is uncommon for a pair of high molecular weight polymers to form completely miscible mixtures, but blends of PS and PPO show a complete solubility on the molecular level over the entire range of compositions.^[1-5] It was reported that the blends are truly homogeneous at the nanometer scale for samples obtained with low M_w PS and cast from chloroform.^[6] However, three factors have been identified to promote micro-heterogeneity of nanometer dimensions: a high polymer M_w , an increase of temperature, and the preparation of a blend using a solvent that induces crystallization of PPO, such as toluene.^[6]

Mixtures of PS and PPO have been extensively investigated also with regard to their high thermal^[4,5] and mechanical^[7,8] properties. PPO exhibits excellent tensile strength, modulus, chemical resistance, and high-temperature dimensional stability, but poor processability. PS is, for various applications, extremely brittle. Blending of PPO with PS can yield a tough material with good processability.^[6,9] More important, the PS-PPO blend system shows a transition from brittle to ductile failure with increasing PPO content by a gradual change in the micro-deformation mechanisms.^[10] The matrix ductility can, therefore, be easily controlled with the composition. Furthermore, both PS and PPO are amorphous polymers; hence problems associated with the presence of fillers or processing conditions, common for a semi-crystalline matrix, are avoided. Van Melick et al.^[11] reported that the glass transition temperature and the rubber modulus (dynamic modulus determined in the rubbery state) of PS/PPO blends increase with increasing PPO fraction. They concluded that the strain hardening modulus is proportional to the network density. However in the temperature dependence of the strain hardening behavior, relaxation might overrule the entropic character of the polymer network and lead to a decreasing trend.

Carbon nanotubes and, more recently, graphene have been extensively used for the improvement of mechanical and/or electrical properties of different polymer matrices. Mechanical reinforcement has been reported by the incorporation of functionalized carbon nanofibers/nanotubes and graphene (or graphene oxide), increasing the tensile strength and Young's modulus of mostly polar, but also apolar thermoplastics.^[12-17] Oxygen functional groups also favor the utilization of these carbon nanostructures in polymer composites, as they can enhance the interfacial adhesion between filler and polymer matrix. However,

these functional groups are structural lattice defects and fundamentally decrease the conductivity of the composite material.

Composites exhibiting a low electrical percolation threshold and high conductivity are usually prepared using liquid-based processes for a better dispersion of the filler inside the polymer matrix.^[18-20] The manufacturing of soluble or dispersible nanotubes/graphene sheets usually involves chemical modification or non-covalent functionalization; this latter is mostly done with the use of surfactants and is considered to have less impact on the structure and properties of the filler. Sodium dodecyl sulfate is known as a good surfactant for dispersion of nanotubes in water systems and subsequent mixture with polymer latex.^[19,21] The reduction of graphite oxide in the presence of poly(sodium 4-styrenesulfonate) formed a stable aqueous dispersion of graphene sheets.^[22] It was also reported that pyrenebutyric acid could be used to non-covalently functionalize graphene sheets via strong π - π interactions between pyrenyl rings and the basal planes of graphenes.^[23] Besides promoting a homogeneous distribution of the filler in the polymer matrix, a drawback of using surfactants for dispersion of fillers or for preparation of polymer latexes, is that they can drastically deteriorate the mechanical properties of the final composites, as the surfactants are not eliminated during processing.

Organic solvents are an alternative to disperse nanotubes or graphene without the use of surfactants.^[24-26] Two main issues are maximum filler concentration and subsequent removal of the solvent. The best solvents tend to have high boiling points and consequently are difficult to remove during composite processing.^[26,27] However, the long-time (~400 h) exfoliation of graphite into graphene in low boiling point solvents, such as chloroform and isopropanol, was reported at relatively high concentrations up to 0.5 mg/ml,^[28] just below 50% of the concentration which can be achieved with high boiling point solvents such as N-methyl-pyrrolidone.^[29]

The graphene surface is reported to be able to adsorb nonpolar polymers on its basal plane through π - π stacking or hydrophobic interactions^[30]. Generally, the π - π stacking interactions are realized by a solvent mixing of two components for a long time, allowing full contact of these two components.^[31] In this work graphene and multi-wall carbon nanotubes (MWCNTs) are dispersed in chloroform via long-time ultra-sonication and subsequently mixed with a PS/PPO polymer blend, which is also dissolved in chloroform. The solution is drop cast and the resulting dried film is pulverized into a powder for subsequent composite processing. We aim for a high performance nanocomposite

exhibiting a low electrical percolation threshold with well-dispersed fillers inside the polymer matrix due to the liquid phase mixing. The stiffness is expected to be improved, as compared to the PS/PPO matrix, especially for the graphene composites, due to interfacial π - π stacking interactions between graphene and the phenyl rings of PS/PPO.

7.2 Experimental

7.2.1 Materials and Characterization

PS/PPO pellets were produced by Sabic Innovative Plastics (The Netherlands). They contained 50 wt.% of PPO (PPO-803, with an average M_w of 30 kg/mol and a polydispersity index of 2.3) blended with PS (*Lacqrene* 1450N manufactured by Arkema, with an average M_w of 220 kg/mol and polydispersity index of 2.4). The blend is not a commercial product and does not contain any stabilizer. Chloroform (AR *Biosolve*, purity 99,9%) was used as solvent.

Thin long MWCNTs (*Nanocyl*® 7000) were provided by Nanocyl SA (Belgium). These are the same CNTs as those used in Chapters 3 and 4. Graphene sheets used were also the same as the ones used in Chapters 3 and 4, and were obtained via graphite (*SP-2 Bay Carbon*) oxidation and a thermo-expansion process.^[32]

UV-Vis absorption spectra were recorded with a Hewlett-Packard 8453 spectrometer operating between 200 and 1100 nm. Samples were taken regularly during the sonicating process and diluted by a certain factor, resulting in filler contents that were suitable for UV-Vis measurements.

The electrical conductivity was measured using the standard four-point method. Parallel contact lines, with 1 cm in length and with a 1 cm interval, were drawn on the composite film with conductive-silver paint (Fluka). All conductivity measurements were performed at room temperature with a Keithley 6512 programmable electrometer. For each sample, conductivity data represent the average over 10 consecutive measurements in a voltage range from 0 to 10 V and at frequencies between 50 and 60 Hz.

Composite films were imaged using a XL30 ESEM (Fei Co.) equipped with a field emission electron source. High vacuum conditions were applied and a secondary electron

detector was used for image acquisition. No additional sample treatment, such as surface etching or coating with a conductive layer, has been applied before surface scanning [22].

A DMA Q800 (TA Instruments) was used for the visualization of the temperature dependent mechanical properties and the determination of the glass transition temperatures (T_g). The measurements were done in tensile mode and the samples were undergoing a sinusoidal deformation, with amplitude of 10 μm at a frequency of 10 Hz, and were simultaneously heated from 0 to 185 $^{\circ}\text{C}$ at a rate of 3 $^{\circ}\text{C}/\text{min}$. The T_g was set to be the temperature at the maximum of the loss modulus (E'') peak. DMA was also used for the acquisition of the elastic modulus, defined here as slope of the stress vs. strain curve in the linear region, at deformation of $\sim 0.3\%$. Differential scanning calorimetry (DSC) was also applied for characterizing the T_g of the pure PS/PPO and the filler composites. A DSC Q2000 (TA instruments) was used, with 2 cycles from 20 to 250 $^{\circ}\text{C}$ at 3 $^{\circ}\text{C}/\text{min}$ ramp. The second cycle was used for recording T_g as the inflection point of the heat flux vs. temperature curve. All samples ranged between 8 and 10 mg weight.

7.2.2 Preparation of dispersions and composite processing

Graphene (0.05 g) and MWCNTs (0.05 g) nanopowders were deposited in bottom-round flasks and mixed with 100 ml of CHCl_3 , resulting in a filler content of 0.05 mg/ml. The dispersions were then bath sonicated (*Bransonic*[®] 1510) for 6 h. The output power provided was 70 W. The flasks were placed in an ice/water bath during sonication in order to prevent temperature rising.

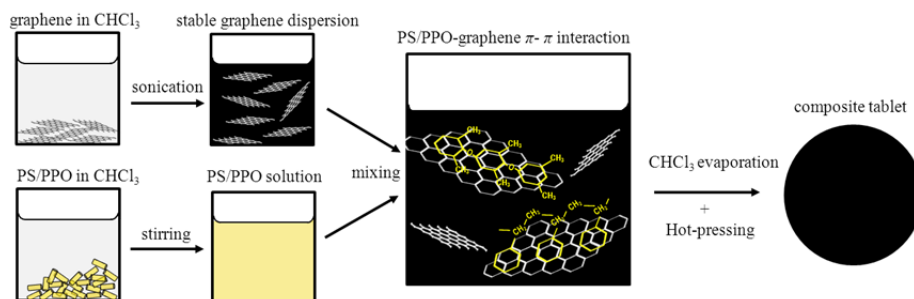


Figure 7.1. Sketch exemplifying the experimental route for the manufacturing of PS/PPO graphene nanocomposites. Same procedure was used for the preparation of PS/PPO MWCNTs composites.

PS/PPO pellets were mixed with chloroform (concentration of 0.05 g/ml) in a closed vessel and stirred for 1 h, achieving a homogeneous solution. A sequence of the whole experimental procedure is sketched in Figure 7.1.

For composite preparation, each filler dispersed in chloroform was mixed with PS/PPO chloroform solution by stirring to a final filler content, after solvent removal, between 0.1 wt.% and 10 wt.%. The dispersions were drop cast into Petri plates of various diameters according to the volume content of solvent. The dispersions were stirred during solvent evaporation at room temperature for 3 days to avoid inhomogeneities or phase separation. The films were then grained into small flakes using a small coffee mill (*Moulinex*, max 85 g) and vacuum dried in an oven at 90 °C for 2 days to remove residual chloroform. The resulting composite powders were heated quickly to 200 °C and then for 20 min until 220 °C between Teflon sheets, using a Collin Press 300G. Subsequently the heated material was compression molded into films of 0.3 to 0.5 mm thickness at 100 bar for 4 minutes. Prior to final compression, the composite was degassed via 3 consecutives quick compressions at 50 bar for 20 seconds.

7.3 Results and discussion

A reported technique to control the MWCNTs filler dispersion in water and other solvents is UV-Vis.^[33] We monitored the UV-Vis absorbance of the graphene (0.5 mg/ml) dispersion in chloroform and used as this approach to indirectly estimate the quality of exfoliation.

We understand that a lot of features might influence the UV-Vis results for graphene dispersions, as e.g. the angle between the incident light and sheets at the acquisition moment, scattering of light, and crumbling of samples in the dispersion. However, we clearly see an increase in absorbance for practically the whole measured spectra range (250 to 750 nm) with increasing sonication time, and a prominent increasing peak at ~275 nm, as was already observed for nanotubes and attributed to 1D van Hove singularities.^[34] The use of long-time ultra-sonication of graphite/graphene was also reported, as mentioned in the introduction.

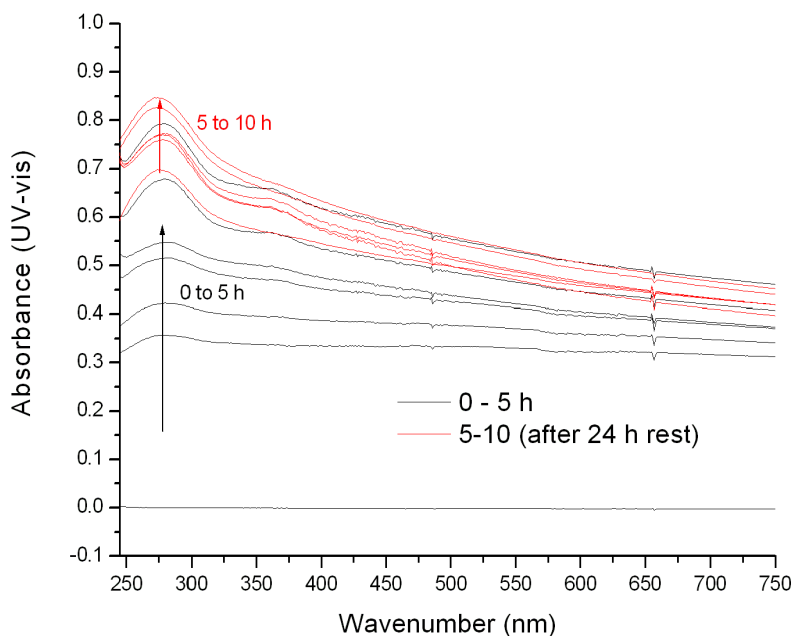


Figure 7.2. Monitoring of UV-Vis absorbance over time for graphene/chloroform dispersion (0.5 mg/ml). The sonication power was set at 70 W.

In this work we monitored (every 0.5 to 1 h) the absorbance of graphene and MWCNTs in chloroform over a total 10 h sonication time with a pause of 24 h between the fifth and sixth hours in order to check the stability of dispersions. We can see in Figure 7.2 that the absorbance increases up to 5 h and, after 24 h rest, a small decrease is observed probably due to some graphene settling. Continuing the sonication from 6 to 10 h results in an oscillation around the maximum peak of absorbance reached. We considered then that 6 h would be sufficient for optimum graphene/chloroform dispersion. The same trend was verified for MWCNTs dispersion, except that the maximum absorbance was considerably lower than the one measured for the graphene system, which indicates a poorer exfoliation/dispersion of MWCNTs in this solvent. Nevertheless, both graphene and MWCNTs dispersions were visually completely black and with no trace of settling (sedimentation) after weeks of rest. The dispersion/organization of the filler in the final composite was investigated via SEM. In Figure 7.3 we can see that the nanotubes and graphene platelets are mostly individually exfoliated and are homogeneously distributed, forming a percolating network through the polymer.

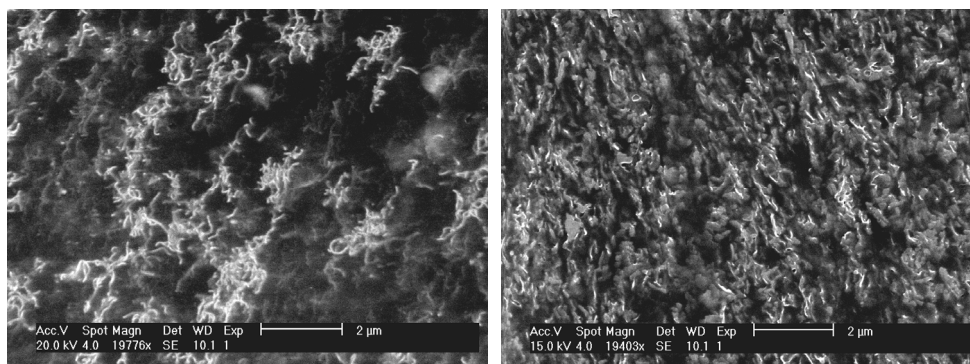


Figure 7.3. SEM micrographs of the surface of a PPO/PS MWCNTs (left) nanocomposite, and the cross-section area of a PPO/PS graphene (right) nanocomposite, containing 1 wt.% of MWCNTs and 4 wt.% of graphene, respectively.

7.3.1 Conductive Percolation Threshold

It is known that the latex technology allows the incorporation of carbon nanotubes and graphene into polymer systems in a well-dispersed and homogeneous way, resulting in the formation of a conductive network at low filler contents.^[18,20] We followed the liquid-phase dispersion concept proposed by the latex technology, with basically two modifications. We substituted water, an environmental friendly solvent, by the organic solvent chloroform, in order to avoid the use of any kind of surfactant which could be detrimental to the mechanical properties. Additionally, freeze-drying, an energy demanding step, was substituted by solvent evaporation at room temperature and atmospheric pressure. By allowing slow solvent evaporation, instead of freeze-drying the well-dispersed liquid system, we suspected that some phase separation could occur, compromising the organization of the graphene/MWCNTs inside the final composite by the creation of micro-heterogeneities; this trend was reported elsewhere.^[35] The degree of exfoliation or organization of fillers inside the composite is a controversial topic. Logically, poor dispersions should result in composites with low ultimate conductivity values and high conductivity percolation threshold. However, some experimental studies, supported by theoretical simulation, indicate that a certain filler entanglement or clustering helps the formation of a conductive network, thereby decreasing the percolation threshold.^[36]

The conductivity percolation thresholds obtained for MWCNTs and graphene PS/PPO nanocomposites are shown in Figure 7.4. The values are low, even when compared to composites prepared via latex technology (references used for comparison in Figure 7.4). The conductivity percolation threshold obtained for PS/PPO MWCNTs samples is as low at 0.2 wt.% filler content, reaching conductivity values of 57 S/m at 4 wt.%. These results are in close agreement with PS/PPO MWCNTs reference samples, which were prepared via latex technology.^[37] For the PS/PPO graphene samples, on average, the percolation threshold starts at ~ 1 wt.% and a maximum conductivity of 0.9 S/m is obtained at 4 wt. %.

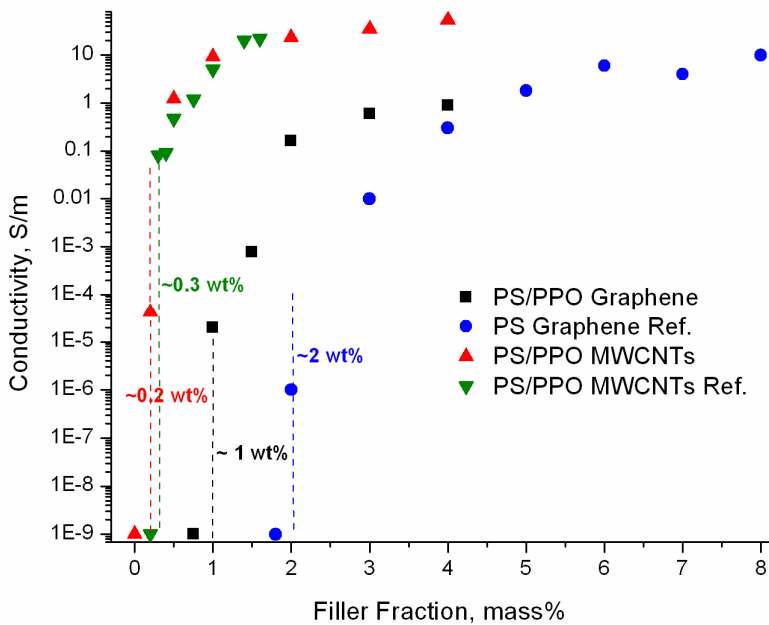


Figure 7.4. Electrical conductivity (four-point measurements) as a function of graphene/MWCNTs loading for composites based on PS/PPO. PS Graphene Reference sample and PS/PPO MWCNTs Reference sample^[37] were prepared using water-based latex technology and are used as reference for comparison. Results represent an average of at least 3 measurements with standard deviations below 10%.

The percolation value is lower as compared to the PS graphene reference, also prepared by our group using a water-based latex concept and reported in Chapter 6 of this thesis. It is important to point out that the viscosity of PS/PPO blend is lower than the viscosity of the very high molecular weight PS (about 5×10^3 Pa.s for PS/PPO and $> 10^5$ Pa.s

for PS), so the processability and consequently movement of filler and final organization inside the polymer matrix are different, factors which might favor the low percolation threshold obtained for PS/PPO graphene samples. Some studies report this positive influence of low viscosity on percolation threshold, giving rise to the so-called ‘dynamic percolation’.^[38,39]

The low percolation threshold obtained for samples prepared via organic solvent dispersion, as compared to samples prepared by water-based latex technology, have to be carefully addressed, considering several factors that differentiate between the two methods. The interaction chloroform-graphene/MWCNTs-PS/PPO is fundamentally different from the interaction water/surfactant-graphene/MWCNTs-PS/PPO. Secondly, the long-time bath ultrasonic exfoliation provides a slow and gentle exfoliation of fillers, compared to the more intense tip sonication. This might result in different MWCNTs lengths or different graphene surface areas. Thirdly, the slow removal of the solvent may result in phase separation as compared to freeze-drying, where the water is removed from a ‘frozen-in’ system. Finally, the use of surfactants may result in an extra insulating material surrounding the filler, hindering direct filler-filler contacts. The entropy of mixing for the two different polymer solutions, one in water and the other in chloroform, are also different, resulting in different thermodynamics parameters.

The goal of this work is to test a new method, also based on liquid-phase dispersion, to produce conductive nanocomposites with low percolation threshold and improved mechanical properties. A more detailed specific comparison regarding the yielding of each sonication technique, solubility parameters, as well as the influence of the speed of solvent removal and the specific influence of surfactant on composite final conductivity, have to be conducted in order to clearly explain how each of these factors influences the observed percolation thresholds.

7.3.2 Thermo-Mechanical Properties

Graphene and MWCNTs are known for their outstanding intrinsic mechanical properties. The use of these materials as reinforcement in polymer composites has been extensively studied and several approaches for the manufacturing of these nanocomposites have been proposed. Dispersion, filler-matrix interface interaction and processing

conditions are crucial issues in order to achieve mechanical improvement. The large surface area of nanofillers like graphene and MWCNTs is an attractive property for an efficient stress transfer from the filler to the polymer matrix. The pre-dispersion of these nanofillers in liquid solvents promotes exfoliation in the form of a stable suspension, constituting also a handy platform for manipulating these fluffy nanofiller powders. As mentioned before, the latex technology concept uses aqueous dispersions as a base to form stable suspensions, with the help of surfactants. The surfactants are usually salts or low molecular weight polymers that act via ionic or steric interactions. Even though some of these surfactants may show some compatibility with the filler and/or the polymer matrix, they usually remain present in the final composite, and depending on the amount, they can drastically reduce the mechanical properties of the composite material. Our proposal, which avoids the use of surfactants by dispersing the MWCNTs and graphene directly in chloroform and dissolve the polymer matrix in the same solvent, looks promising, especially after we confirmed the formation of stable chloroform-filler suspensions, and subsequently composites with low electrical percolation threshold.

Three series of composite mixtures were produced for each nanofiller, with concentrations ranging from 0.1 wt.% to 4.0 wt.% of filler content. The mixtures of MWCNTs/graphene dispersions and PS/PPO solutions, both using chloroform, resulted in a black homogeneous fluid for all concentrations. The drop-cast films, after drying, were smooth and visually completely black, for concentrations of graphene or MWCNTs higher than 1 wt.%. For MWCNTs and graphene concentrations from 0.1 to 0.75 wt.% some macroscopic heterogeneities could be visualized on the films. All films with 0.1 wt.% were partially transparent. After grinding the drop-cast films into small flakes, and subsequently hot pressing these flakes into tablets, all the graphene and MWCNTs composite samples with concentration from 0.5 wt.% to 4.0 wt.% of filler content exhibited a shiny black surface, with no visual heterogeneities. Surprisingly, all composites with 0.1 wt.% for both graphene and MWCNTs, presented small air bubbles trapped inside their structure, even though the drying process and degasification before hot-pressing were carried out in an identical way for all the mixtures. Reference pure PS/PPO samples, without any filler content, were prepared using exactly the same procedure as used for the nanocomposites preparation. Tablets of PS/PPO were partially transparent and smooth, with no bubbles. Hence the presence of the bubbles remains obscure and samples with 0.1 wt.% filler content were discarded.

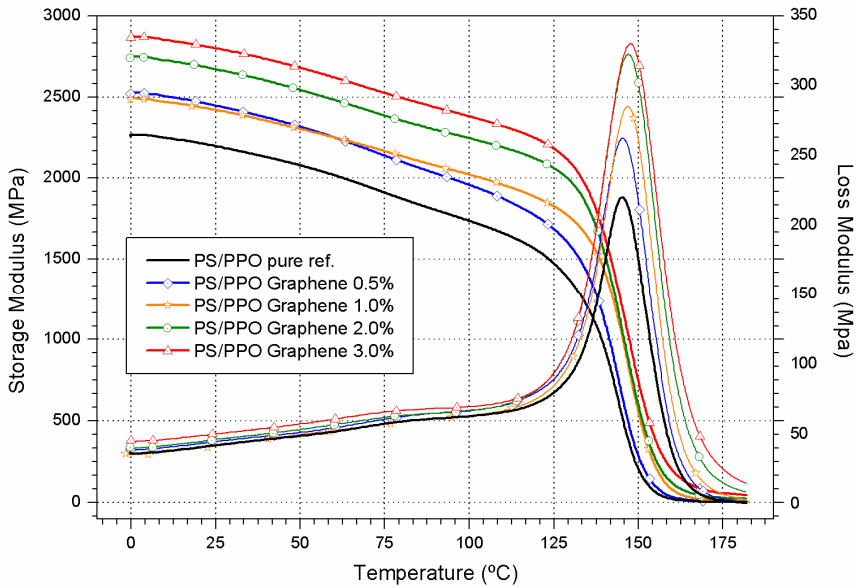


Figure 7.5. Storage and Loss Moduli as function of temperature for PS/PPO graphene composites at different filler contents. Results represent an average of at least 3 measurements with standard deviations below 5%.

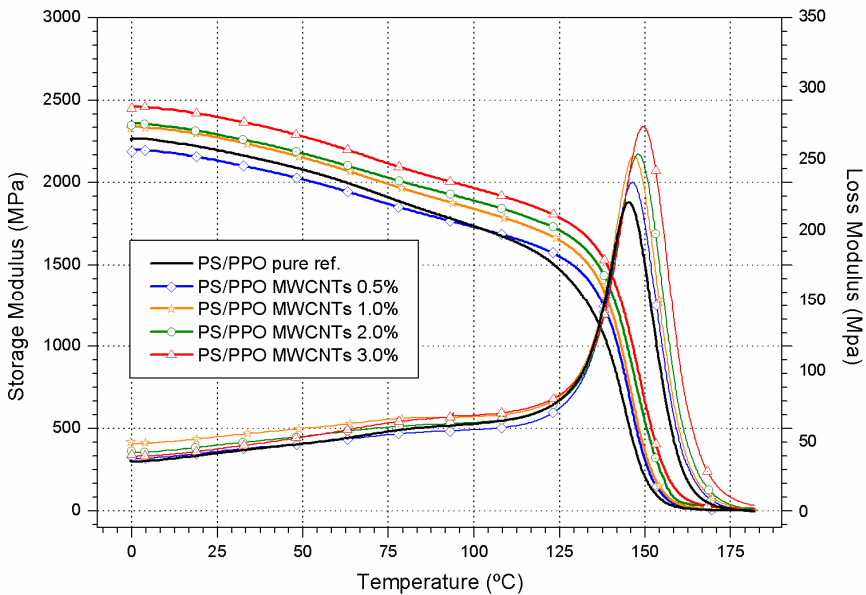


Figure 7.6. Storage and Loss Moduli as function of temperature for PS/PPO MWCNTs composites at different filler contents. Results represent an average of at least 3 measurements with standard deviations below 5%.

The dynamic thermo-mechanical behavior of the PS/PPO composites is compared in Figure 7.5 and Figure 7.6 for the different filler contents. The static elastic modulus (E), at $\sim 0.3\%$ of deformation was also measured using the DMA machine. The average properties values are shown in Table 7.1. Each curve or value represents an average of at least 3 measurements on distinct samples with the same concentration, with deviations below 5%. For comparison, only samples with concentration between 0.5 and 3 wt.% were considered. Samples with 4 wt.% of graphene in PS/PPO were discarded basically due to brittleness during analysis. Most of these samples broke during static modulus measurement, hampering further comparison.

The addition of 0.5 wt.% or 1 wt.% of graphene to a 50/50 wt./wt. PS/PPO clearly enhances the dynamic modulus of the composite. This improvement reaches 17% when we compare PS/PPO graphene 1 wt.% with pure PS/PPO at 100 °C. It is important to point out that practically all samples exhibited a storage modulus (E') value higher than 2000 MPa up to 100 °C. Probably due to the presence of micro-heterogeneities during film preparation, graphene samples from 0.5 to 1 wt.% content showed a slightly higher standard deviation of measured E' values. Nevertheless, a clear trend indicating improvement of the E modulus was obtained.

The DMA analysis of PS/PPO MWCNTs composites showed a similar trend behavior as observed for PS/PPO graphene samples. However, the percentage of improvement was clearly lower for all concentrations as compared to PS/PPO graphene, reaching a maximum E' improvement of $\sim 6\%$ for 1 wt.% MWCNTs content at 100 °C as compared to the pure polymer. This improvement is really close to the 5% maximum standard deviation measured, preventing reliable considerations on any improvement trend up to this filler content. Samples with 4 wt.% of MWCNTs PS/PPO, besides less brittle than graphene ones at the same loading, were also discarded due to brittleness. Samples with 0.5 wt.% of MWCNTs showed a higher deviation on E' values as compared to the ones with higher filler loadings, exhibiting, on average, a lower E' value than pure PS/PPO at temperatures below 100 °C. It is important to mention that the M_w of PS is much higher than PPO, factor which can cause preferential adsorption of PS on the surface of the fillers. This trend was reported^[40] for silica particles in PS matrix and we suspect that the incorporation of graphene or MWCNTs in PS, especially at low filler contents, can cause phase separation and/or inhomogeneities in the composites, decreasing their average E modulus and increasing deviations during measurements.

The Halpin-Tsai model^[41] is widely used in the fiber composites field to describe the tensile modulus of unidirectional composites as a function of aspect ratio. The equations can deal with a variety of reinforcement geometries including discontinuous filler reinforcement such as fiber-like or flake-like structures. The E_c modulus of a composite is proposed to be

$$\frac{E_c}{E_m} = \frac{(1+\zeta\eta V_f)}{(1-\eta V_f)} \quad (1)$$

where

$$\eta = \left(\frac{E_f}{E_m} - 1\right) / \left(\frac{E_f}{E_m} - \zeta\right) \quad (2)$$

and E_c , E_m , E_f are Young's modulus of the composite, polymer matrix and fibers, respectively. V_f is the filler volume fraction and ζ is a shape parameter dependent on filler geometry and loading direction. In particular $\zeta = 2(l/d)$ for fibers^[41], and $2(l/t)$ for disc-like^[41] platelets, when calculating the composite modulus in the longitudinal direction ($E_{||}$). l , d and t are the length, diameter and thickness of the dispersed fillers respectively. When calculating the composite modulus in the transversal direction (E_{\perp}) the parameter ζ is set to be 2. For composites containing randomly distributed fibers, the composite modulus can be calculated by the following^[42]:

$$E_c = \frac{3}{8}E_{||} + \frac{5}{8}E_{\perp} \quad (3)$$

Equation 3 was used to estimate the Young's modulus of the composite materials (E_c Model) and the results are compared in Table 7.1 with the results measured experimentally (E_c Exper.) for all the filler contents. One can see that the calculated Young's moduli are much higher than the measured ones, especially at higher filler loadings. These results are a clear indication that interface adhesion filler-matrix is not ideal or that the fillers do not have a minimum length (minimum size in the case of graphene) for maximum stress transfer. Residual porosity might also influence, decreasing the modulus obtained experimentally. It is important to mention that the modulus of the fillers E_f used was 1 TPa for both graphene and nanotubes; this high value, vastly defined and used in literature for a single particle, might not reflect reality.

In polymer composites, the quality of fiber reinforcement is usually described in terms of the ‘critical fiber length’. This parameter is small for strong interfaces and is defined as 2 times the distance over which the strain rises from the fiber ends to a plateau level. It is generally accepted that in order to obtain good fiber reinforcement the fiber length should be at least 10 times the ‘critical length’.^[43] The mechanics of nano-reinforcement for graphene monolayers was reported to be probed directly in a poly (methyl methacrylate) matrix.^[44] Applying this theory for pure single layer graphene, relatively large graphene flakes ($> 30 \mu\text{m}$) will be needed before efficient reinforcement can take place.^[44] As mentioned in Chapter 6, our exfoliation process produced graphene platelets no larger than a few hundred nanometers across, so it is expected to yield no or poor reinforcement. According to experimental results, an improvement of almost 30% in the E or E' modulus was obtained for PS/PPO graphene 3 wt.% samples as compared to the pure polymer (see Table 7.1). For most practical applications these results are highly satisfactory, even if the Halpin-Tsai moduli were not achieved experimentally.

In composites with pure graphene or MWCNTs, interfacial stress transfer will only be taking place through van der Waals bonding across an atomically smooth surface. Pi interaction, or π - π stacking, refers to attractive, non-covalent interactions between neutral closed-shell systems. Despite intense experimental and theoretical interest, there is no unified description of the exact factors that contribute to π - π stacking interactions. Grimme^[45] recommends using the term with care. For systems with about ten carbon atoms or less, there is little theoretical evidence for a special role of the π orbitals. This view is supported by experimental phase change data for hydrocarbons, and even extreme cases, such as intramolecular π - π stacking in cyclophanes, fit in.^[45] Thus, the term “ π - π stacking” should be used as a geometrical descriptor of the interaction mode in unsaturated molecules and to understand π - π interactions as a special type of electron correlation (dispersion) effect that can only act in large unsaturated systems when they are spatially close, which is only possible in a stacked orientation. As mentioned in the introduction, some studies reported that graphene is able to adsorb nonpolar polymers on its basal plane through π - π stacking or hydrophobic interactions. We speculate then, that due to a more suitable and larger planar structure for the formation of π - π stacking with the aromatic rings of PPO/PS, the composites with graphene nanofiller exhibit a higher interaction with the matrix and consequently higher mechanical improvement than composites prepared with MWCNTs. Interaction filler-matrix might be also simply entropic for system.

Table 7.1. Mechanical properties and glass transition temperature of graphene and MWCNTs composites in a PS/PPO matrix. Modulus values correspond to an average of at least 3 measurements on distinct samples, with standard deviations below 5%.

Sample	Filler (wt.%)	E_c Model (MPa)	E Exper. (MPa)	E' at 100 °C (MPa)	T_g from E'' (°C)
PS/PPO	0	1962	1962	1735	145.2
PS/PPO Graphene	0.5	2949	2369	1959	145.3
PS/PPO Graphene	1	3949	2167	2022	146.8
PS/PPO Graphene	2	5940	2438	2247	146.9
PS/PPO Graphene	3	7961	2533	2380	147.5
PS/PPO MWCNTs	0.5	2620	1934	1731	146.3
PS/PPO MWCNTs	1	3159	1951	1841	146.8
PS/PPO MWCNTs	2	4368	2029	1890	147.9
PS/PPO MWCNTs	3	5591	2103	1968	149.4

The thermal properties of the pure PS/PPO and the composites were first characterized by DSC. Pure PS/PPO pellets were analyzed prior to any dispersion or processing. The analysis of the second heating run shows a glass transition temperature (T_g) of 146.5 °C. After dissolving the polymer in CHCl_3 and removing the solvent by evaporation (3 days at room temperature and air pressure), PS/PPO showed a T_g of 136 °C (via DSC second heating run analysis), value which is 10 °C lower than the T_g of the pellets. The results clearly indicate that CHCl_3 that is not removed can act as a plasticizer. For PS/PPO tablets that were submitted to further vacuum drying and hot pressing after solvent evaporation, the T_g was 145.2 °C, value which is more consistent with the value of the pure raw material, and points to almost the absence of a plasticizing (solvent) effect. This material was obviously used for comparison with composites, as it was processed in identical way.

For the PS/PPO graphene composites analyzed by DSC, a small increase of T_g was observed for samples with an increase in the filler concentration, reaching a maximum of 147.5 °C for the composite with 3 wt.% of filler content. The same trend was not observed for PS/PPO MWCNTs composites, for which all samples at all nanofiller concentrations (from 0.5 to 3 wt.%) exhibited a similar $T_g \sim 145$ °C, consistent with the value obtained for pure PS/PPO.

Thermo-gravimetric analysis (TGA) was also utilized for characterization of the thermal stability of the composites. Pure PS/PPO and PS/PPO graphene and MWCNTs composites were submitted to identical standard heating ramps of 10 °C/min up to 700 °C, in air. A comparison of the degradation temperature at 20 wt.% loss shows, on average, a small improvement from 414 °C to 416-418 °C for the composite samples as compared to the pure polymer. No clear trend related to filler concentration or type of filler could be identified.

The thermal properties of the materials were also studied based on the ASTM D 4065-2001 norm, which recommends defining the T_g in terms of the maximum loss modulus E'' . It can be seen in Table 7.1 that the addition of the nanofillers graphene or MWCNTs slightly increases the T_g of the composites. In brief, it is possible to see a trend, the T_g increases as the filler concentration also increases, for both materials. The same increase was not obtained for PS/PPO MWCNTs samples analyzed by DSC. Analyzing the first DSC heating run of PS/PPO MWCNTs, we could not verify a conclusive trend of increasing T_g . We speculate then, that after the second DSC heating run, where some tension or/and CNTs entanglement/orientation can be released, no clear increase in T_g for these composites can be considered.

Unfortunately, tensile tests were not conducted due to the lack of available material. New masterbatches are being prepared and the stress-strain behavior will be explored in a future work.

7.4 Conclusions

MWCNTs and graphene were successfully dispersed in a PS/PPO polymer matrix via organic solvent dispersion. The long-term ultra-sonication of MWCNTs and graphene suspensions in chloroform, with pre-defined filler concentration (0.5 mg/mL), were monitored via UV-Vis until the achievement of an optimum exfoliation time (6 h). The mixture of the filler suspensions with PS/PPO solution, both in chloroform solvent, and subsequent drying and processing yield for most of samples visually homogeneous shiny black composite tablets. SEM confirmed the well-dispersed organization of MWCNTs and graphene inside the polymer matrix.

Conductivities of up to 57 S/m were obtained for MWCNTs composites, with a percolation threshold as low as 0.2 wt.% of filler content. These values are in close agreement with results obtained using water-based latex technology for the same filler/polymer system. PS/PPO graphene composites exhibited an electrical percolation threshold around 1 wt.% and a maximum conductivity of 0.9 S/m. The percolation threshold value for the solvent-based recipe is lower when compared to similar filler/polymer systems produced via latex technology.

Finally, the thermo-mechanical properties (E' , E'') of the composites showed substantial improvement by the addition of the nanofillers, specially at concentrations ≥ 1 wt.%. For PS/PPO graphene samples an increase in the E' of up to 29% was obtained for composites with 3 wt. %, with a storage modulus higher than 2500 MPa at temperatures up to 75 °C. The mechanical improvement obtained for PS/PPO MWCNTs was lower for all wt.% concentrations as compared to PS/PPO graphene samples. Thermal analysis indicates that, in general, the T_g slightly increases as the filler, namely graphene, concentration increases. DSC measurements clearly indicate a plasticizing effect caused by the presence of non-removed CHCl_3 in the samples, so the drying process has to be optimized thoroughly. Bubbles found trapped inside some samples may also be an effect of the presence of CHCl_3 .

In summary, we conclude that it is possible to produce highly conductive MWCNTs/graphene polymer composites with low electrical percolation threshold using liquid-phase dispersion, without the use of surfactants. Non-polar polymers, like PS/PPO blends, with oriented aromatic rings along its structure, can interact with the basal carbon plane of graphene via π - π stacking, improving the mechanical properties of the composite as compared to pure polymer. We suspect that due to a more suitable and larger planar structure for the formation of π - π stacking with the aromatic rings of PPO/PS, the composites with graphene nanofiller exhibited higher interaction with the matrix and consequently a more pronounced mechanical improvement than composites prepared with MWCNTs.

References

- [1] S. T. Wellinghoff, J. L. Koenig, E. Baer, *J. Polym. Sci., Part B: Polym. Phys.* **1977**, *15*, 1913.
- [2] W. M. Prest, R. S. Porter, *J. Polym. Sci., Part B: Polym. Phys.* **1972**, *10*, 1639.
- [3] C. G. Robertson, G. L. Wilkes, *J. Polym. Sci., Part B: Polym. Phys.* **2001**, *39*, 2118.
- [4] N. E. Weeks, F. E. Karasz, W. J. Macknight, *J. Appl. Phys.* **1977**, *48*, 4068.
- [5] J. Yang, L. J. An, T. Xu, *Polymer* **2001**, *42*, 7887.
- [6] S. Li, L. C. Dickinson, J. C. W. Chien, *J. Appl. Polym. Sci.* **1991**, *43*, 1111.
- [7] A. F. Yee, *Polym. Eng. Sci.* **1977**, *17*, 213.
- [8] L. W. Kleiner, F. E. Karasz, W. J. Macknight, *Polym. Eng. Sci.* **1979**, *19*, 519.
- [9] B. Tekkanat, R. Gibala, *J. Thermoplast. Compos. Mater.* **1991**, *4*, 190.
- [10] S. T. Wellinghoff, E. Baer, *J. Appl. Polym. Sci.* **1978**, *22*, 2025.
- [11] H. G. H. van Melick, L. E. Govaert, H. E. H. Meijer, *Polymer* **2003**, *44*, 2493.
- [12] M. Ghislandi, L. A. S. d. A. Prado, A. d. I. V. Oyerviedes, H. Wittich, K. Schulte, A. Barros-Timmons, *J. Polym. Sci., Part A: Polym. Chem.* **2008**, *46*, 3326.
- [13] H. Kim, A. A. Abdala, C. W. Macosko, *Macromolecules* **2010**, *43*, 6515.
- [14] M. Moniruzzaman, K. I. Winey, *Macromolecules* **2006**, *39*, 5194.
- [15] M. Fang, K. Wang, H. Lu, Y. Yang, S. Nutt, *J. Mater. Chem.* **2009**, *19*, 7098.
- [16] H. Deng, E. Bilotti, R. Zhang, T. Peijs, *J. Appl. Polym. Sci.*, *118*, 30.
- [17] Z. Wang, P. Ciselli, T. Peijs, *Nanotechnology* **2007**, *18*, 9.
- [18] E. Tkalya, M. Ghislandi, A. Alekseev, C. Koning, J. Loos, *J. Mater. Chem.* **2010**, *20*, 3035.
- [19] J. Yu, K. Lu, E. Sourty, N. Grossiord, C. E. Koning, J. Loos, *Carbon* **2007**, *45*, 2897.
- [20] N. Grossiord, J. Loos, O. Regev, C. E. Koning, *Chem. Mater.* **2006**, *18*, 1089.
- [21] J. Yu, N. Grossiord, C. E. Koning, J. Loos, *Carbon* **2007**, *45*, 618.
- [22] S. Stankovich, D. A. Dikin, G. H. B. Dommett, K. M. Kohlhaas, E. J. Zimney, E. A. Stach, R. D. Piner, S. T. Nguyen, R. S. Ruoff, *Nature* **2006**, *442*, 282.
- [23] H. Bai, Y. Xu, L. Zhao, C. Li, G. Shi, *Chem. Commun.* **2009**, 1667.
- [24] H. T. Ham, Y. S. Choi, I. J. Chung, *J. Colloid Interface Sci.* **2005**, *286*, 216.
- [25] J. L. Bahr, E. T. Mickelson, M. J. Bronikowski, R. E. Smalley, J. M. Tour, *Chem. Commun.* **2001**, 193.
- [26] Y. Hernandez, M. Lotya, D. Rickard, S. D. Bergin, J. N. Coleman, *Langmuir* **2010**, *26*, 3208.

- [27] Y. Hernandez, V. Nicolosi, M. Lotya, F. M. Blighe, Z. Y. Sun, S. De, I. T. McGovern, B. Holland, M. Byrne, Y. K. Gun'ko, J. J. Boland, P. Niraj, G. Duesberg, S. Krishnamurthy, R. Goodhue, J. Hutchison, V. Scardaci, A. C. Ferrari, J. N. Coleman, *Nat. Nanotechnol.* **2008**, *3*, 563.
- [28] A. O'Neill, U. Khan, P. N. Nirmalraj, J. Boland, J. N. Coleman, *J. Phys. Chem. C* **2011**, *115*, 5422.
- [29] U. Khan, A. O'Neill, M. Lotya, S. De, J. N. Coleman, *Small* **2010**, *6*, 864.
- [30] S. Z. Zu, B. H. Han, *J. Phys. Chem. C* **2009**, *113*, 13651.
- [31] Y. Cao, J. Zhang, J. Feng, P. Wu, *ACS Nano* **2011**, *5*, 5920.
- [32] M. J. McAllister, J.-L. Li, D. H. Adamson, H. C. Schniepp, A. A. Abdala, J. Liu, M. Herrera-Alonso, D. L. Milius, R. Car, R. K. Prud'homme, I. A. Aksay, *Chemistry of Materials* **2007**, *19*, 4396.
- [33] N. Grossiord, O. Regev, J. Loos, J. Meuldijk, C. E. Koning, *Anal. Chem.* **2005**, *77*, 5135.
- [34] A. G. Ryabenko, T. V. Dorofeeva, G. I. Zvereva, *Carbon* **2004**, *42*, 1523.
- [35] A. Saalbrink, A. Lorteije, T. Peijs, *Composites Part A* **1998**, *29*, 1243.
- [36] E. Tkalya, *Graphene-based polymer nanocomposites*, PhD thesis, Technische Universiteit Eindhoven (Eindhoven), **2012**..
- [37] N. Grossiord, *A latex-based concept for making carbon nanotube/polymer nanocomposites*, PhD thesis, Technische Universiteit Eindhoven (Eindhoven), **2007**.
- [38] R. Zhang, A. Dowden, H. Deng, M. Baxendale, T. Peijs, *Compos. Sci. Technol.* **2009**, *69*, 1499.
- [39] H. Pang, C. Chen, Y.-C. Zhang, P.-G. Ren, D.-X. Yan, Z.-M. Li, *Carbon*, *49*, 1980.
- [40] S. Jain, J. G. P. Goossens, G. W. M. Peters, M. van Duin, P. J. Lemstra, *Soft Matter* **2008**, *4*, 1848.
- [41] J. C. Halpin, J. L. Kardos, *Polym. Eng. Sci.* **1976**, *16*, 344.
- [42] J. C. Halpin, N. J. Pagano, *J. Comp. Mat.* **1969**, *3*, 720.
- [43] A. Kelly, N. H. Macmillan, *Strong solids*, Clarendon Press, **1986**.
- [44] L. Gong, I. A. Kinloch, R. J. Young, I. Riaz, R. Jalil, K. S. Novoselov, *Adv. Mater.* **2010**, *22*, 2694.
- [45] S. Grimme, *Angew. Chem. Int. Ed.* **2008**, *47*, 3430.

Technology Assessment

Carbon fillers, and more recently carbon nanofillers, have been widely used for different industrial applications; from inexpensive carbon black, used as additives in a polymer matrix for simple reinforcement purposes, to continuous oriented carbon fibers used as textiles embedded in a thermoset resin for high-performance aerospace applications. The actual technologies that deal with carbon fillers having nanometric dimensions, like MWCNTs or graphene, are therefore still not completely developed in a way to fulfill the requirements for most of the industrial applications in composites. The interactions filler-filler and filler-matrix are still not totally exploited in order to yield the expected improvement. The processing conditions are not fully controlled and understood; henceforth most of the research still remains in the academic level.

Most of the final applications that utilize these nano-scaled carbon structures as fillers in composites are directed to devices which have macroscopic dimensions. Hence, the detailed study of the mechanical and conductive behavior of these carbon nanofillers agglomerated in the form of a bulk powder could generate important insights on their macroscopic properties. In industry, the powder pressing method, studied in Chapter 3 of this thesis, can be a simple and reliable tool suitable for processing control of filler production. The technique can be easily scaled up, and some companies, as Nanocyl S.A. (Belgium), already use a simplified model of the process in an industrial plant. Therefore, the detailed study can be useful for improvement of the actual process and proper characterization of the bulk electrical properties of these carbon materials.

The conductivity of a composite is directly related to the formation of a conductive network through the polymer matrix and its understanding depends, at least partly, on the knowledge of the electrical behavior of the nanoparticles agglomerates. The conductivity values for composites above the percolation threshold described in this dissertation are in agreement with results obtained for powder compacts. We could identify a clear sign that for composites at low filler contents (1-5 wt.%) it is impossible to reach the high conductivities obtained for powders compacts, due to huge mismatch of effective densities of conductive fillers. This information was not completely clear and was explored in order

to provide a realistic estimation of achievable conductivity values for carbon-based polymer composites. We assume that the results presented most probably will be helpful when designing new formulations and processes in the production field. Overall, carbonaceous nanofiller/polypropylene composites exhibiting really low conductivity percolation thresholds were successfully produced using a latex technology process. The process can also be scaled up to industrial scale. The preparation of polymer latex is versatile, and can be done either by emulsion polymerization or by polymer emulsions which can be artificially brought into latex form. This is a known and studied field in polymer science. On the other hand, sonication of large volumes of aqueous surfactant-filler dispersions require some adaptations, such as the use of a stirring system combined with the use of a long probe for the tip sonicator. Some of these types of aqueous dispersion are already commercially available.

The bottleneck for the transfer of this technology from laboratory to industry might be the cost of the process. In particular, the raw materials carbon nanotubes and graphene are still expensive. The manufacturing of 'good' quality material is still an issue and remains a niche industry restricted to higher-value industrial sectors. Manufacturers of carbon nanotubes are aware of this and can already produce tons of MWCNTs per year, which could bring the price per kilogram of finished product down to 10 euros. Graphene is a more recent material; this ultrathin form of carbon - a single atomic layer thick in some cases, a handful of layers in others - has been the focus of an enormous research effort for the past couple of years. With so many graphene application papers being published now and a steady stream of media reports touting graphene as the miracle material that may replace silicon, it's easy to get lost in the hype. Graphene has a number of extremely useful properties, including very fast electron mobility and high mechanical strength. But many of the extreme values that have been reported apply only to isolated graphene. It is necessary to study graphene's properties under the complex conditions that are present in real technological devices. For any application to be successful, extensive research is needed, requiring a lot of time.

Thin and highly pristine graphene films are made by various chemical vapor deposition (CVD) methods. The CVD-quality samples generally play a key role in advanced electronics. The films can also be isolated from thin graphite flakes by successively splitting the flakes apart with adhesive tape. The Scotch tape method, as it's

known in the field, was central to the Nobel Prize work. However, these methods are (still?) not suitable for large scale production of fillers to be used in composites.

In this dissertation, we utilized and compared methods for graphene production that treats graphite with strong acids and oxidizers or that simply expose graphite to long-term ultrasonic exfoliation. The first procedure exfoliates graphite and yields a high-surface-area product consisting of defective oxidized crystallites. Researchers typically refer to the product as graphite oxide or graphene oxide. Oxidation is followed by chemical or thermal treatment, which partially reduces the material and renders it electrically conducting. This rougher form of graphene tends to be used in composite materials and energy storage devices. Two companies, Vorbeck (USA) and XG Sciences (USA), have already exceeded the ton level production of graphene utilizing these oxidation/reduction methods. Of course one has to note that these companies currently produce a form of graphene known as graphene nanoplatelets (small stacks of graphene sheets). In addition to raw graphene, these companies offer materials made with graphene. XG Sciences, for example, works with resin and polymer compounders to provide commercial customers with new graphene-polymer composites. Depending on the material's intended use - for example to manufacture parts for the automotive and aerospace industries - polymers may be blended with graphene nanoplatelets to increase stiffness, electrical conductivity, and thermal stability or to reduce solvent and gas permeability relative to the pure polymer. Graphene-based electrically conductive inks are another family of commercial products. Vorbeck makes such products under the trade name Vor-ink for the printed-electronics industry. The company also manufactures sheets and rolls of preprinted Vor-ink-based circuits.

For production of graphene we utilized the oxidation/reduction methods described above which can be scaled up, and is already being used commercially, and compared with another promising method (still not commercially available) that utilizes simply long-time mechanical exfoliation of graphite in a solvent. The resulting graphene sheets were characterized and used to produce conductive polymer composites via latex technology.

Focusing on industrial application one can say that the production of graphene via oxidation of graphite and subsequent thermal reduction of graphite oxide looks more attractive than the other two methods: graphite oxidation followed by chemical reduction or the liquid phase sonication of graphite into graphene. In short, thermal reduction has an important advantage over the latter two methods in terms of time needed for the preparation of graphene. It also exhibits a clear advantage over graphene prepared via liquid phase

exfoliation in terms of a lower percolation threshold and higher conductivity levels, which can be reached at relatively low filler loadings.

A last attempt for the preparation of carbon-based polymer nanocomposites utilizing organic solvents was also planned with focus on industrial application. The conductive composites prepared via latex technology are environmentally friendly (water/surfactant used as solvent) but have limited applicability due to their poor mechanical properties. The latex technology process utilizes a high amount of surfactant, for stabilization of the system, compromising the mechanical structure of the final product. Furthermore, the free-drying of the aqueous filler/latex dispersion is a relatively lengthy and expensive process in terms of operating costs and energy consumption. With the new approach, we successfully produced highly conductive MWCNTs/graphene polymer composites, and with low electrical percolation threshold, using organic solvents and without the use of surfactants. Overall, the composites exhibited high conductivity values, reaching 10-50 S/m, values which might be enough for antistatic and even for electromagnetic interference (EMI) shielding applications. The processing method was simple and fast. Non-polar polymers, like PS/PPO blends, with oriented aromatic rings which can interact with the basal carbon plane of graphene, should be used. The results showed that it is possible to produce composites with improved mechanical properties, suitable for a wide range of applications where certain stiffness is required. A drawback of the technique is the use of organic solvents, like chloroform, for dispersion of the filler and the polymer. They are more expensive than water and may offer health risk.

Summary

The manufacturing of low density conductive plastics, that could replace metals in many applications, is a challenging target that has been pursued by several technological segments. The incorporation of carbon nanofillers, namely carbon nanotubes and graphene, into a polymer matrix is a recent and promising approach. The achievement of highly conductive nanocomposites, with low electrical percolation threshold, depends mostly on the intrinsic properties of the fillers and their state of dispersion throughout the matrix. In this system the macroscopic properties of the composite are undoubtedly governed by the nature and extension of the interactions between filler particles, as well as between filler and polymer matrix. This doctoral dissertation therefore examines the macroscopic electrical behavior of carbon fillers, at initial stage, still as a powder, and subsequently when inserted into polymer matrix to form conductive nanocomposites.

The latex technology has proven to be efficient on promoting a homogenous incorporation of exfoliated CNTs into any kind of viscous polymer which can be artificially brought into latex form, or which can be synthesized via emulsion polymerization. One objective of this dissertation is henceforth to study the scope and limitations of multifunctional graphene-based nanocomposites, using the superior DPI-owned water-based latex concept developed for CNTs, for dispersing the two-dimensional graphene nanofiller in polymer matrices (PS, PP, PS/PPO). For comparison, zero-dimensional (statistically spherical) carbon black nanoparticles, one-dimensional MWCNTs, and three-dimensional graphite are also evaluated. We strive to understand differences observed for the different carbon allotropes, each with a high surface-to-volume ratio

Special attention is given to graphene as nanofiller, whose properties may be highly variable depending on the preparation method. In order to assess a collective understanding of the main routes utilized in this work for preparation of graphene, Chapter 2 introduces a systematic literature review on the particularities of each preparation method. Techniques used for characterization of single sheet properties and its organization inside polymer composites are presented, with focus on atomic force microscopy and Raman spectroscopy.

The conductive performance of a composite is directly related to the formation of a conducting network through the polymer matrix and its understanding depends critically on

the knowledge of the electrical behavior of the agglomerated nanoparticles, e.g. in the form of a bulk powder or a paper film. In literature there is still a lack of information concerning these macroscopic bulk properties of carbon powders. Chapter 3 studies the electrical conductivity of the nanofillers MWCNTs, graphene, carbon black and graphite, using compacts produced by a paper preparation process and by powder compression. Powder pressing assays show that the bulk conductivity depends not only on the intrinsic material properties but is also strongly affected by the number of particle contacts and the packing density. Conductivities at high pressure (5 MPa) for the graphene, nanotube and carbon black show lower values ($\sim 10^2$ S/m) as compared to graphite ($\sim 10^3$ S/m). For nanotube, graphene and graphite particles, the conductive behavior during compaction is governed by mechanical particle arrangement/deformation mechanisms while for carbon black this behavior is mainly governed by the increasing particle contact area. The materials resulting from the paper preparation process for carbon black and graphite showed similar conductivity values as for the compacts, indicating a limited effect of the surfactant on the conductivity. The paper preparation process for the large surface area nanotube and graphene particles induces a highly preferred in-plane orientation, thereby yielding largely the single particle intrinsic conductivity for the in-plane direction, with values in the order of 10^3 S/m.

In Chapter 4, the percolation thresholds and final conductivities of polypropylene (PP) composites, prepared with the fillers studied in Chapter 3, are evaluated and compared with powder and paper results. The latex technology concept is used for the incorporation of the carbon fillers in the polymer. The fillers are first dispersed in water (assisted by surfactants) using ultra-sonication, subsequently mixed with PP latex, then freeze-dried and, finally, hot-pressed into composite tablets. PP composites produced in this work showed well-dispersed fillers inside the polymer, with percolation thresholds as low as 0.3 wt.%. The maximum conductivity obtained for the composites is approximately ~ 1 S/m, not reaching the high value of $\sim 10^3$ S/m, which are obtained for graphene and nanotube-based paper films or graphite compacts.

Chapter 5 focuses on the characterization of graphene layers via micro-Raman spectroscopy, tip-enhanced Raman spectroscopy (TERS) and tip-enhanced Raman spectroscopy mapping (TERM). In particular TERM allows for the investigation of individual graphene sheets with high Raman signal enhancement factors and allows imaging of local defects with nanometer resolution. Enhancement up to 560% of the

graphene Raman bands intensity was obtained using TERS. TERM (with resolution better than 100 nm) showed an increase in the number of structural defects (D band) on the edges of both graphene and graphite regions.

Continuing the investigation of graphene structures, Chapter 6 compares graphene sheets produced from graphite powder using the three best known water-based conversion approaches. The first two are based on chemical oxidation methods, only differing in the reduction process, either by the use of hydrazine or by thermal expansion, respectively. The third one is based on long-term ultrasonic exfoliation. Water/surfactant solutions were prepared with these three nanofillers and latex technology was applied for the preparation of conductive graphene/polystyrene composites with well-dispersed graphene platelets. The samples were characterized with respect to filler properties and morphology, and their influences on electrical conductive properties of the composites were compared. Microscopic studies showed that both reduction processes lead to agglomeration/wrinkling of the nanoplatelets, even though they yield composites with high conductivity and low percolation threshold. Although mechanical ultrasound exfoliation of graphite produces less defective multi-layer graphene, these platelets have a smaller lateral size and their composites exhibit a higher percolation threshold.

As a final attempt, in Chapter 7, the concept of liquid-phase dispersion, inspired on the latex technology, was applied for the preparation of well-dispersed suspensions of multi-wall carbon nanotubes and graphene in chloroform, using long-time ultra-sonication, without the use of surfactants. The dispersions with pre-defined filler concentration (0.5 mg/ml) were monitored via UV-Vis until the achievement of optimum exfoliation (6 h). The mixture of the filler suspensions with a PS/PPO solution, both using chloroform as solvent, subsequent drying and hot pressing, yielded for most of the samples a visually homogeneous and shiny black composite tablet. The well-dispersed organization of the fillers inside the polymer matrix, visualized with scanning electron microscopy, resulted in ultimate conductivities and percolation thresholds of 57 S/m and 0.2 wt.% for nanotubes composites, and 0.9 S/m and ~1 wt.% for graphene composites, respectively. Dynamic mechanical analysis showed that an increase in the storage moduli of the PS/PPO matrix could be gradually obtained by the insertion of fillers, e.g. reaching ~30% of enhancement by the addition of 3 wt.% of graphene filler. The same trend in improvement, at lower augmentation, was observed for the corresponding nanotubes-based composites.

Acknowledgements

One more step has come to an end and it is time to acknowledge all the people that somehow contributed to its completion. First of all, I'd like to express my sincere gratitude to my promoter prof. Bert de With, firstly for giving me the opportunity to work in SMG group, but especially for becoming my daily supervisor after the leaving of Joachim. We have had important discussions and after a bit of re-management of ideas, I think we could find a proper way to a smooth and interesting final flow of the project.

Prof. Joachim Loos, thanks a lot for being my supervisor the first two years and for the initial vibrant working atmosphere you always tried to create in our group. It was the start-up of ideas that gave rise to this thesis. Thanks also to dr. Kangbo Lu, that helped me a lot with the initial experiments.

Prof. Cor Koning, I thank you for always being present and active, since the beginning, in all the important steps of the project. All the discussions and positive support were really important for the completion of the Russian-Brazilian strategy.

The committee members, professors Cor Koning, Paul van der Schoot, Han Goossens and Ton Peijs, are also acknowledged for reading and giving interesting suggestions for the improvement of the thesis. Prof. Alex van Herk is thanked for chairing the PhD defense. DPI, in the name of Jan Stamhuis, is acknowledged for technical and financial support.

Evgeniy, thanks a lot for being daily part of the project. All the discussions, measurements, reports and ping-pong challenges were really serious business but fun. It seems the mission was accomplished and a strong friendship was settled. Paul, Ronald and Charline, thank you also for your active participation and contribution to all the project issues.

During my PhD project, I have had the great chance to interact with several people that helped me with technical and theoretical support. The SPM lab was the place where most of the work arose. Sasha Alekseev, Marco Hendrix, and Günter Hoffmann, thank you for being patient and teaching me something (or at least try to). Part of this thesis belongs to you. Sasha Kodentsov and Huub van der Palen, you were great with all the amazing technical solution for all kind of non-sense problems we used to come up with. Thank you also for the organization and all the fruitful discussions we all used to have on last Friday

of each month (late hours of hard work). Niek Lousberg, thanks for the SEM enlightenment and thank you Paul Bomans for the TEM analyses. Imanda Scholten, I really appreciate your help since the beginning of my PhD. You make our lives much easier. Jos Laven is thanked for Raman instructions and advices. Gingling, thanks for the help, always in a nice mood, with the DMA. Thank you, Heiner Friedrich, for thesis corrections and interesting suggestions. Catarina Esteves, *muito obrigado*, first for letting me know about the position and after for all the measurements support, suggestions and nice time I could have with you and Pedro.

I would like to express my appreciation to all the students that concluded their work with me. Bernardo, Guillaume, Eric, Simon, Pieter, and all the OGO students, I feel that together we could create and learn something.

My SMG and TU/e friends, you could make life in Eindhoven much brighter than one could expect from the Dutch weather. Indu and Camille, thank you for appreciating good live music in the office in the past 3 or 4 years. The daily lunch commission Camille, Isabelle, Vladimir and Ivelina, thanks a lot for your real friendship since the beginning, in the university, and for the strong ones, at Stratum afterwards. Then I have to include Mark (thanks, the coffee mill was really useful), Delei, Baris, Hesam, Gökhan, Dina, Jos, Beulah, Niels, Koen, Marcel, João, Maarten, Fabio, Laura, Beryl, Katya, Nico and all the members of the SMG family. Thank you all for the nice time we spent together.

I cannot forget the great football teams we had in the department. Benjamin, Mr. Tkalya, Vlado, Mark, Donglin, Miguel, Ariel, Esteban, Miran, Tom, Hector, Carlos, Maria, and all the others that played for the Spartak SPC, the Vlackers, and recently for the SuPerStars. It was a pleasure to play with all of you.

I also would like to acknowledge the international friends from outside the university. My roommates Jorge and Nicolas (El Cordobes), and all the Brazilian community: Gerry, Vinicius, Gustavo, Gaucho, Mauricio, Paulo, Ariel, Ivan, Ana, Iana, Alexandre, Lorena, Bruna, Vivian and many others, together with members of the rest of the world: Gosia, Sami, Olga, Can, Armando, Vera, Vsevo and all the other nationalities; I think we could make Eindhoven feel like home, at least from time to time.

Finally I would like to dedicate a lot of this to my family: Carlos, Christina, Janaína and Daniel (including family), and to my girlfriend, Manuela, that could, even from far away, bring a bit more of poetry and a lot of inspiration (also a lot of travelling) to my life during the stay.

Curriculum Vitae

Marcos Gomes Ghislandi was born on the 28th of March 1981 in Goiânia, Brazil. After finishing the secondary school in 1998, he studied Materials Engineering in the Federal University of Santa Catarina, Brazil. In 2004 he received his bachelor diploma in Engineering, with final project related to polymer composites. From 2005 to 2007 he coursed the Joint European Master in Materials Science (EMMS) at the Technical University of Hamburg-Harburg (Germany) and the University of Aveiro (Portugal), where he received the degree of Master in Materials Science, with final work focused on fiber reinforced composites.

In 2008 he started a PhD project in the Laboratory of Materials and Interface Chemistry at the Eindhoven University of Technology (the Netherlands), under the supervision of prof. dr. G. de With. The most important results of this work are presented in this dissertation.

List of Publications

- ❖ M. Ghislandi, E. Tkalya, S. Schillinger et al. High performance graphene and MWCNTs-based PS/PPO composites via organic solvent dispersion. (in preparation)
- ❖ M. Ghislandi, E. Tkalya, B. Marinho et al. Electrical conductivities of carbon powder nanofillers and their latex-based polymer composites. *Composites: Part A*, 2012. (submitted)
- ❖ M. Ghislandi, E. Tkalya, A. Alekseev et al. Electrical conductivity of polymer composites prepared with aqueous graphene dispersions. *Nanotechnology*, 2012. (submitted)
- ❖ M. Ghislandi, G. Hoffmann, L. Xue et al. Tip-enhanced Raman spectroscopy and mapping of graphene sheets. *Applied Spectroscopy Reviews*, 2012. (accepted)
- ❖ M. Ghislandi, E. Tkalya, G.d. With, C.E. Koning. The use of surfactants for dispersing carbon nanotubes and graphene to make conductive nanocomposites. *Current Opinion in Colloid and Interface Science*, 2012. (accepted)
- ❖ B. Marinho, M. Ghislandi, E. Tkalya et al. Electrical conductivity of compacts of graphene, multi-wall carbon nanotubes, carbon black, and graphite powder. *Powder Technology* 221:351-358, 2012.
- ❖ A. Alekseev, D. Chen, E. E. Tkalya, M.G. Ghislandi et.al. Local organization of graphene network inside graphene/polymer composites. *Advanced Functional Materials* 22:1311-1318, 2012.
- ❖ E. Tkalya, M. Ghislandi, A. Alekseev et al. Latex-based concept for the preparation of graphene-based polymer nanocomposites. *Journal of Materials Chemistry* 20: 3035-3039, 2010.